

# Fingerprinting of soil organic matter composition by FTIR-ATR spectroscopy

---

**Kapeni, Sofia**

**Master's thesis / Diplomski rad**

**2024**

*Degree Grantor / Ustanova koja je dodijelila akademski / stručni stupanj:* **University of Zagreb, Faculty of Agriculture / Sveučilište u Zagrebu, Agronomski fakultet**

*Permanent link / Trajna poveznica:* <https://um.nsk.hr/um:nbn:hr:204:763106>

*Rights / Prava:* [In copyright](#) / [Zaštićeno autorskim pravom.](#)

*Download date / Datum preuzimanja:* **2025-04-01**



*Repository / Repozitorij:*

[Repository Faculty of Agriculture University of Zagreb](#)



UNIVERSITY OF ZAGREB  
FACULTY OF AGRICULTURE

**FINGERPRINTING OF SOIL ORGANIC  
MATTER COMPOSITION BY FTIR-ATR  
SPECTROSCOPY**

MASTER THESIS

Sofia Kapeni

Zagreb, July, 2024.

**UNIVERSITY OF ZAGREB  
FACULTY OF AGRICULTURE**

Graduate study programme:

Danube AgriFood Master - DAFM

**FINGERPRINTING OF SOIL ORGANIC  
MATTER COMPOSITION BY FTIR-ATR  
SPECTROSCOPY**

MASTER THESIS

Sofia Kapeni

Mentor:

Prof. Željka Zgorelec

Co-Mentor:

Prof. Apolka Ujj

Zagreb, July, 2024.

**UNIVERSITY OF ZAGREB  
FACULTY OF AGRICULTURE**

**STUDENT STATEMENT  
ON THE ACADEMIC INTEGRITY**

I, **Sofia Kapeni** JMBAG 01781381467, born on 27 March 1999 in Amarousio, Athens, Greece, declare that I independently prepared the Master thesis entitled:

**FINGERPRINTING OF SOIL ORGANIC MATTER COMPOSITION BY FTIR-ATR  
SPECTROSCOPY**

With my signature I guarantee:

- that I am the sole author of this Master thesis;
- that all literature sources used, both published and unpublished, are appropriately cited or paraphrased and listed in the reference list at the end of the Master thesis;
- that this Master thesis does not contain any parts of work previously submitted to the Faculty of Agriculture or other higher education institutions for the purpose of completing university or specialist study programme
- that the electronic version of this Master thesis is identical to the printed version which has been reviewed by the Committee and approved by the mentor
- that I am acquainted with the regulations of the Code of Ethics of the University of Zagreb (Article 19).

In Zagreb, on \_\_\_\_\_

\_\_\_\_\_  
*(date) (signature of the student)*

UNIVERSITY OF ZAGREB  
FACULTY OF AGRICULTURE

REPORT  
ON EVALUATION AND DEFENSE OF GRADUATE THESIS

Master thesis of the student **Sofia Kapeni** JMBAG 01781381467 entitled

FINGERPRINTING OF SOIL ORGANIC MATTER COMPOSITION BY FTIR-ATR  
SPECTROSCOPY

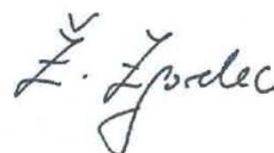
was defended and evaluated with the grade (5) excellent on 24/07/24.

Committee:

signatures:

1. Prof. Željka Zgorelec, PhD

mentor



2. Prof. Apolka Ujj, PhD

co-mentor



3. Assoc. Prof. Lidija Svečnjak, PhD

member



4. Assoc. Prof. Ivana Šestak, PhD

member



## **Acknowledgment**

I hereby express my sincere gratitude to my mentors, Željka Zgorelec and Lidija Svečnjak, for their invaluable support, and guidance, throughout this research. Their expertise and dedication has been of immense value for the completion of this thesis, as well as for my personal development. I deeply appreciate their understanding, patience, and kindness throughout this whole year.

I am also deeply grateful to the members of my thesis committee, for their constructive feedback and suggestions, which have significantly improved the quality of this work.

Furthermore, I would like to express my heartfelt gratitude to my parents, Athanasios and Georgia, and my brother, Georgios, who have always believed in me and supported me in every possible way throughout the challenges of this journey. Their encouragement has been invaluable for completing this Master's degree.

I would also like to thank my aunt, Maria, who has always supported me and shared her excitement with me throughout this journey. Lastly, my deepest thanks to my grandfather, Georgios, whose generous support made it possible for me to pursue my Master's studies abroad.

To everyone who has been a part of this journey, thank you for your contribution.

# Content Table

1. Introduction .....	1
1.1 Objectives of the research .....	1
2. Literature Overview .....	3
2.1 Soil .....	3
2.1.1 Soil quality .....	3
2.1.2 Soil organic matter (SOM) .....	3
2.1.3 Soil organic matter fractionation .....	4
2.2 Soil spectroscopy.....	5
2.2.1 Fourier Transform Infrared Spectroscopy (FTIR) .....	7
2.2.2 FTIR spectroscopy and soil analysis .....	8
3. Materials and Methods .....	19
3.1 Research preparation .....	19
3.1.1 Soil samples.....	19
3.1.2 Reference physicochemical analysis .....	22
3.1.3 FTIR-ATR analysis and IR spectra acquisition .....	22
3.1.4. Statistical analysis .....	24
4. Results .....	25
4.1 Physicochemical characteristics .....	25
4.2 FTIR-ATR spectra .....	27
4.2.1 Assignment of molecular vibrations in soil spectra.....	27
4.2.2 Comparison of the characteristic bands between the soil types .....	29
4.2.3 Correlation of spectra with physicochemical parameters.....	30
5. Discussion .....	31
6. Conclusion.....	33
7. References .....	34
8. Appendices .....	39
8.1 Average FTIR-ATR spectra obtained by Shimadzu IRTracer 100 Spectrometer. ....	39
8.2 Linear Regression of FTIR spectral peaks and Organic Matter Content (OM%). ....	40
8.3 Linear Regression of FTIR spectral peaks and pH.....	43
8.4 Linear Regression of FTIR spectral peaks and Total Nitrogen Content (TN%). ....	46
8.5 Linear Regression of FTIR spectral peaks and Phosphorus Content (P).....	49
8.6 Linear Regression of FTIR spectral peaks and Potassium Content (K). ....	52
8.7 Linear Regression of FTIR spectral peaks and Clay Content (%). ....	55
Biography .....	58

# Summary

Of the Master thesis of student **Sofia Kapeni**, entitled

## **FINGERPRINTING OF SOIL ORGANIC MATTER COMPOSITION BY FTIR-ATR SPECTROSCOPY**

Soil plays a critical role in food production, carbon sequestration, and climate regulation. Ensuring soil security aligns with several United Nations Sustainable Development Goals (SDGs) and is essential for global sustainability. Soil organic matter (SOM) is an important indicator of soil quality and plays a multifaceted role in soil functionality. However, the heterogeneous nature of SOM makes it highly vulnerable to climate change, that can affect the composition and stability of SOM. Therefore, advancing soil assessment techniques is crucial for protecting soil resources. Infrared spectroscopy (IR), as a non-destructive method, is of great importance for detecting changes in soil dynamic properties such as SOM. Fourier transform infrared-attenuated total reflectance (FTIR-ATR) spectroscopy is a powerful tool for SOM characterization, providing insights into SOM functional groups and their degree of humification. The aim of this study is to evaluate the applicability of FTIR-ATR spectroscopy in characterizing SOM in different soil types in Croatia, including a comparative assessment of two FTIR-ATR spectrometers to evaluate their performance. The soil types examined were Luvisol, Regosol acric, Gleysol vertic, Dystric Stagnosol and Chernozem, which differ in various soil indicators including organic matter content (OM), pH, total nitrogen (TN), plant available phosphorus ( $P_{AL}$ ) and potassium ( $K_{AL}$ ), and clay content. According to our findings, FTIR-ATR spectroscopy provided insights into the hydrophilic fraction of SOM. However strong absorbance bands attributed to minerals and other inorganic constituents of soils masked distinct SOM constituents, highlighting the need for advanced chemometric modelling techniques for fingerprinting SOM composition using FTIR-ATR spectroscopy.

**Keywords:** Croatia, soil quality, soil degradation, FTIR spectroscopy, SOM



# Sažetak

Diplomskog rada studentice **Sofia Kapeni**, naslova

## KARAKTERIZACIJA ORGANSKE TVARI TLA UPOTREBOM FTIR-ATR SPEKTROSKOPIJE

Tlo igra ključnu ulogu u proizvodnji hrane, sekvestraciji ugljika i regulaciji klime. Osiguravanje sigurnosti tla kao resursa usklađeno je s nekoliko ciljeva održivog razvoja Ujedinjenih naroda i ključno je za globalnu održivost. Organska tvar tla (*Eng. Soil Organic Matter, SOM*) važan je pokazatelj kvalitete tla i igra višestruku ulogu u funkcionalnosti tla. Međutim, heterogena priroda SOM-a čini ga vrlo osjetljivim na klimatske promjene, koje mogu utjecati na sastav i stabilnost SOM-a. Stoga su napredne tehnike procjene kvalitete tla ključne za zaštitu tla kao resursa. Infracrvena spektroskopija (IR), kao nedestruktivna metoda, od velike je važnosti za otkrivanje promjena u dinamičkim svojstvima tla kao što je SOM. Infracrvena spektroskopija s Fourierovom transformacijom i prigušenom totalnom refleksijom (FTIR-ATR) moćan je alat za karakterizaciju SOM-a, pružajući uvid u funkcionalne skupine SOM-a i njihov stupanj humifikacije. Cilj ove studije je utvrditi primjenjivost FTIR-ATR spektroskopije u karakterizaciji SOM-a u različitim tipovima tala u Hrvatskoj, uključujući usporednu analizu dva FTIR-ATR spektrometra za procjenu njihove učinkovitosti. Ispitivani tipovi tla bili su Luvisol (crvenica/terra rossa), Regosol acric (regosol na eolskom pijesku), Gleysol vertic (glejno vertično), Dystric Stagnosol (pseudoglej) i Chernozem (černozem/crnica), koji imaju različita svojstva (deskriptore) tla uključujući sadržaj organske tvari (SOM), pH, ukupni dušik (TN), biljni pristupačni fosfor ( $P_{AL}$ ) i kalija ( $K_{AL}$ ), te sadržaja gline. Prema našim rezultatima, FTIR-ATR spektroskopija omogućila je uvid u hidrofilnu frakciju SOM-a. Međutim, jake vrpce apsorpcije koje se pripisuju mineralima i drugim anorganskim spojevima u tlu maskirale su različite komponente SOM-a, naglašavajući potrebu za naprednim tehnikama kemometrijskog modeliranja za karakterizaciju sastava SOM-a pomoću FTIR-ATR spektroskopije.

**Ključne riječi:** Hrvatska, kvaliteta tla, degradacija tla, FTIR spektroskopija, SOM

# 1. Introduction

The development of alternative soil assessment techniques is becoming increasingly important for achieving global sustainability due to the adverse effects of the climate crisis on the environment. Soil degradation poses a severe threat to future generations (Maynard and Johnson 2018) and sustaining soil quality has been emphasized in several Sustainable Development Goals (SDGs), including SDG 2 (Zero Hunger), SDG 3 (Good Health and Well-being), SDG 12 (Responsible Consumption and Production), SDG 13 (Climate Action), SDG 15 (Life on Land), and SDG 17 (Partnerships for the Goals) (United Nations 2015). Monitoring soil properties is fundamental for maintaining soil health amidst agroecosystem disturbances (Maynard and Johnson 2018; Lehman et al. 2015; Metzger et al. 2020; Jensen et al. 2020; and Ghebleh-Goydaragh et al. 2021a).

Soil organic matter (SOM) is a critical indicator of soil quality and fertility (Haynes 2005; Xing et al. 2021; Ghebleh-Goydaragh et al. 2021a). SOM is a dynamic soil attribute that is highly sensitive to climate change, since it interacts with climatic and topographical features, as well as land management practices (Pärnpuu et al. 2022). However, assessing soil organic matter has several challenges. Traditional laboratory analyses of SOM require extensive sample preparations, which are often costly and extremely time-consuming (Xing et al. 2021). These methods can alter the inherent properties of the soil and often do not provide comprehensive data on the interactions between the organo-mineral complexes within the SOM continuum (Volkov et al. 2021). Therefore, there is a need for more efficient, non-destructive methods to assess SOM.

This research is based on the hypothesis that Fourier transform infrared spectroscopy (FTIR) can be used to assess soil quality (Volkov et al. 2021; Nuzzo et al. 2020). In addition, it is hypothesized that FTIR-ATR spectroscopy can effectively characterize SOM in different soil types and that the spectral features will show significant correlations with soil physicochemical properties obtained by traditional laboratory analysis.

This study aims to investigate the applicability of Fourier transform infrared-attenuated total reflectance (FTIR-ATR) spectroscopy in fingerprinting soil organic matter of distinct soil types in Croatia. The primary focus of this thesis is to evaluate the effectiveness of FTIR-ATR spectroscopy in characterizing SOM in different soil types. The comparative evaluation of FTIR-ATR spectrometers aims to further enhance the reliability and applicability of this analytical approach in soil assessment, thereby contributing valuable insights into the non-destructive evaluation of soil organic matter.

## 1.1 Objectives of the research

1. To conduct a comprehensive literature review to establish the state of the art in soil spectroscopy and soil organic matter characterization, providing a foundation for the current study.

2. To determine the effectiveness of FTIR-ATR spectroscopy in characterizing soil organic matter across various soil types in Croatia.
3. To compare the spectroscopic fingerprints between the soil types as well as between the two different FTIR-ATR spectrometers.
4. To correlate the spectroscopic data with physicochemical properties of soils, which are organic matter (OM %), pH, total nitrogen (TN %), plant available phosphorus (P), plant available potassium (K) and particle size distribution.

## **2. Literature Overview**

### **2.1 Soil**

Soil is a polyphasic, dynamic living body, which constitutes a fundamental component of the natural environment (Helfenstein et al. 2021). Soil, as a non-renewable resource (Williams et al. 2020), is recognized as one of the most important components of the environment (Jensen et al. 2020), as it plays a significant role in the functionality of ecosystems, by regulating water storage, nutrient cycling, waste decomposition, carbon sequestration, and climate regulation (Helfenstein et al. 2021; Williams et al. 2020; Santos et al. 2020). In the pressing urgency to mitigate the detrimental impacts of climate change, the study of soil attributes is becoming imperative for preserving soil resources (Krivoshein et al. 2022; Williams et al. 2020).

#### **2.1.1 Soil quality**

Soil quality and health are often used interchangeably and they refer to the ability of the soil to facilitate ecosystem purposes (Maynard and Johnson 2018). Soil health is distinguished by inherent and dynamic features, which reflect the history of a specific region and serve as an information repository of the soil, known as pedomemory (Williams et al. 2020). Inherent soil properties, including structure, texture, and porosity, are shaped by natural soil-forming factors such as parent material, topography, climate, biota, and time. These static properties form in response to the anthropogenic activities such as land use, crop cultivation, and fertilization (Ma et al. 2017). Conversely, anthropogenic activities predominantly influence the dynamic properties of the soils, including soil organic matter (SOM) and microbial populations (Maynard and Johnson 2018; Lehman et al. 2015; Cooperband 2002; Wang et al. 2023).

#### **2.1.2 Soil organic matter (SOM)**

Soil organic matter (SOM), is a crucial indicator of soil quality (Pärnpuu et al. 2022; Cooperband 2002; Xing et al. 2016). SOM, despite constituting a relatively small proportion of soil, which typically ranges from 1% to 6%, has a profound effect on the soil physicochemical and biological properties (Pärnpuu et al. 2022; Cooperband 2002; Xing et al. 2021; Baumann et al. 2016), such as in carbon sequestration. Carbon sequestration reduces soil susceptibility to degradation, while enhancing soil fertility (Cooperband 2002), thus mitigating global warming (Wang et al. 2023; Rial et al. 2016). In this regard, SOM assessment is important for securing global sustainability (Krivoshein et al. 2022; Teong et al. 2016; Allo et al. 2020).

Soil organic matter (SOM) constitutes the principal reservoir of carbon within ecosystems (Volkov et al. 2021; Jiménez-González et al. 2019; Rial et al. 2016), comprising approximately 50% of the soil organic carbon (SOC) (Bot and Benites 2005). SOM primarily derives from plant and animal residues that undergo varying degrees of degradation (Bot and Benites 2005). Upon its formation, SOM exists in an equilibrium state, that can be found adsorbed, precipitated, or in an insoluble form within the soil solution (Haynes 2005).

SOM plays a vital role in the soil's food web, due to the microbial decomposition known as humification (Haynes 2005; Bot and Benites 2005; Xing et al. 2021). Humification refers to the physical breakdown of the organic material followed by the biochemical transformation of the

degraded products by soil microorganisms (Bot and Benites 2005). The rate and speed of humification depend on the structural complexity of organic materials, including carbohydrates, hemicelluloses, celluloses, and lignins, highlighting the heterogeneity of organic matter composition in soil ecosystems (Cooperband 2002). During the process of humification, the stable SOC fraction facilitates the formation of carbon aggregates in the soil (Bot and Benites 2005; Lal et al. 2015) offering biological stability to SOM (Dhillon et al. 2017). SOM bonding and binding agents play a crucial role in the stabilization of SOM through organo-mineral complexation (Cooperband 2002; Jiménez-González et al. 2019). Bonding refers to the cohesion of mineral particles with organic decomposed products, such as polysaccharides, while binding, refers to the connection of soil aggregates with plant roots and fungal hyphae (Cooperband 2002). One of the factors that affect the soil's ability to adsorb organic matter is the presence of metal oxides, such as aluminum (Al) and iron (Fe) hydrous oxides. Specifically, the negatively charged humic molecules create strong bonds with the surfaces of Al and Fe, either with electrostatic bonding or Van der Waals interactions, resulting in the formation of macroaggregates (Haynes, 2005; Nath et al. 2022). These processes influence the physical, chemical, and biological properties of the soil, and subsequently soil quality (Jensen et al. 2020; Volkov et al. 2021).

### **2.1.3 Soil organic matter fractionation**

Soil organic matter (SOM) can be classified into stable and labile fractions (Figure 1). The lability of soil organic matter influences how effectively soil microorganisms can assimilate the humified compounds (Pärnpuu et al. 2022). Based on the susceptibility to microbial breakdown, SOM can be also categorized into the active fraction, characterized by a short degradation time of 1 – 2 years, the intermediate fraction whose degradation time is about 2 – 5 years, and the stable fraction which its degradation time exceeds the 10 years. Notably, active fraction is directly associated with the nutrient supply within the soil. Although the stable fraction provides fewer nutrients compared to the active fraction, it plays a crucial role in enhancing soil fertility by inhibiting soil compaction and crusting. The stable fraction of organic matter constitutes 70 – 96% of soil organic carbon (SOC) and is predominantly composed of humus (Cooperband 2002). Humus is the final product of the humification process that is resistant to further degradation (Cooperband 2002). This resistance allows humus to significantly impact soil properties, particularly the cation exchange capacity (CEC), which in turn affects the availability and exchange of macro- and micronutrients in the soil (Metzger et al. 2020; Cooperband 2002). Humus is composed of fulvic acids, humic acids, and humin (Bot and Benites 2005; Jiménez-González et al. 2019). Humin, in particular, is rich in aliphatic compounds such as long-chain fatty acids, alcohols, and alkanes, as well as aliphatic biopolymers like cutin, suberin, cutan, and suberan. These aliphatic characteristics of humin significantly influence soil properties (Nuzzo et al. 2020).

Conversely, the labile fraction of SOC refers to the decomposable matter that is readily available for plant uptake (Pärnpuu et al. 2022; Haynes 2005). The labile SOC constitutes 2 – 30% of SOC and consists of a wide range of organic compounds, including aliphatic organic acids, phenolic compounds, and free amino acids, as well as more complex humic molecules such as hydrophobic acids (Haynes 2005). According to Haynes (2005), the labile SOC encompasses

portions of water-extractable organic carbon (WEOC) and permanganate oxidizable organic carbon (POXC) represent the most labile fractions, highlighting the multifaceted functions of organic matter in soil processes. Studies by Pärnpuu et al. (2022) and Jensen et al. (2020), have demonstrated that WEOC provides valuable information regarding the degradation index of soil organic matter (SOM), emphasizing the crucial role of labile carbon fractions in assessing the qualitative and quantitative characteristics of SOM. As a result, understanding the SOM fractions is of great significance for evaluating soil dynamics and ecosystem functions (Cooperband 2002).

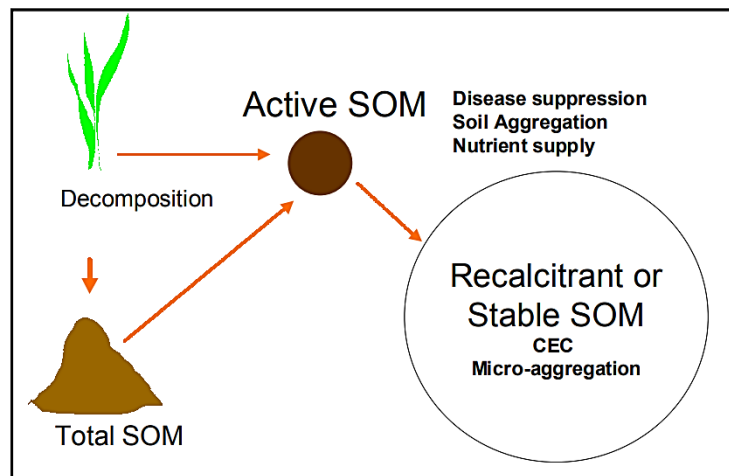


**Figure 1.** The different fractions of soil organic matter (active and stable)  
Source: Cooperband et al. (2002)

Soil organic matter (SOM) is mainly detected in the topsoil (Haynes 2005) since the majority of organic material is concentrated in the top 15 centimeters (6 inches) of soil (Cooperband 2002). Anthropogenic activities have a significant influence on soil organic matter, and affect the susceptibility of soil to degradation. This degradation initiates a series of events that alter the microenvironment of soil organisms (Bot and Benites 2005). Consequently, the ecosystem faces the risk of losing its resilience and adaptability to the continuously shifting environmental conditions due to climate change (Williams et al. 2020).

## 2.2 Soil spectroscopy

The analysis of SOM significantly contributes to the assessment of soil quality, due to the dynamic equilibrium in its chemical composition, as it is represented as an organo-mineral continuum of high- and low-molecular organic and inorganic substances in a finely dispersed state (Krivoshein et al. 2022). However, the evaluation of soil properties and their impact on soil quality has been hindered by the limitations of traditional methods (Bot and Benites 2005). Conventional laboratory analysis includes standard procedures and preparatory steps that typically rely on physical, chemical, biological, and mineralogical analytical techniques, such as digestion, and titration, that may alter soil composition (Helfenstein et al. 2021; Krivoshein et al. 2022; Maynard and Johnson 2018; Xing et al. 2016). Therefore, there is a growing need for incorporating rapid, and easily repeatable methods for the qualitative and quantitative characterization of soil quality (Maynard and Johnson 2018). In this context, Fourier Transform

Infrared Spectroscopy (FTIR) holds significant importance in detecting soil's dynamic properties, and therefore in the overall determination of soil health (Maynard and Johnson 2018).

Over the past three decades, spectroscopy has emerged as a cost- and time-effective tool for assessing soil quality, including the determination of SOM, SOC, pH, and soil texture (Allo et al. 2020; Nath et al. 2022; Rial et al. 2016). Due to minimal labor, sample preparation, and the small quantity of soil samples required, soil spectroscopy enables more precise analysis compared to traditional techniques (Xing et al. 2021; Breure et al. 2021). Moreover, spectroscopy has proven advantageous in studying interactions between organic and mineral components within soil, whereas conventional laboratory methods are less effective in providing insights into these interactions (Volkov et al., 2021).

The versatility of soil spectroscopy is reflected in its ability to utilize different wavelengths: visible (VIS) in 400 – 700 nm frequency, near-infrared (NIR) in 701 – 1100 nm frequency, and mid-infrared (MIR) in 2500 – 25000 nm frequency of the electromagnetic spectrum (Helfenstein et al. 2021; Jensen et al. 2020), as illustrated in Figure 2. Infrared spectroscopy (IR), has been primarily used in assessing SOM, humic substances (aliphatics, aromatics, and amides), minerals (clay, silt, sand, carbonates), potassium (K), phosphorus (P), lattice water, pH, and CEC (Metzger et al. 2020; Wang et al. 2023; Helfenstein et al. 2021; Jensen et al. 2020; Nath et al. 2022; Xu et al. 2020; Rial et al. 2016; Santos et al. 2020). The abovementioned soil components are recognized as spectrally active compounds, that can develop fundamental overtone and combination absorptions in the infrared region, unveiling the impacts of the interactions between soil forming properties and land use (Metzger et al. 2020).

The research of Šestak et al. (2019) investigates the applicability of hyperspectral visible and near-infrared reflectance (VNIR) sensing for predicting organic and inorganic soil constituents. VNIR spectroscopy successfully estimated soil chemical properties such as total carbon (TC), pH, and total nitrogen content (TN) non-destructively in arable soils, confirming its effectiveness in precision farming. In an additional investigation by Šestak et al. (2018), VNIR spectral data were used to distinguish nitrogen fertilization treatments and predict soil organic matter (SOM) content and pH in a field-scale evaluation, underscoring VNIR's effectiveness in soil assessment. Finally, a recent study by Šestak et al. (2022) evaluates VNIR spectroscopy's capability to assess post-fire soil chemical properties, including pH, organic carbon (SOC), and soil nutrients, and to differentiate fire severity based on soil spectra, highlighting the use of soil reflectance to predict soil properties.

However, many studies have demonstrated the superiority of MIR over NIR range of spectrum in distinguishing molecular vibrations, particularly of the organic and inorganic constituents of SOM (Helfenstein 2021; Ghebleh-Goydaragh et al. 2021a). One of the main advantages of MIR spectroscopy is its capability to effectively characterize various soil properties using a single spectrum (Nath et al. 2022). This is because the MIR spectrum (wavenumber range 4000 – 400  $\text{cm}^{-1}$ ) provides a greater number of molecular absorptions with clearer peak resolution compared to the NIR spectrum. The spectroscopic analysis is based on the excitation, stretching, and bending of carbon (C) atoms during the absorption of carbon molecules, resulting from

their molecular vibrations in this range. As a result, MIR spectrum can offer a comprehensive overview of soil biochemical data (University of California 2023).

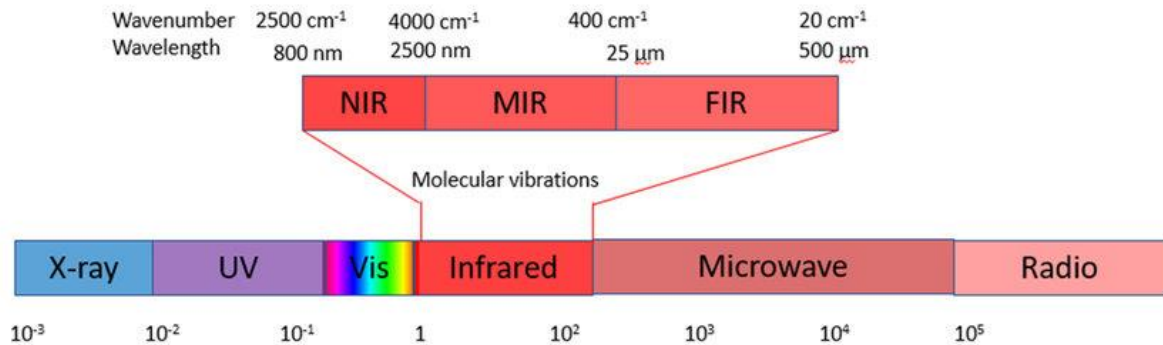


**Figure 2.** Electromagnetic spectrum in wavelengths (nm) and wavenumbers ( $\text{cm}^{-1}$ )  
Source: Fox (2020)

MIR analysis can be conducted using various methods, including Transmission, Diffuse Reflectance Infrared Fourier Transform (DRIFT), and Fourier Transform Infrared coupled with Attenuated Total Reflectance (FTIR-ATR) spectroscopy (Margenot et al. 2017), as shown in Figure 3. The attenuated total reflectance function is based on the principle of total internal light reflection following the selective absorption of the sample components within the IR range, resulting in a linear range of band intensities (Xing et al. 2021). This technique serves as a valuable means for the characterization of SOM, as it enables the assessment of both organic and inorganic functional groups (Parolo et al. 2017). Xing et al. highlighted that ATR spectroscopy offers significant advantages in dealing with challenges observed in other IR methods, such as in infrared transmission spectroscopy. However, as SOM constitutes a small proportion of soil (less than 5%), its characterization remains challenging (Pärnpuu et al. 2022).

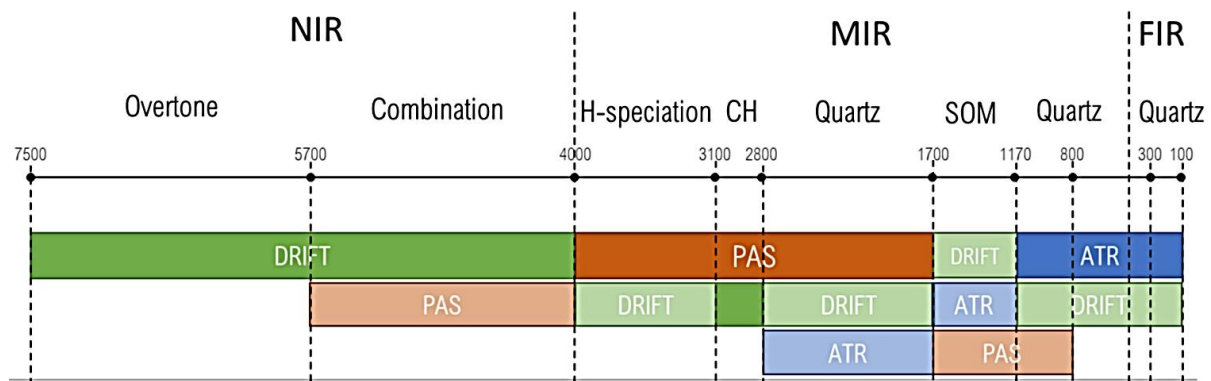


**Figure 3.** Applicability of FTIR methods: DRIFT, ATR-FTIR, and FTIR-PAS for soil analysis.  
Source: Volkov et al. (2021)

### 2.2.1 Fourier Transform Infrared Spectroscopy (FTIR)

Fourier Transform Infrared Spectroscopy (FTIR) serves as a powerful tool in distinguishing SOM constituents (Teong et al. 2016; Maynard and Johnson 2018), including carbohydrates, lignins, cellulose, fats and lipids (Artz et al. 2008). Its effectiveness lies in the capability to detect functional groups that change dipole moments and can absorb infrared radiation. These



functional groups contain oxygen (O), nitrogen (N), and sulfur (S) molecules, exhibiting high chemical reactivity, such as cation-exchange capacity and metal sorption (Maynard and Johnson 2018). FTIR enables the direct detection of SOM compounds, without the need of chemical extraction, thereby avoiding interference from secondary chemical reactions and artefacts associated with extraction processes (Maynard and Johnson 2018; Pärnpuu et al. 2022; Nath et al. 2022). Particularly, the incorporation of attenuated total reflectance (ATR) accessories, such as diamond ATR (Figure 4), has significantly enhanced the application of FTIR spectroscopy in the analysis of soils (Artz et al. 2008).

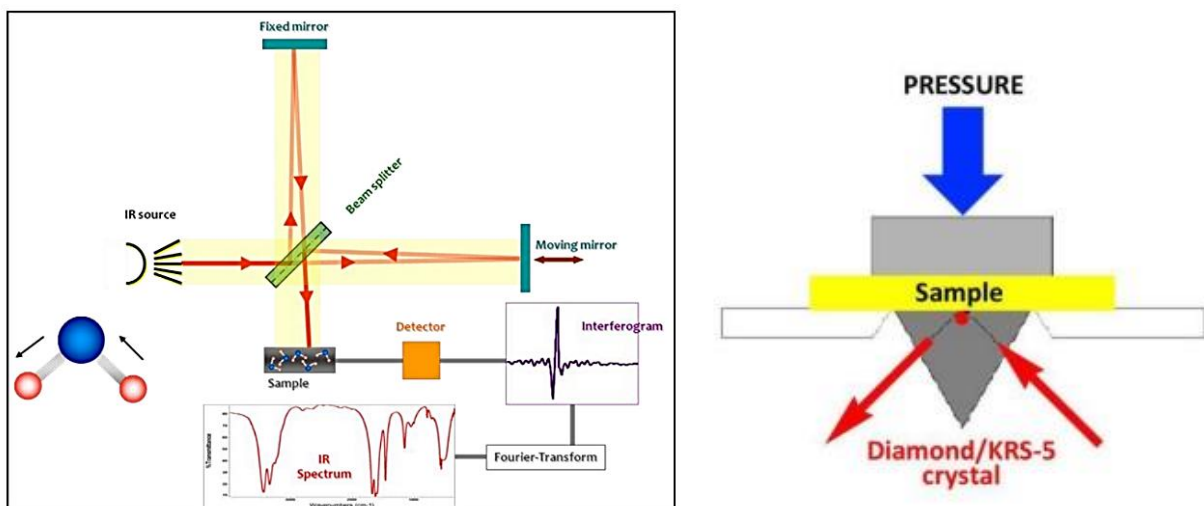


**Figure 4.** Schematics of an FTIR spectrometer and of a diamond ATR. Source: Robertson et al. (2013)

### 2.2.2 FTIR spectroscopy and soil analysis

The study of Volkov et al. (2021) emphasizes the importance of FTIR-ATR in achieving enhanced sensitivity in the determination of SOM and SOC. Additionally, Bot and Benites (2005) underline the successful application of FTIR combined with chemometric modeling for soil type identification. Their findings indicate that there is a significant relationship between the labile SOC fraction, particulate water-extractable organic carbon (p-WEOC), and degradation index (DDI) of SOM, that influence soil's capacity to sequester carbon. The degradation and humification index of SOM are also investigated in the study of Obeng et al. (2023). The study conducted by Teong et al. (2016) suggests that FTIR can effectively distinguish peat soil and clay soil, by identifying and associating FTIR spectral peaks with clay minerals and distinct SOM functional groups, such as aromatics, carbonyls, alkanes, and alcohols. Margenot et al. (2017) suggest that the presence of absorbance bands that correspond to aliphatic and aromatic compounds within the soil spectrum, indicates the level of humification, and thus SOM characterization.

In addition, FTIR has been successfully used to evaluate the hydrophobicity, along with the degradation of SOM, due to its content in aliphatic substances (Pärnpuu et al. 2022; University of California 2023). SOM is characterized by hydrophobic functional groups which present

distinct absorption bands in the IR spectrum (Margenot et al. 2017; Parolo et al. 2017). Parolo et al. (2017) emphasize the critical role of hydrophilic and hydrophobic functional groups in shaping the spatial arrangement and structure of carbon chains within SOM. More specifically, the hydrophilic and hydrophobic constituents of SOM can develop hydrogen bonds, and cation exchanges with adsorbates, such as clay minerals, thus influencing SOM's chemical properties like pH. These findings agree with the research of Helfenstein et al. (2021) that proves the efficacy of FTIR spectroscopy in predicting soil pH, CEC, and exchangeable ions, such as calcium ( $\text{Ca}^{2+}$ ), and magnesium ( $\text{Mg}^{2+}$ ).

Several studies have identified characteristic molecular vibrations corresponding to soil organic and inorganic constituents within the FTIR spectra (Table 1). MIR range includes molecular vibrations of the O–H region spanning from 3775 to 3100  $\text{cm}^{-1}$ , the C–O region from 3100 to 2560  $\text{cm}^{-1}$ , the SOM region from 2000 to 1340  $\text{cm}^{-1}$ , the matrix region II from 1340 to 840  $\text{cm}^{-1}$ , and the matrix region I below 840  $\text{cm}^{-1}$ .

The review study of Tinti et al. (2015) confirmed that the Si–OH and Fe–O stretching vibrations at 3698  $\text{cm}^{-1}$  and 3622  $\text{cm}^{-1}$  are indicative of phyllosilicate vibrations within clay minerals like kaolinite and gibbsite. Similar findings of silicates are also observed in several other studies, such as O–H stretching between 3696  $\text{cm}^{-1}$  and 3618  $\text{cm}^{-1}$  (Pärnpuu et al. 2022; Parolo et al. 2017; Volkov et al. 2021; Xing et al. 2021; Fakhry et al. 2016), as well as (Al)/(Mg)Si–OH stretching in the range 3620 – 3613  $\text{cm}^{-1}$ , indicative of kaolinite, montmorillonite and smectite (Krivoshein et al. 2022; Volkov et al. 2021; Xing et al. 2021; Fakhry et al. 2016; Xu et al. 2020; Peltre et al. 2014). Moreover, Fe–O stretching of aluminosilicates like kaolinite and gibbsite are observed at 3622  $\text{cm}^{-1}$  (Tinti et al. 2015).

Various studies also highlight the overlapping of clay minerals and organic compounds in the region 3600 – 3351  $\text{cm}^{-1}$  which is characterized by O–H and N–H stretching vibrations, attributed to both clay minerals such as gibbsite and carboxyl and hydroxyl groups of soil organic matter, including amines, amides, alcohols, phenols, and carboxylic acids (Tinti et al. 2015; Pärnpuu et al. 2022; Parolo et al. 2017; Krivoshein et al. 2022; Teong et al. 2016; Nuzzo et al. 2020; Volkov et al. 2021; Ghebleh-Goydaragh et al. 2021b; Fakhry et al. 2016; Xu et al. 2020; Peltre et al. 2014), emphasizing the complex interaction between clay minerals and organic compounds within soil. Additionally, Artz et al. 2007 reported the presence of cellulose at 3340  $\text{cm}^{-1}$ . Organic compounds are also present in the region 3270 – 3042  $\text{cm}^{-1}$ , including aromatic phenols and alcohols (Teong et al. 2016; Artz et al. 2007).

Furthermore, many studies have reported prevalent C–H stretching vibrations in the region 3000 – 2850  $\text{cm}^{-1}$ , indicative of aliphatic compounds, such as fats, waxes, and lipids. These compounds constitute the hydrophobic fraction of SOM and demonstrate the presence of organic matter in the soil (Tinti et al. 2015; Pärnpuu et al. 2022; Parolo et al. 2017; Krivoshein et al. 2022; Teong et al. 2016; Artz et al. 2007; Helfenstein et al. 2021; Nuzzo et al. 2020; Maynard and Johnson 2018; Volkov et al. 2021; Ghebleh-Goydaragh et al. 2021b; Fakhry et al. 2016; Baumann et al. 2016; Dhillon et al. 2017; Peltre et al. 2014). Obeng et al. (2023) reported the presence of humic acids, fulvic acids and humin in the range 2856 – 2849  $\text{cm}^{-1}$ . Besides, C–H stretching vibrations around 2850  $\text{cm}^{-1}$  are attributed to both aliphatics and polysaccharides (Teong et al. 2016; Artz et al. 2007; Nuzzo et al. 2020).

Similarly, the presence of carbonates within soil spectra has been confirmed by several studies. The C–H vibrations the region  $1800 - 1783 \text{ cm}^{-1}$  attributed to the carbonate minerals like aragonite, calcite and dolomite (Tinti et al. 2015; Volkov et al. 2021) Furthermore, Krivoshein et al. (2022) indicated the presence of clay minerals, quartz, and carboxylic acids at  $1880 - 1866$  and  $1783 \text{ cm}^{-1}$ .

The hydrophilic fraction of SOM is extensively observed in soil spectra within the MIR range. Particularly the range of  $1730 - 1700 \text{ cm}^{-1}$  is characterized by the prevalence of C=O stretching vibrations indicative of carboxylic acids (Tinti et al. 2015; Nuzzo et al. 2020; Volkov et al. 2021; Ghebleh-Goydaragh et al. 2021b; Peltre et al. 2014). The studies of Volkov et al. (2021) and Artz et al. (2007) reported the presence of aromatic esters at  $1730 - 1720 \text{ cm}^{-1}$  and carboxylic acids at  $1720 - 1700 \text{ cm}^{-1}$ . A broader range of bands related to SOM constituents, like C=C and C=O stretching vibrations and N–H bending vibrations, are observed in the range  $1660 - 1444 \text{ cm}^{-1}$ , indicative of aromatics, aliphatics, phenolics, amides I and II, phenols, ketones and quinones, lignin (Tinti et al. 2015; Parolo et al. 2017; Krivoshein et al. 2022; Teong et al. 2016; Artz et al. 2007; Nuzzo et al. 2020; Maynard and Johnson 2018; Volkov et al. 2021; Xing et al. 2021; Obeng et al. 2023; Ghebleh-Goydaragh et al. 2021b; Jiménez-González et al. 2019; Fakhry et al. 2016; Baumann et al. 2016; Dhillon et al. 2017; Xu et al. 2020; Peltre et al. 2014).

The range of  $1479 - 1408 \text{ cm}^{-1}$  is dominated by C–H and N–H stretching vibrations, attributed to amide II and aliphatics, as well as O–H stretching vibrations of carbonates according Tinti et al. (2015). Organo-mineral complexes are observed at  $1465 - 1460 \text{ cm}^{-1}$  due to SiO–H vibrations of silicates along with C–O–H and C–H vibrations of aliphatics (Krivoshein et al. 2022; Helfenstein et al. 2021; Maynard and Johnson 2018; Volkov et al. 2021; Jiménez-González et al. 2019; Peltre et al. 2014). Moreover, various studies have reported both inorganic and organic compounds arising within the range  $1453 - 1410 \text{ cm}^{-1}$ , due to C–O stretching. These vibrations are associated with carbonate minerals such as calcite and dolomite, and organic compounds such as aromatics, aliphatics, phenolics and humic acids (Pärnpuu et al. 2022; Parolo et al. 2017; Artz et al. 2007; Xing et al. 2021; Ghebleh-Goydaragh et al. 2021b; Jiménez-González et al. 2019; Fakhry et al. 2016; Baumann et al. 2016; Dhillon et al. 2017; Xu et al. 2020; Peltre et al. 2014). Artz et al. (2007) observed C–O, C=C, and O–H stretching vibrations indicative of humic acids, aromatics, and aliphatics at  $1426 \text{ cm}^{-1}$ . Volkov et al. (2021) observed (Mg)–OH and C–O vibrations at  $1420 \text{ cm}^{-1}$ , associated with clay minerals and carboxylic acids respectively. Pärnpuu et al. (2022) reported C–H and O–H deformations and C–O, C=O stretching vibrations of aliphatics and carbonates at  $1417 \text{ cm}^{-1}$ . The presence of benzoic acid is also reported at  $1415 \text{ cm}^{-1}$  by Tinti et al. (2015).

In the range from  $1410$  to  $1400 \text{ cm}^{-1}$ , Krivoshein et al. 2022 as well as Artz et al. (2007) attributed the (Mg)–OH and C–O stretching vibrations to quartz and carboxylic acids respectively. Maynard and Johnson (2018) reported the presence of carbonates, including calcite and dolomite, in the spectral region from  $1396$  to  $1383 \text{ cm}^{-1}$  due to the C–O stretching vibrations. In addition, C–H deformations of phenolics, aliphatics and carboxyls at  $1380 \text{ cm}^{-1}$  are reported by Tinti et al. (2015) and at  $1371 \text{ cm}^{-1}$  by Artz et al. (2007). Interestingly, at  $1370 \text{ cm}^{-1}$ , Dhillon et al. (2017) attributed the C–O vibrations to lignin-derived phenols. In the range of  $1342 - 1307 \text{ cm}^{-1}$  the C–N stretching vibrations observed are indicative of aromatic amines,

such as sulfonamides as stated by Tinti et al. (2015). In the range of 1320 – 1310  $\text{cm}^{-1}$ , C–O stretching vibrations are observed, attributed to amide III and carboxylic acids (Pärnpuu et al. 2022), while at 1320  $\text{cm}^{-1}$ , O–H deformation of carbonates are also observed by Volkov et al. (2021).

In the range from 1293 to 1256  $\text{cm}^{-1}$ , and at 1230  $\text{cm}^{-1}$  C–O stretching vibrations are indicative of bentonite and benzoic acid (Tinti et al. 2015). Moreover, C–O stretching vibrations at 1285 – 1280  $\text{cm}^{-1}$  indicative of aromatics and carboxylic acids are reported by Krivoshein et al. (2022). Further C–O stretching vibrations of phenolics, and lignin were also reported at 1265  $\text{cm}^{-1}$  by Artz et al. (2007) and at 1240  $\text{cm}^{-1}$  by Maynard and Johnson (2018). Besides, Nuzzo et al. (2020) reported C–O stretching vibrations in the range of 1235 – 1225  $\text{cm}^{-1}$  indicative of carboxylic acids. Apart from carboxylic acids, Tinti et al. (2015) reported the presence of several other organic and inorganic compounds at 1230  $\text{cm}^{-1}$ , including bentonite, phenols, and amides. Lignin structures are reported at 1130  $\text{cm}^{-1}$  according to the findings of Jiménez-González et al. (2019).

In the range 1170 – 1153  $\text{cm}^{-1}$ , Si–O vibrations are attributed to quartz, and C–O vibrations are attributed to aliphatics (Krivoshein et al. 2022; Volkov et al. 2021) and polysaccharides (Dhillon et al. 2017; Peltre et al. 2014). It is noteworthy that Dhillon et al. (2017) also referred to the presence of cellulose within the range 1160 – 1030  $\text{cm}^{-1}$  due to the C–OH vibrations. Silicates and other non-aromatic compounds, such as polysaccharides, have been extensively reported within the range 1095 – 945  $\text{cm}^{-1}$ , due to the Si–O, and C–OH, C–O, C–N vibrations. Interestingly, these silicates are associated with the clay minerals of kaolinite, illite and smectite (Tinti et al. 2015; Krivoshein et al. 2022; Volkov et al. 2021; Baumann et al. 2016; Artz et al. 2007; Nuzzo et al. 2020). Moreover, Si–O, C–O and C=C stretching, as well as C–H out-of-plane bending of aluminosilicates, and aromatics is reported at 975  $\text{cm}^{-1}$  by Tinti et al. (2015) and Volkov et al. (2021).

Additionally, (Al)–OH deformations of aluminosilicates are reported at 990  $\text{cm}^{-1}$  (Xing et al. 2021) and within the range 926 – 910  $\text{cm}^{-1}$  (Tinti et al. 2015; Nuzzo et al. 2020; Xing et al. 2021; Fakhry et al. 2016; Xu et al. 2020; Peltre et al. 2014). In the range of 945 – 887  $\text{cm}^{-1}$  the presence of C=C stretching vibrations are attributed to benzoic acid, carbohydrates, and cellulose (Tinti et al. 2015; Krivoshein et al. 2022; Volkov et al. 2021). In addition, at 910 – 900  $\text{cm}^{-1}$ , C–H out-of-plane bending vibrations are assigned to aromatics (Nuzzo et al. 2022). The SiO–H stretching vibrations at 887 – 866  $\text{cm}^{-1}$  are attributed to carbonates, quartz, and clay minerals (Tinti et al. 2015; Krivoshein et al. 2022; Volkov et al. 2021; Peltre et al. 2014). Particularly Fakhry et al. (2016) reported that the O–H vibrations at 891 – 870  $\text{cm}^{-1}$  are assigned to the carbonate mineral of calcite. Moreover, C–H bending vibrations of aromatics are observed by Krivoshein et al. (2022) at 875  $\text{cm}^{-1}$ , and by Tinti et al. (2015) at 870  $\text{cm}^{-1}$ . In the range of 820 – 752  $\text{cm}^{-1}$  O–H stretching vibrations of clay minerals, quartz, and carbonates, as well as and C–C stretching vibrations of phenols are exhibited as mentioned by Tinti et al. (2015).

The absorption bands of Si–O below 800  $\text{cm}^{-1}$  unveil the dominance of quartz and clay minerals (Tinti et al. 2015; Krivoshein et al. 2022; Artz et al. 2007; Nuzzo et al. 2020; Volkov et al. 2021;

Fakhry et al. 2016; Peltre et al. 2014). Several studies noted the presence of carbonates around 720 – 713  $\text{cm}^{-1}$  (Tinti et al. 2015; Parolo et al. 2017; Artz et al. 2007), as well as at 630 – 620  $\text{cm}^{-1}$  (Volkov et al. 2021). In addition, at 630 – 620  $\text{cm}^{-1}$  Ca–OH and C–S stretching of hydroxyapatite and sulfates are reported by Volkov et al. (2021). Vibrations of metal oxides, mainly Fe oxides, are reported by Parolo et al. (2017), Volkov et al. (2021) and Peltre et al. (2014) at 700 – 600  $\text{cm}^{-1}$ , and by Fakhry et al. (2016) at 536 – 525  $\text{cm}^{-1}$ . In addition, C–H bending vibrations indicative of aromatic compounds are detected at 750  $\text{cm}^{-1}$ , 715  $\text{cm}^{-1}$  and 675 – 670  $\text{cm}^{-1}$  (Krivoshein et al. 2021), and at 698 – 686  $\text{cm}^{-1}$  (Parolo et al. 2017). N–H vibrations of primary and secondary amines are evident in the studies of Xu et al. (2020) arising at 780  $\text{cm}^{-1}$ , and of Peltre et al. (2014) within the range 750 – 700  $\text{cm}^{-1}$ . Lastly Si–O bending vibrations below 535  $\text{cm}^{-1}$  are attributed to quartz and clay minerals such as kaolinite, illite, and smectite (Tinti et al. 2015; Krivoshein et al. 2022; Nuzzo et al. 2020; Volkov et al. 2021). The abovementioned spectral peaks along with their assigned functional groups, are summarized in the table below (Table 1).

**Table 1.** IR absorption band positions with the assignment of the underlying molecular vibrations according to the literature and references therein.

Band position (cm <sup>-1</sup> )	Functional group assignment and type of vibration	Associated soil components (literature data*)
3698	Si-OH, Fe-O stretching	clay minerals (kaolinite, gibbsite) <sup>1</sup>
3696	Si-OH stretching	clay minerals <sup>11</sup>
3697– 3689	O-H stretching	kaolinite <sup>15</sup>
3694	O-H stretching	clay minerals, quartz <sup>2</sup>
3690 – 3680	Si-OH, O-H stretching	clay minerals <sup>10</sup>
3629 – 3618	O-H stretching	clay minerals (kaolinite) <sup>3</sup>
3622	Si-OH, Fe-O stretching	clay minerals (kaolinite, gibbsite) <sup>1</sup>
3620	(Al)/(Mg)Si-OH stretching	clay minerals (kaolinite, montmorillonite) <sup>4,10,11,18,19</sup>
3620 – 3613	(Al)-OH stretching	smectite <sup>15</sup>
3617	O-H stretching	clay minerals, quartz <sup>2</sup>
3600 – 3000	O-H stretching	alcohols, phenols, water <sup>17</sup>
3600 – 2800	O-H, N-H stretching	alcohols, phenols, amides, water <sup>19</sup>
3553 – 3542	O-H stretching	phenols <sup>15</sup>
3500 – 3300	O-H, N-H stretching	alcohols, phenols, carboxylic acids, amides <sup>13</sup>
3500 – 3200	O-H, N-H stretching	alcohols, phenols, amine, amide, carboxyl and hydroxyl groups <sup>18</sup>
3490	O-H stretching	alcohols, phenols, carboxylic acids <sup>4,10</sup>
3460	O-H stretching	clay minerals (gibbsite) <sup>1</sup>
3450	O-H stretching	clay minerals, water <sup>8</sup>
3450 – 3420	O-H stretching	clay minerals <sup>15</sup>
3440 – 3320	O-H, N-H stretching	clay minerals, amines <sup>1</sup>
3430	O-H stretching	water <sup>1</sup>
3430 – 3401	O-H stretching	water, carboxyl and hydroxyl groups of SOM <sup>3</sup>
3365	O-H, N-H stretching	phenols, alcohols, carboxylic acids, amides and amines <sup>2</sup>
3360	O-H stretching	clay minerals <sup>11</sup>
3351	O-H stretching	alcohols <sup>5</sup>
3340	O-H stretching	cellulose <sup>6</sup>
3270	O-H, C=O stretching	phenols, alcohols, carboxylic acids <sup>4,10</sup>
3107 – 3042	C=C stretching	aromatics <sup>1</sup>
3000 – 2800	C-H stretching	aliphatics <sup>19</sup>
2983	C-H asymmetric stretching	aliphatics <sup>12</sup>
2960	C-H stretching	aliphatics <sup>13</sup>
2947 – 2858	C-H stretching	aliphatics (fats, wax, lipids) <sup>3</sup>
2940	C-H asymmetric stretching	aliphatics (fats, wax, lipids) <sup>4</sup>
2930 – 2910	C-H asymmetric stretching	aliphatics <sup>10</sup>
2930	C-H asymmetric stretching	aliphatics <sup>1,7</sup>
2929 – 2917	C-H symmetric stretching	humic acids, fulvic acids, humic <sup>15</sup>
2925	C-H stretching	aliphatics <sup>16</sup>
2921	C-H asymmetric stretching	aliphatics <sup>2, 12</sup>
2920	C-H asymmetric stretching	aliphatics <sup>5,6,8,17</sup>
2910	C-H asymmetric stretching	aliphatics <sup>9</sup>
2879	C-H stretching	aliphatics <sup>13</sup>
2860 – 2850	C-H symmetric stretching	aliphatics (fats, wax, lipids) <sup>10</sup>

Band position (cm <sup>-1</sup> )	Functional group assignment and type of vibration	Associated soil components (literature data*)
2860	C–H symmetric stretching	aliphatics (fats, wax, lipids) <sup>4</sup>
2858	C–H stretching	aliphatics <sup>16</sup>
2856 – 2849	C–H asymmetric stretching	humic acids, fulvic acids, humic <sup>15</sup>
2855	C–H symmetric stretching	aliphatics (fats, wax, lipids) <sup>7</sup>
2852	C–H asymmetric stretching	aliphatics <sup>2</sup>
2850	C–H symmetric stretching	aliphatics (fats, wax, lipids) <sup>5,6,8,17</sup> , polysaccharides <sup>5,6,8</sup>
2627	C–H stretching	carbonates (aragonite) <sup>1</sup>
2592	C–H stretching	carbonates (calcite) <sup>1</sup>
2520	C–H stretching	carbonates (calcite, aragonite) <sup>1, 19</sup>
2514 – 2507	C–O vibration	carbonates (calcite, dolomite) <sup>3</sup>
2500	O–H stretching	carbonates <sup>7</sup>
2200 – 2000	C–OH vibration	carbohydrates <sup>19</sup>
2000	Si–O stretching	quartz <sup>1</sup>
2000 – 1790	Si–O stretching	quartz <sup>19</sup>
1900 – 1700	C=O stretching	humic acids <sup>15</sup>
1885	C=O stretching	carboxylic acids <sup>10</sup>
1880 – 1866	Si–O, C=O stretching	quartz, clay minerals, carboxylic acids <sup>4</sup>
1865	C=O stretching	carboxylic acids <sup>10</sup>
1800	C=O stretching	carbonates (calcite) <sup>1</sup>
1790 – 1783	C=O stretching	carbonates (calcite) <sup>10</sup>
1783	Si–O, C=O stretching	clay and quartz minerals, carboxylic acids <sup>4</sup>
1730 – 1700	C=O stretching	carboxylic acids (humic acids) <sup>1,8</sup>
1730 – 1720	C=O stretching	carboxylic acids <sup>10</sup>
1720 – 1710	C=O stretching	carboxylic acids <sup>19</sup>
1720 – 1700	C=O stretching	carboxylic acids <sup>13</sup>
1720	C=O stretching	carboxylic acids, aromatic esters <sup>6,14</sup>
1713	C=O stretching	aromatics <sup>12</sup>
1710 – 1707	C=O stretching	carboxylates, aromatic esters, free organic acids <sup>6</sup>
1710 – 1680	C=C stretching, N–H bending	amines, alkenes (aromatics) <sup>10</sup>
1703	C=C, C=O stretching	carboxylic acids, esters <sup>17</sup>
1702	C=O stretching	carboxylic acids <sup>5</sup>
1660 – 1640	C=O stretching	amides <sup>19</sup>
1660 – 1600	C=O stretching	aromatics <sup>19</sup>
1653	C=O stretching	aromatics, amides, ketones, quinones, lignins <sup>6</sup>
1650 – 1600	C=C, C=O stretching	aromatics, aliphatics, ketones, lignin <sup>6,13</sup>
1650 – 1640	O–H, C=C stretching	primary water, quartz, aromatics, aliphatics (amide I) <sup>4,10</sup>
1650	C=O, C=N stretching	amide I, ketones, carboxyls, quinones, lignins <sup>1,9</sup>
1647 – 1633	N–H, O–H bending	amides <sup>3</sup>
1644	C=O stretching	aromatics, amides, ketones, lignin, humic acids <sup>17</sup>
1643 – 1615	C=O stretching	carboxylates <sup>15</sup>
1642 – 1569	C=C, C=O stretching	amide II, aromatics, quinones, carboxylates <sup>1</sup>
1640	C=O stretching	amides <sup>12</sup>
1634	C=O stretching	aromatics <sup>16</sup>

<b>Band position (cm<sup>-1</sup>)</b>	<b>Functional group assignment and type of vibration</b>	<b>Associated soil components (literature data*)</b>
1630	C=O, C=C stretching	aromatics, amides <sup>18</sup> , water <sup>19</sup>
1620 – 1610	Si–O, C=O stretching, N–H bending	silicates, aromatic amide I <sup>4,10</sup>
1610	C=O, C=C stretching	aromatics, ketones <sup>12</sup> , amines <sup>19</sup>
1606	C=O stretching	aromatic amines <sup>5</sup>
1600 – 1598	C=C stretching	aromatics <sup>10</sup>
1600 – 1570	C=C stretching	aromatics, carboxylates <sup>19</sup>
1584	C=O, C=C stretching	aromatic phenols lignin, humic acids <sup>17</sup>
1580	C=C, C=O asymmetric stretching	aromatics <sup>10</sup>
1580 – 1551	C=C, C=O asymmetric stretching	aromatics, alkenes <sup>8</sup>
1570 – 1540	N–H and C–N in-plane bending	amide II <sup>19</sup>
1564	C=O stretching	amide II <sup>16</sup>
1550	N–H in-plane stretching, C=C stretching	amide II <sup>6</sup> , aromatics <sup>11</sup>
1540 – 1520	C=C stretching	aromatics (amide II) <sup>10,14</sup>
1530 – 1510	C=C stretching	aromatics (amide II), phenols, lignin <sup>1</sup>
1520	C=C stretching	aromatics (amides) <sup>12,13</sup>
1515	C=C stretching	aromatics, amide II <sup>8,19</sup>
1515 – 1513	C=C stretching	aromatics, phenolics, lignin <sup>6</sup>
1510	C=C stretching	lignin <sup>14</sup>
1509	C–H, C=C stretching	aromatics <sup>17</sup>
1508	C=C stretching	lignin <sup>5,6</sup>
1490	C=C stretching	aromatics <sup>9</sup>
1479 – 1444	C–H, N–H stretching	amide II, aliphatics <sup>1</sup>
1479 – 1408	O–H stretching	carbonates <sup>1</sup>
1465	C–H stretching	aliphatics, organo-clay complexes <sup>19</sup>
1460	SiO–H, C–OH stretching, C–H scissoring	silicates, aliphatics <sup>4,7,9,10</sup> , lignin <sup>14</sup>
1453 – 1416	C–O stretching, C–H bending	calcite, dolomite, aromatics, phenolics <sup>3</sup>
1450 – 1370	C–H bending	aromatics <sup>13</sup>
1450	C–H deformation	aromatics, phenolics, aliphatics, lignin <sup>6</sup>
1445 – 1350	C–H deformation	methyls <sup>19</sup>
1440	C–O, O–H stretching	carboxylic acids <sup>10</sup> , carbonates <sup>11,13,18</sup>
1435 – 1419	C–O stretching	calcite <sup>15</sup>
1430	C–O stretching	carbonates <sup>17,19</sup>
1434	C–H bending	aliphatics <sup>17</sup>
1426	C–O, C=C, O–H stretching	humic acids, aromatics, aliphatics <sup>6</sup> clay minerals, carboxylic acids <sup>10</sup> , lignins <sup>14</sup> , carboxylates, aromatics, amides <sup>16</sup>
1420	(Mg)–OH, C–O stretching	aliphatics, carbonates <sup>2</sup>
1417	C–H, O–H deformation, C–O, C=O stretching	
1415	C–O stretching, C–H bending	phenolics, carboxylic acids (benzoic acid) <sup>1</sup>
1410	C–O, O–H stretching	phenolics <sup>12</sup>
1410 – 1400	(Mg)–OH, C–O stretching	quartz, carboxyls <sup>4</sup>
1400	C–H symmetric stretching	carboxylic acids <sup>8</sup>
1397 – 1384	C–O stretching	carboxylates <sup>15</sup>
1396 – 1383	C–O stretching	carbonates (calcite, dolomite) <sup>3</sup>
1393	C–O stretching	carboxylates <sup>19</sup>



Band position (cm <sup>-1</sup> )	Functional group assignment and type of vibration	Associated soil components (literature data*)
1380	C-H, C-O, O-H bending	phenolics, carboxyls <sup>1</sup>
1371	C-H deformation	phenolics, aliphatics, lignin <sup>6</sup>
1370	C-H, C-O stretching	aliphatics, lignin-derived phenols <sup>17</sup>
1342 – 1307	C-N stretching	aromatic amines (sulfonamides) <sup>1</sup>
1320	O-H deformation	carbonates <sup>7</sup>
1320 – 1310	C-H, C-O stretching	aromatic amide III, carboxylic acids <sup>10</sup>
1320 – 1230	C-N stretching	amide III <sup>19</sup>
1295 – 1220	C-OH, C-H bending	phenols, aromatics <sup>19</sup>
1293 – 1256	C-O stretching	bentonite, benzoic acid, ethers <sup>1</sup>
1285 – 1280	Si-O, C-O, C-N stretching	clay minerals, aromatics, carboxylic acids <sup>10</sup>
1270	C-O stretching	aliphatics <sup>8</sup> , lignin <sup>14</sup>
1265	C-O stretching	phenolics, ethers, lignin <sup>6</sup>
1240	C-O stretching	phenolics, aliphatics, lignin <sup>9</sup>
1238	Si-O stretching	silicates <sup>1</sup>
1235 – 1225	C-O stretching	carboxylic acids <sup>8</sup>
1230	C-O stretching, O-H deformation	bentonite, phenols, ethers, amide III, acetates, carboxylic acids (benzoic acid) <sup>1</sup> , lignin <sup>14</sup>
1170 – 1060	C-O stretching	polysaccharides, proteins <sup>19</sup>
1165	Si-O stretching	quartz <sup>4</sup>
1165 – 1153	Si-O, O-H, C-O stretching	quartz, aliphatics <sup>10</sup>
1162	C-O stretching	polysaccharides <sup>17</sup>
1160	C-OH stretching	aliphatics, alcohols, carbohydrates <sup>1</sup>
1160 – 1030	Si-O, C-OH stretching	clay minerals, quartz, cellulose <sup>17</sup>
1136 – 1070	Si-O, SiO-H, C-OH stretching	silicates, sulfates, alcohols, ethers <sup>1</sup>
1130	C-H bending	lignin <sup>14</sup>
1113	Si-O stretching	silicates <sup>4</sup>
1110	C-OH stretching	alcohols <sup>12</sup>
1107 – 914	Si-O stretching	silicates <sup>15</sup>
1103	C-O stretching	polysaccharides <sup>17</sup>
1100 – 1000	Si-O stretching	silicates (quartz) <sup>19</sup>
1095	Si-O, C-H in plane bending	silicates, non-aromatics <sup>4,10</sup>
1085	Si-O, C-H in plane bending	minerals, polysaccharides <sup>16</sup>
1080 – 1075	Si-O stretching, C-N stretching	clay minerals (kaolinite, illite), polysaccharides <sup>10</sup>
1080 – 1030	C-O stretching, O-H deformation	polysaccharides <sup>6</sup>
1070	Si-O stretching	silicates (kaolinite, illite) <sup>4,8</sup>
1056 – 945	SiO-H, C-OH stretching, C-H bending	aluminosilicates (kaolinite, illite, smectite), carbohydrates (polysaccharides), sulfones, aromatics <sup>1</sup>
1050	C-O stretching	polysaccharides <sup>12,13,19</sup>
1046 – 1025	Si-O stretching	silicates (kaolinite, illite) <sup>3</sup>
1039 – 1024	Si-O stretching	montmorillonite <sup>15</sup>
1037	(Al)-OH, Si-O stretching, C-H bending	clay minerals (kaolinite, illite) <sup>10</sup> , polysaccharides <sup>10,17</sup>
1035 – 1020	Si-O stretching, C-H bending	silicates (kaolinite, illite), non-aromatics <sup>4</sup>
1033	Si-O, C-H in-plane bending	minerals, polysaccharides <sup>16</sup>
1030	C-H bending	lignin <sup>14</sup>

Band position (cm <sup>-1</sup> )	Functional group assignment and type of vibration	Associated soil components (literature data*)
1030	C–H bending	lignin <sup>14</sup>
1030 – 950	Si–O stretching	clay minerals <sup>19</sup>
1010 – 995	Si–O stretching	kaolinite, illite <sup>10</sup>
1002	Si–O, C–O stretching	silicates (kaolinite, illite), polysaccharides <sup>2</sup>
1000	Si–O lattice stretching	silicates (kaolinite, illite) <sup>4,18</sup>
990	(Al)–OH deformation	aluminosilicates, clay minerals <sup>11</sup>
975	Si–O, C–O, C=C stretching, C–H out of plane bending	aluminosilicates (kaolinite, illite, smectite), sulfones, aromatics <sup>1,10</sup>
975 – 675	C–H out of plane bending	aromatics <sup>19</sup>
945 – 887	C=C stretching	benzoic acid, carbohydrates, cellulose <sup>1</sup>
930 – 910	Si–O, O–H stretching	aluminosilicates, benzoic acid, carbohydrates, cellulose <sup>4,10</sup>
926 – 912	(Al)–OH deformation	aluminosilicates <sup>15</sup>
925	(Al)–OH deformation	kaolinite <sup>18</sup>
920	(Al)–OH deformation	aluminosilicates (kaolinite) <sup>1</sup>
915	(Al)–OH deformation	kaolinite, smectite <sup>19</sup>
910 – 900	C–H out of plane bending	aromatics <sup>8</sup>
910	(Al)–OH deformation	aluminosilicates, clay minerals <sup>11</sup>
900	C–H out of plane bending	cellulose <sup>6</sup>
891 – 870	O–H stretching	calcite <sup>15</sup>
887 – 866	O–H stretching	carbonates, quartz and clay minerals <sup>1</sup>
875	SiO–H stretching, C–H bending	carbonates (calcite) <sup>10,19</sup> , aromatics <sup>10</sup>
870	C–H, C=C stretching	aromatics <sup>1</sup>
860	(Al)–OH stretching	clay minerals <sup>4,10</sup>
850 – 750	N–H out-of-plane bending	primary amines <sup>19</sup>
835	C–H out of plane stretching	aromatics, lignin <sup>1,6</sup>
820 – 752	O–H, C–C stretching	clay minerals (kaolinite), quartz, carbonates, phenols <sup>1</sup>
800	Si–O stretching	quartz, silicates <sup>8,19</sup>
798 – 779	Si–O stretching	quartz, silicates <sup>3</sup>
796	Si–O lattice stretching	silicates <sup>4,10</sup>
794 – 777	Fe(II)–OH stretching	clay minerals <sup>15</sup>
780	Si–O stretching, N–H out-of-plane bending	quartz, silicates <sup>8</sup> , primary amines <sup>18</sup>
774	Si–OH, (Al)/ (Mg)–OH stretching	clay minerals <sup>10</sup>
750	Si–OH, (Al)/(Mg)–OH stretching, C–H bending	clay minerals, polyaromatics <sup>10</sup>
750 – 700	N–H wag	secondary amines <sup>19</sup>
720	C–H bending (CH <sub>2</sub> wag)	carbonates (calcite), alkanes <sup>1,6</sup>
716 – 713	C–O vibrations	carbonates (calcite) <sup>3</sup>
715	O–H, C–H bending	aromatics <sup>10</sup>
700	Si–O bending	silicates <sup>1,19</sup>
700 – 600	Fe–O vibrations	iron oxides <sup>19</sup>
697	Si–O lattice bending	silicates, quartz <sup>4,10</sup>
695	Si–O lattice bending	silicates, quartz <sup>8</sup>
693 – 673	Si–O bending	quartz <sup>15</sup>
698 – 686	C–H out-of-plane bending	aromatics <sup>3</sup>

Band position (cm <sup>-1</sup> )	Functional group assignment and type of vibration	Associated soil components (literature data*)
675 – 670	C–H bending	aromatics <sup>10</sup>
655 – 650	Si–O bending, Fe–O stretching	silicates <sup>1,4,10</sup>
645 – 640	Si–O, S–C, O–H stretching	silicates (bentonite), sulfates, water <sup>10</sup>
630 – 620	Ca–OH, C–S stretching	hydroxyapatite, carbonates and sulfates <sup>10</sup>
536 – 525	O–H stretching	metal oxides <sup>15</sup>
535 – 525	Si–O–Al bending	clay minerals (kaolinite) <sup>10</sup>
520	Si–O–Al bending	silicates <sup>1</sup>
517 – 513	Si–O lattice bending	quartz <sup>10</sup>
490	Si–O lattice bending	silicates, water <sup>4,10</sup>
470	Si–O lattice bending	silicates <sup>1,4,8</sup>
470 – 420	Si–O lattice bending	clay minerals (kaolinite, illite, smectite) <sup>1</sup>
455 – 450	Si–O lattice bending	silicates <sup>4</sup>
430 – 420	(Al/Mg) –OH stretching, C–C deformation	clay minerals (kaolinite, illite, smectite), quartz <sup>4,8</sup>
400	Si–O lattice bending	silicates <sup>4</sup>

\* <sup>1</sup> Tinti et al. (2015); <sup>2</sup> Pärnpuu et al. (2022); <sup>3</sup> Parolo et al. (2017); <sup>4</sup> Krivoshein et al. 2022; <sup>5</sup> Teong et al. (2016); <sup>6</sup> Artz et al. (2007); <sup>7</sup> Helfenstein et al. (2021); <sup>8</sup> Nuzzo et al. (2020); <sup>9</sup> Maynard and Johnson (2018); <sup>10</sup> Volkov et al. (2021); <sup>11</sup> Xing et al. (2021); <sup>12</sup> Obeng et al. (2023); <sup>13</sup> Ghebleh-Goydaragh et al. 2021b); <sup>14</sup> Jiménez-González et al. 2019; <sup>15</sup> Fakhry et al. (2016); <sup>16</sup> Baumann et al. (2016); <sup>17</sup> Dhillon et al. (2017); <sup>18</sup> Xu et al. (2020); <sup>19</sup> Peltre et al. (2014).

## 3. Materials and Methods

### 3.1 Research preparation

#### 3.1.1 Soil samples

Croatia is characterized by diverse topographic configurations contributing to a wide variety of soil types. Five soil samples were collected from the topsoil (10 cm and 30 cm depth) of various locations across Croatia (Figure 5). The classification of these soil types was carried out in accordance with the World Reference Base for Soil Resources (WRB), as defined by the Food and Agriculture Organization (FAO 2015). The sampling parameters for the studied areas in Croatia, including soil type, sample location, region, type of land use, sampling depth, and year of sampling, are summarized in Table 2.

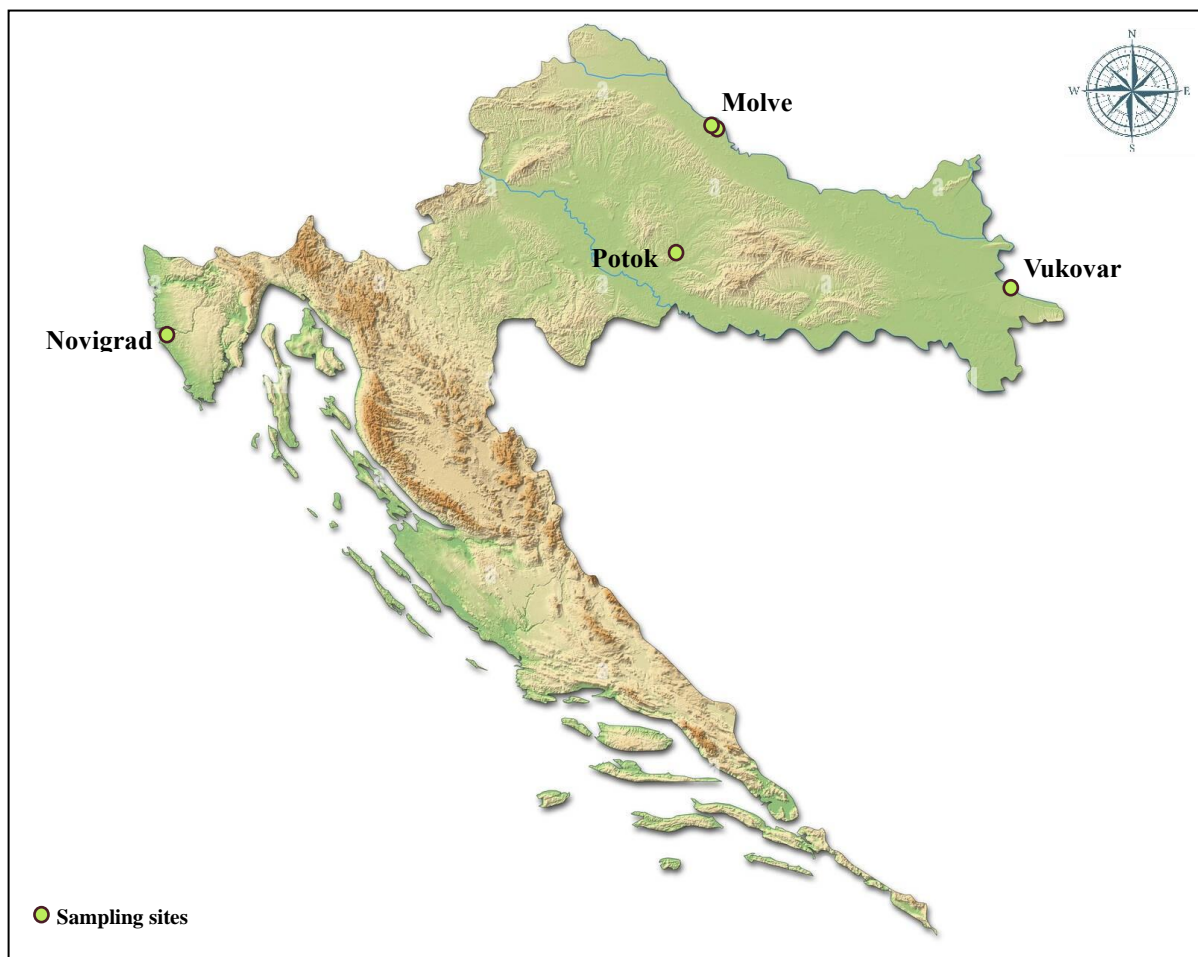


**Figure 5.** Spatial distribution of soil sampling sites across Croatia (West: Novigrad, Central: Potok, North: Molve, East: Vukovar).

**Table 2.** Sampling parameters in the studied areas of Croatia.

Soil type (FAO, WRB, 2015)	Sample location	Region	Type of land use	Sampling depth (cm)	Sampling year
Luvisol	Novigrad	Western Croatia (Istra peninsula)	Olive trees – Fire range	0 – 10	2020
Regosol acric	Molve 40	Northern Croatia	Arable cropland	0 – 30	2023
Gleysol vertic	Molve 9	Northern Croatia	Meadow	0 – 30	2023
Dystric Stagnosol	Potok	Central Croatia	Conventional agriculture	0 – 30	2018
Chernozem	Vukovar	Eastern Croatia	Conventional agriculture	0 – 30	2015

In western Croatia, within the Istria Peninsula, the region of Novigrad was selected for soil sampling. The soil sample was obtained from an area combining olive tree cultivation with fire range, and was classified as Luvisol (Figure 6), which is also known as "terra rossa" in the Croatian context. Luvisol is the most widely distributed soil across Croatia (Bašić 2013). The parent material of Luvisols may vary from non-calcareous to limestone substrates. Silicate substrates typically have a lower concentration of clay minerals compared to limestones. Luvisols are characterized by the accumulation of inorganic and organic materials in the upper horizons, resulting in the formation of a surface layer enriched with organic matter. Within Luvisols, humification leads to the formation of organic compounds with low molecular weight that can easily bind with aluminum and iron ions under acidic conditions. Consequently, mineral leaching occurs, thus reducing the stability of clay minerals like montmorillonite (Bašić 2013).

In northern Croatia, within the region of Molve, the two soil types selected were the Regosol acric and Gleysol vertic (Figure 6). Regosol acric was obtained from an arable land in Molve 40, while Gleysol vertic was obtained from meadow land in Molve 9. Regosols are undeveloped soils primarily formed by erosion processes, particularly water erosion, that gradually remove soil materials (Bašić 2013). Gleysols are characterized by heavy texture and high clay content, particularly of montmorillonite. Chemically, Gleysols are distinguished by their high organic matter content, ranging from 1.4% to 9.1%, high cation exchange capacity (CEC), and absence of acidic properties. As a result, Gleysols are rich in available nutrients, however, under anaerobic conditions their nutrient availability and, thus, the soil dynamics are affected (Bašić 2013).

In the northeastern part of Croatia, in the region of Potok, the soil type of Dystric Stagnosol was collected from an arable cropland (Figure 6). Stagnosol, also known as Pseudogley, is distinguished by waterlogging conditions caused by excessive rainwater, leading to gleyization processes extending up to 100 cm deep. Stagnosols are typically formed from leached loess or

fluviatile/colluvial sediments in non-calcareous clay minerals and are characterized by high silt content due to eolian sedimentations. Notably, Stagnosols (Pseudogleys) are the second most widely distributed soil across Croatia, after Luvisol (Bašić 2013).

Within Vukovar in Eastern Croatia, which is a region extensively known for its conventional agricultural use, the soil sampled belongs to the class of Chernozem (Figure 6). Chernozems are characterized by a loamy texture, which is predominantly composed of illite clay minerals, and are known for accumulating high-quality organic matter. Chernozems are naturally rich in nutrients, especially in phosphorus and potassium. However, due to anthropogenic interventions and intensive agricultural practices, they may experience a decline in organic matter content and the overall soil fertility (Bašić 2013).



**Figure 6.** Pictures of the collected soil types: Luvisol, Regosol acric, Gleysol vertic, Dystric Stagnosol, and Chernozem.

### 3.1.2 Reference physicochemical analysis

The collected soil types originated from regions with varying pedogenic characteristics and land use practices, thereby indicating differences in soil quality characteristics. The physicochemical characteristics of the soils were first analyzed by using standardized methods. Soil sample preparation involved drying, grinding, sieving and homogenizing of soil samples following the guidelines of HRN ISO 11464:2006. The particle size distribution was defined by sieving (HRN ISO 11464:2006). The pH was measured in three different solutions 0.01 M CaCl<sub>2</sub>, 1 M KCl, and H<sub>2</sub>O, modified at a 1:2.5 w/v ratio, according to the standard HRN ISO 10390:2004. The organic matter (OM) content was determined as a percentage of dry matter (% DM) using the sulfochromic oxidation method (modified Tjurin method) in accordance with HRN ISO 14235:2004. Total nitrogen (TN) content was determined as a percentage of dry matter (% DM) using dry combustion method («elemental analysis»), following the standard HRN ISO 13878:2004. The availability of phosphorus (P) and potassium (K) were determined by the ammonium lactate (AL) method with an extraction using ammonium lactate acetic acid at a 1:20 w/v ratio (Škorić 1982).

### 3.1.3 FTIR-ATR analysis and IR spectra acquisition

The archived air-dried soil samples were analyzed by Fourier transform infrared spectroscopy (FTIR) coupled with Attenuated Total Reflectance (ATR) recording technique. FTIR-ATR spectra of the soil samples were acquired using the Cary 660 FTIR spectrometer (Agilent Technologies) with the Golden Gate single-reflection diamond ATR accessory (Specac) (Figure 7) and the Shimadzu IRTracer 100 Spectrometer equipped with QATR 10 Single-Reflection ATR with a Diamond Crystal (Figure 8). Absorbance spectra were recorded in the mid-infrared region (spectral range: 4000 – 400 cm<sup>-1</sup>) at a nominal recording resolution of 4 cm<sup>-1</sup>. Before the spectral analysis, samples were pulverized into fine homogenates with a mortar (Figure 9). For spectra acquisition, approximately 10 mg of the homogenized soil sample was pressured on the diamond ATR plate using a self-leveling sapphire anvil to obtain the FTIR-ATR spectrum of a thin uniform layer of each sample. Spectra were recorded in absorbance mode (32 scans/spectrum) in the mid-IR spectral range from 4000 to 400 cm<sup>-1</sup>. Four replicate spectra of each sample were acquired by using different aliquots and the average of those was calculated. The spectral purity was checked by recording the spectrum of the empty ATR element that was thoroughly cleaned with triple distilled water and dried with soft tissue paper prior to each spectrum acquisition. A background spectrum was recorded between each sample acquisition. The laboratory temperature was maintained at 23 ± 1 °C during measurements. The assignment of the molecular vibrations of the soil spectra was conducted based on spectral atlas, i.e. Socrates's tables and charts of IR spectra and characteristic group frequencies (2001), and spectral data from the scientific literature related to soil FTIR-ATR spectra.

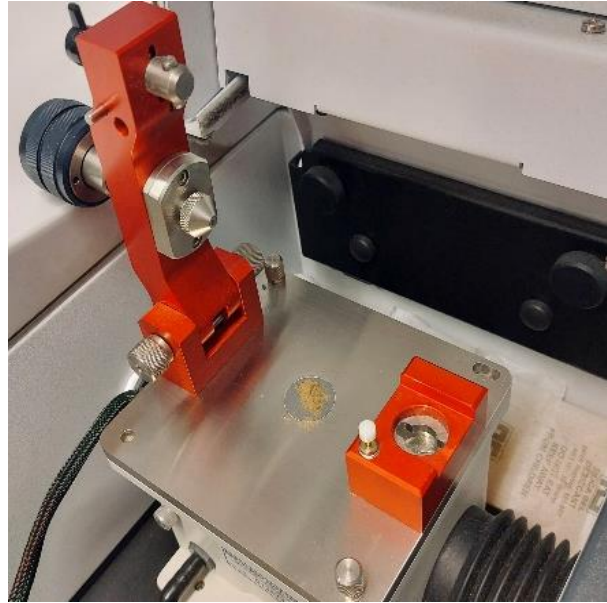


**Figure 7.** The FTIR-ATR spectrometer setup with the Agilent Technologies Cary 660 FTIR Spectrometer and single-reflection diamond ATR accessory \*.

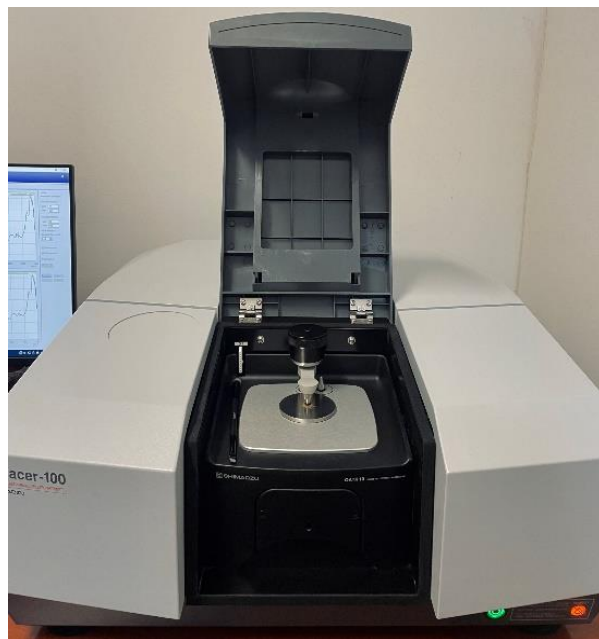


**Figure 8.** The FTIR-ATR spectrometer setup with the Shimadzu IRTracer 100 Spectrometer and single-reflection diamond ATR accessory \*\*.

\* provided by the Department of Fisheries, Apiculture, Wildlife management and special Zoology under the supervision of Associated Professor Lidija Svečnjak.

\*\* provided by the Department of Animal Science and Technology under the supervision of Professor Ivica Kos.





**Figure 9.** Preparation of soil samples prior to FTIR analysis: Five soil samples (Regosol acric, Dystric Stagnosol, Luvisol, Chernozem, Gleysol vertic (from left to right) and pulverization into fine homogenates using a mortar.

### 3.1.4. Statistical analysis

The raw spectral data were stored and pre-analyzed using the Resolutions Pro version 5.3.0 software package. Further spectral data analysis and processing were carried out using Origin 8.1 (OriginLab Corporation).

## 4. Results

### 4.1 Physicochemical characteristics

Physical and chemical analysis was performed on the soil samples. The results of particle size distribution (Table 3) showed that the texture of examined soils varied. Soils were classified into 2 main textural soil groups, clay soils including the soil types of Luvisol, Gleysol vertic, and Chernozem, and sandy soils, which included the types of Regosol acric and Dystric Stagnosol.

**Table 3.** Physical characteristics of the examined soil types.

Soil type (WRB-FAO, 2015)	Particle size distribution (%)			Texture
	clay	silt	sand	
Luvisol	57	40	3	Silty Clay
Regosol acric	7	11	82	Loamy sand
Gleysol vertic	54	39	7	Clay
Dystric Stagnosol	14.1	30.3	55.7	Sandy loam
Chernozem	29.4	67.3	3.3	Silty clay loam

The organic matter content (OM%) of the samples varied between 1.3 – 10.9 % (Table 4). Dystric Stagnosol is characterized by low organic matter content (1.3% OM), thus classifying it as a weakly humic soil. In contrast, Luvisol, Chernozem, and Regosol acric showed higher organic matter contents of 3.4%, 3.3%, and 2.4%, respectively, and are characterized as quite humic soils. Gleysol vertic, with OM 10.9%, is characterized as extremely highly humic soil (Šoštarić et al. 2017; Zebec et al. 2017; Škorić 1982). Notably, Gleysol vertic, characterized by clay texture (54% clay content), displayed the highest organic matter content among the studied soils. Conversely, Dystric Stagnosol, with a sandy loam texture (14.1% clay content), had the lowest organic matter content.

The pH values ranged from acidic (4.83) in Gleysol vertic to neutral (6.80) in Chernozem (Table 4). Luvisol had a pH level slightly below neutral (pH=6.3). Dystric Stagnosol and Regosol acric exhibit acidic pH with a value of 4.84 and 5.32 respectively. Gleysol vertic, despite its high OM content, is characterized by low pH values (pH=4.83).

The total nitrogen content ranged from 0.08% to 0.71% (Table 4). Dystric Stagnosol showed the lowest content in total nitrogen (0.08%), therefore characterized as soil weak supplied in nitrogen. Gleysol vertic and Chernozem showed the highest amount of TN, with 0.71% and 0.451% TN respectively, classified as soils very rich in nitrogen. Luvisol was characterized as a soil well supplied in nitrogen, with a TN of 0.237 %.

The concentration of available phosphorus (P) ranged from 30 to 315 mg/kg of soil (Table 4). The highest P content was observed in Chernozem (315 mg/kg), classifying it as a soil very rich in phosphorus, while the lowest content was observed in Gleysol vertic (30 mg/kg) and was characterized as a soil very poorly supplied with phosphorus. Regosol acric and Dystric

Stagnosol had a moderate phosphorus content of 136 mg/kg and 106 mg/kg respectively, while Luvisol was characterized by a very weak phosphorus content of 41 mg/kg.

Potassium (K) ranged from 129 mg/kg in Dystric Stagnosol to 431 mg/kg in Chernozem (Table 4). Chernozem and Luvisol were characterized as soil very rich in potassium, with 431 mg/kg and 256 mg/kg of K respectively. Regosol acric and Gleysol vertic with 184 mg/kg and 194 mg/kg respectively were characterized as well supplied soils in K. Dystric Stagnosol, with 129 mg/kg of K, was characterized as moderately supplied soil in potassium (Zebec et al. 2017).

**Table 4.** Chemical characteristics of the examined soil types including: pH, Organic Matter (OM%), Total Nitrogen (TN %), plant available Phosphorus ( $P_{AL}$ ) and plant available Potassium ( $K_{AL}$ ).

Soil type ( WRB-FAO, 2015)	pH <sub>KCl</sub>	OM (%)	TN (%)	$P_{AL}$ , (mg/kg soil)	$K_{AL}$ , (mg/kg soil)
Luvisol	6.30	3.4	0.237	41	256
Regosol acric	5.32	2.4	0.118	136	184
Gleysol vertic	4.83	10.9	0.710	30	194
Dystric Stagnosol	4.84	1.3	0.080	106	129
Chernozem	6.80	3.3	0.451	315	431

## 4.2 FTIR-ATR spectra

### 4.2.1 Assignment of molecular vibrations in soil spectra

The FTIR-ATR spectra of the different soil types (obtained as an average spectrum for each soil sample) with the assignment of the major underlying molecular vibrations are presented in Figure 10. According to Figure 10, soil constituents are represented by weak bands of functional groups in the range  $3725 - 3200 \text{ cm}^{-1}$  and at  $1635 \text{ cm}^{-1}$ , as well as intensive overlapping absorptions of inorganic and organic constituents observed in the fingerprinting region between  $1400$  and  $500 \text{ cm}^{-1}$ . These bands are characteristic and similar for several soil types according to the literature. The spectral region between  $3725 \text{ cm}^{-1}$  and  $3200 \text{ cm}^{-1}$  (H-bond region) is characterized by weak signals, peaking around  $3697 \text{ cm}^{-1}$  and  $3623 \text{ cm}^{-1}$  attributed to the SiO-H and Fe-O stretching vibrations of phyllosilicates within clay minerals, particularly kaolinite and gibbsite (Tinti et al. 2015; Pärnpuu et al. 2022; Krivoshein et al. 2022; Artz et al. 2007; Parolo et al. 2017; Volkov et al. 2021). A shoulder band was also observed at  $3646 \text{ cm}^{-1}$  in the spectrum of Luvisol. The broad weak peak arising at  $3415 \text{ cm}^{-1}$  ( $3500-3000 \text{ cm}^{-1}$ ) can be assigned to O-H, Fe-O and FeO-H and N-H stretching vibrations of both clay minerals and SOM constituents, such as alcohols, phenols, carboxylic acids, amides and amines (Margenot et al. 2017; Tinti et al. 2015; Pärnpuu et al. 2022; Parolo et al. 2017; Krivoshein et al. 2022; Teong et al. 2016; Artz et al. 2007; Volkov et al. 2021; Ludwig et al. 2008). No IR absorption bands were observed in the spectral region from  $3000$  to  $1800 \text{ cm}^{-1}$  of analysed soils spectra. The weak peak at  $1635 \text{ cm}^{-1}$  is assigned to C=C stretching and N-H bending vibrations of amides (amide I, II), and C=C, C=O stretching vibrations aromatic ketones, aldehydes, quinones, and carboxylic acids (benzoic acid) (Pärnpuu et al. 2022; Parolo et al. 2017; Nuzzo et al. 2020).

The spectral region between  $1200 \text{ cm}^{-1}$  and  $500 \text{ cm}^{-1}$  (fingerprint region) is populated by a number of absorption bands. The most prominent spectral feature in the fingerprint region is the absorption bands occurring at  $994 \text{ cm}^{-1}$  and  $523 \text{ cm}^{-1}$  due to the Si-O stretching vibrations of silicates. The shoulder band at  $1164 \text{ cm}^{-1}$  is assigned to Si-O stretching vibrations of quartz, and C-O stretching vibrations of aliphatics, alcohols and carbohydrates (Tinti et al. 2015; Krivoshein et al. 2022; Volkov et al. 2021). The shoulder bands peaking at  $1114 \text{ cm}^{-1}$  and  $1024 \text{ cm}^{-1}$  are ascribed to SiO-H vibrations of aluminosilicates (kaolinite, illite, smectite), and CO-H stretching and C-H bending vibrations of polysaccharides (Krivoshein et al. 2022; Tinti et al. 2015; Margenot et al. 2017). Notably, the band at  $1114 \text{ cm}^{-1}$  was only observed in the spectrum of Luvisol, and can therefore be identified as Luvisol-specific. The intensive band at  $994 \text{ cm}^{-1}$  was followed by a medium intensity signal occurring at  $912 \text{ cm}^{-1}$ , both attributed to Mg/Al-O-H stretching of aluminosilicates and C-H deformations of benzoic acid, carbohydrates, and cellulose (Tinti et al. 2015; Krivoshein et al. 2022; Volkov et al. 2021; Nuzzo et al. 2020). The very weak band peaking at  $831 \text{ cm}^{-1}$  can be attributed to C-H vibrations of aromatics and lignin (Tinti et al. 2015; Artz et al. 2007).

The most complex absorption region of the IR spectrum of soil arises below  $800 \text{ cm}^{-1}$  due to the numerous overlapping bands of inorganic and organic compounds present in soil (Figure 11). The medium bands peaking at  $794 \text{ cm}^{-1}$ ,  $777 \text{ cm}^{-1}$ ,  $748 \text{ cm}^{-1}$ , and  $692-686 \text{ cm}^{-1}$  are assigned to Si-O, (Mg/Al)-OH stretching vibrations of quartz and aluminosilicates, and C-H bending

of aromatics (Krivoshein et al. 2022; Volkov et al. 2021; Nuzzo et al. 2020; Parolo et al. 2017). The very weak band at  $646\text{ cm}^{-1}$  is attributed to Si–O, S–C, O–H stretching vibrations of silicates, like bentonite, and sulfates (Krivoshein et al. 2022). The most prominent absorption in this region is a broad band with a peak at  $523\text{ cm}^{-1}$  assigned to Si–O bending vibrations of clay minerals (kaolinite) and quartz (Tinti et al. 2015; Volkov et al. 2021). These spectral differences between bands of the studied soils below  $500\text{ cm}^{-1}$  might be attributed to artefacts.

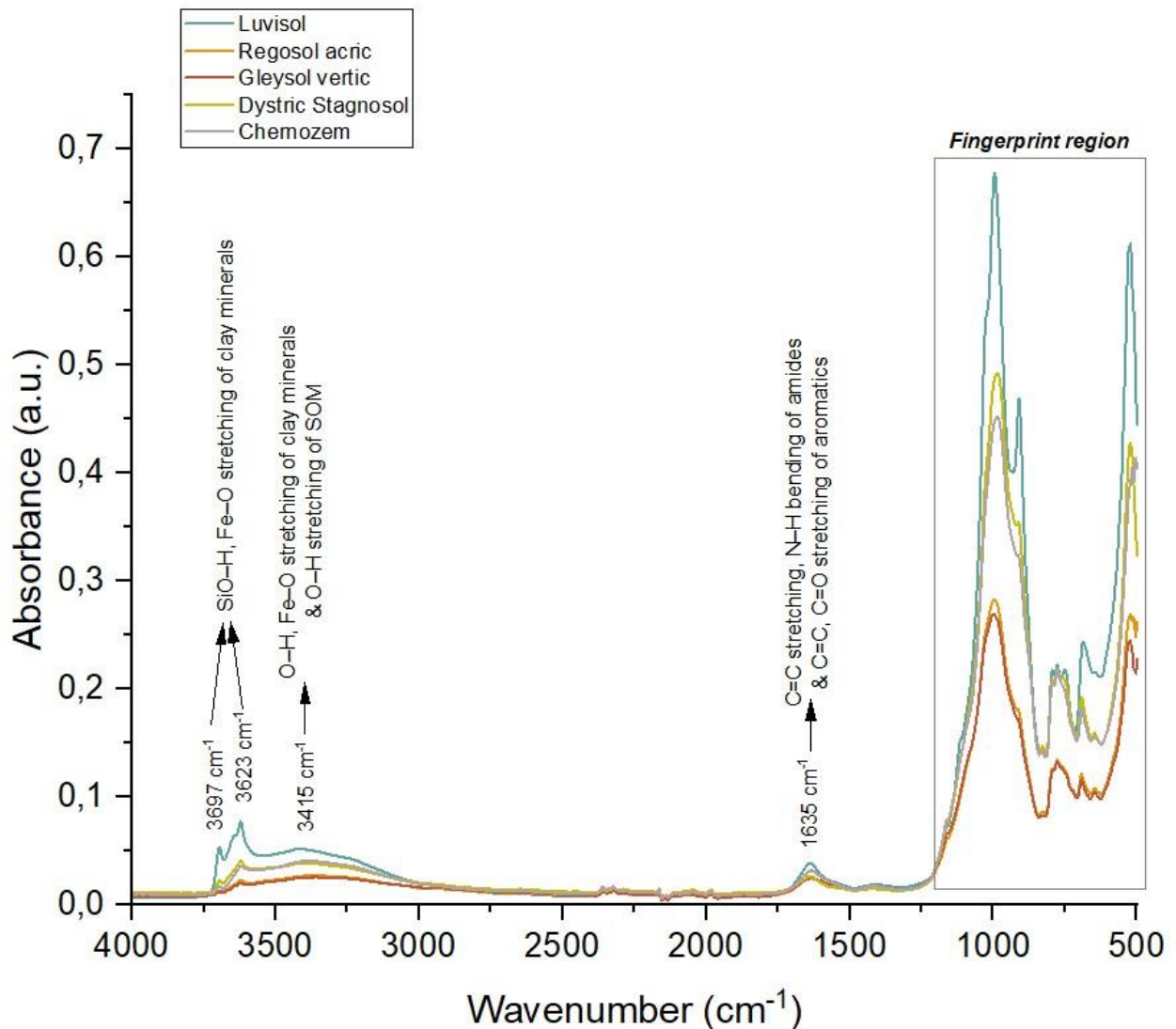


**Figure 10.** Average FTIR-ATR spectra of different soil types collected across Croatia: comparative spectral features with the assignment of major underlying molecular vibrations (whole spectral region:  $4000$  to  $500\text{ cm}^{-1}$ )

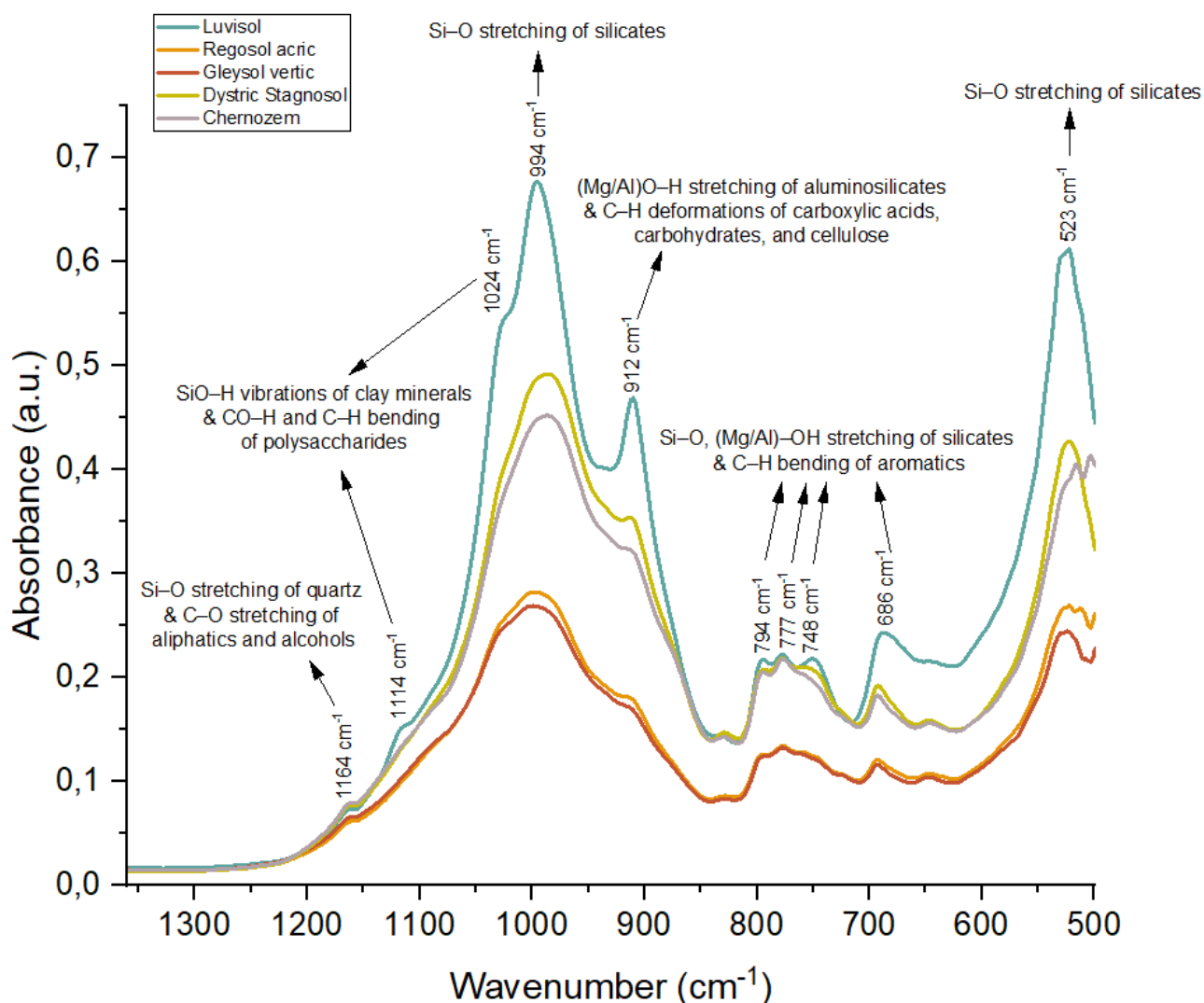


**Figure 11.** Average FTIR-ATR spectra of different soil types collected across Croatia: comparative spectral features with the assignation of major underlying molecular vibrations (fingerprint region: 1400 to 500  $\text{cm}^{-1}$ )

#### 4.2.2 Comparison of the characteristic bands between the soil types

Overall the integral spectral features appear to be similar among the different soil types, however variations in absorbance intensities were noticeable. The intensities of the bands in the region between 3700 – 3000  $\text{cm}^{-1}$  region assigned mainly to clay minerals showed variations between the studied soil types. Luvisol had the highest absorbance peaking at 3697  $\text{cm}^{-1}$ , 3623  $\text{cm}^{-1}$ , 3415  $\text{cm}^{-1}$  while the lowest intensity of absorbance was observed in Gleysol vertic and Regosol acric. As mentioned before, there were no significant molecular vibrations in the region between 3000  $\text{cm}^{-1}$  and 1800  $\text{cm}^{-1}$  in any of the soil types examined, indicating that there were no predominant constituents of the soils arising within this range of wavelength. The vibration of amide bands occurring at 1635  $\text{cm}^{-1}$ , resulted in a higher intensity in the spectrum of Luvisol, followed by Chernozem, while Dystric Stagnosol, Gleysol vertic and Regosol acric showed the lowest intensity of absorbance.

The shoulder band at  $1164\text{ cm}^{-1}$  assigned to vibrations of both inorganic (clay minerals and quartz) and organic compounds (aliphatics, alcohols, carbohydrates), exhibited the highest intensity within the spectra of Chernozem, Dystric Stagnosol, and Luvisol, while Gleysol vertic and Regosol acric had lower intensities. The shoulder band arising at  $1114\text{ cm}^{-1}$ , was present only in the spectrum of Luvisol whereas it was not evident in the other soil spectra. The highest intensity of the shoulder band at  $1024\text{ cm}^{-1}$  was recorded in Luvisol, while the lowest was observed in Gleysol vertic and Regosol acric.

Within the spectral region between  $1050\text{ cm}^{-1}$  and  $850\text{ cm}^{-1}$  there were differences between absorbance bands of the soil types, indicating variability related to constituents of the distinct soil types. The bands at  $993\text{ cm}^{-1}$  and  $912\text{ cm}^{-1}$  appeared as sharp peaks with the highest intensity in the spectrum of Luvisol, while Gleysol vertic and Regosol acric displayed the lowest intensities. In addition, the very weak band absorbance observed at  $831\text{ cm}^{-1}$  had a higher intensity in Chernozem, Dystric Stagnosol and Luvisol, and a lower intensity in Gleysol vertic and Regosol acric. The soil spectra of Luvisol, Chernozem and Dystric Stagnosol within the series of bands at  $794\text{ cm}^{-1}$ ,  $777\text{ cm}^{-1}$  and  $748\text{ cm}^{-1}$  resulted in higher intensities compared to Regosol acric and Gleysol vertic. Finally, at the peak of  $692\text{--}686\text{ cm}^{-1}$  and  $523\text{ cm}^{-1}$  Luvisol resulted in the highest intensity while Gleysol vertic and Regosol acric exhibited the lowest intensities.

### **4.2.3 Correlation of spectra with physicochemical parameters**

The observed spectral features did not show statistically significant correlations with the data obtained by the conventional analysis of OM content ( $R^2$  range: 0.06992 – 0.36904) (Appendix 8.1),  $\text{pH}_{\text{KCL}}$  ( $R^2$  range: 0.1193 – 0.61417) (Appendix 8.2), TN content ( $R^2$  range: 0.00517 – 0.15393) (Appendix 8.3), plant available P content ( $R^2$  range: 0.00292 – 0.2165) (Appendix 8.4), plant available K content ( $R^2$  range: 0.00362 – 0.2665) (Appendix 8.5), and clay content ( $R^2$  range: 0.00104 – 0.20599) (Appendix 8.6). Correlations were examined specifically for the wavelengths that revealed distinct peaks within the FTIR spectra, including:  $3697\text{ cm}^{-1}$ ,  $3623\text{ cm}^{-1}$ ,  $3415\text{ cm}^{-1}$ ,  $1635\text{ cm}^{-1}$ ,  $1164\text{ cm}^{-1}$ ,  $1114\text{ cm}^{-1}$ ,  $1024\text{ cm}^{-1}$ ,  $993\text{ cm}^{-1}$ ,  $912\text{ cm}^{-1}$ ,  $831\text{ cm}^{-1}$ ,  $794\text{ cm}^{-1}$ ,  $777\text{ cm}^{-1}$ ,  $748\text{ cm}^{-1}$ ,  $686\text{ cm}^{-1}$ ,  $646\text{ cm}^{-1}$ ,  $523\text{ cm}^{-1}$ . While these were not statistically significant, substantial correlations were observed between specific spectral absorbances and certain physicochemical data. The complex interactions between minerals and organic matter, along with the small number of samples and lack of repetitions, likely hindered the establishment of correlations between the spectral features and the physicochemical properties.

## 5. Discussion

In general, the FTIR-ATR spectra obtained from the five distinct soil types showed similarities within the MIR range. The absorbance intensities of the observed functional group vibrations apart from the H-bond region ( $4000 - 3100 \text{ cm}^{-1}$ ) and the fingerprinting region ( $1400 - 500 \text{ cm}^{-1}$ ) were similar among the soil types (Figure 10). The strong absorbance bands observed at  $3697 \text{ cm}^{-1}$  and  $3623 \text{ cm}^{-1}$  in all soil types are consistent with the dominance of clay minerals within soil, which is in compliance with findings from several other studies as presented in Table 1.

However, a unique shoulder band at  $3646 \text{ cm}^{-1}$  in Luvisol, not observed in the other soil types, suggests a distinctive mineralogical composition. This may be attributed to the high content of metal oxides (Fe oxides) which is evident by its characteristic red color (terra rosa) (Padilla et al. 2014; Ghebleh-Goydaragh et al. 2021b). Several studies have demonstrated that Fe oxides influence ion retention and soil color (Margenot et al. 2017; Rial et al. 2016). During the soil formation, the weathering of minerals, influences the concentration of Fe oxides, which in turns affects the ability of the soil to adsorb SOM (Haynes 2005; Nath et al. 2022). The reactive surfaces of minerals that contain Fe oxides—such as goethite ( $\alpha\text{-FeOOH}$ ), hematite ( $\alpha\text{-Fe}_2\text{O}_3$ ), ferrihydrite, lepidocrocite, maghemite, magnetite, and schwertmannite—provide sites for the formation of organo-mineral complexes (Margenot et al. 2017; Maynard and Johnson 2018; Cooperband 2002; Jiménez-González et al. 2019). This mechanism is particularly important during the processes of humification and SOM stabilization (Bot and Benites 2005). As a result, the presence of the band at  $3646 \text{ cm}^{-1}$ , exclusively observed in Luvisol, can be attributed to the high concentration of Fe oxides bound to the minerals of Luvisol. These qualitative spectral observations highlight the differences in the inorganic constituents between Luvisol, characterized by the presence of minerals such as goethite and hematite, and the other studied soil types, dominated by kaolinite and gibbsite. Additionally, this implies that Luvisol might be characterized by a higher content of the stable SOM fraction compared to the other studied soils. Besides, this also suggests that the higher absorptions of Luvisol and Chernozem might be due to an increased amount of organo-mineral complexes, particularly comprised of hydrophilic compounds, that are more easily adsorbed onto clay mineral surfaces (Pärnpuu et al. 2022).

The FTIR-ATR spectra of the studied soil types in the range of  $3000 - 1800 \text{ cm}^{-1}$  did not result in significant absorptions, indicating the absence of functional groups related to the hydrophobic fraction of SOM. This may be due to the fact that hydrophobic substances, such as aliphatics, can be degraded more easily by soil microorganisms than the hydrophilic compounds, while hydrophilic compounds are less accessible to soil microorganisms (Pärnpuu et al. 2022).

The range between  $2500$  and  $800 \text{ cm}^{-1}$  is mainly indicative for the presence of organic matter constituents within the soil. According to our FTIR-ATR spectra, the peak at  $1635 \text{ cm}^{-1}$  is the only significant band that demonstrates the presence of amides and other aromatic compounds, such as ketones, aldehydes, quinones, and carboxylic acids (benzoic acid), related to the



hydrophilic part of SOM (Pärnpuu et al. 2022; Parolo et al. 2017). Although we did not observe significant intensity variations between the soil types in this wavelength, Luvisol and Chernozem demonstrated higher absorbance, which in turn indicates a higher concentration of the hydrophilic part of SOM, compared to the other soil types.

Our findings exhibited overlapping absorptions of minerals with soil organic matter in the fingerprint region between  $1200\text{ cm}^{-1}$  and  $500\text{ cm}^{-1}$ . In the  $1200 - 1000\text{ cm}^{-1}$  range only weak shoulder bands were observed at  $1164\text{ cm}^{-1}$ ,  $1114\text{ cm}^{-1}$  and  $1024\text{ cm}^{-1}$  attributed to silicates and masked aliphatics compounds, as highlighted in the literature (Table 1). It is noteworthy that the weak band at  $1114\text{ cm}^{-1}$  was only observed in the spectrum of Luvisol according to our findings. This indicates a different composition of Luvisol within this range compared to the other soils. In addition, the range  $1050 - 950\text{ cm}^{-1}$  was dominated by strong absorbances observed in all soil spectra. Luvisol had the highest absorptions, possibly caused by strong influence of iron oxides and organo-mineral complexes (Fakhry et al. 2016). This overlapping can mask the characteristic absorption bands of SOM, making it difficult to resolve the specific contributions of SOM and clay minerals.

Interestingly, Gleysol vertic although characterized by high clay content (54%) and an extremely high soil organic matter content (SOM 10.9 %) (Table 4), as obtained by the conventional analysis in the laboratory, did not reflect such a high SOM content within the FTIR-ATR spectrum. This suggests that FTIR spectra might not distinctly reflect the high SOM content due to the dominance of minerals. Therefore, given the complexity of soil composition and the overlapping spectral features, it is possible that the high SOM content in Gleysol vertic soil is primarily due to the formation of macroaggregates in the soil (Bot and Benites 2005; Haynes 2005; Nath et al. 2022).

However, the difference between the spectral intensities between the clay soils of Gleysol vertic and Luvisol, throughout the MIR range, reflects different soil composition. Luvisol, is a soil quite humic with a relatively high clay content, and slightly acidic pH (6.30). On the other hand, Gleysol vertic is an extremely highly humic soil, with high clay content, and acidic pH (4.83). As a result, the difference between the pH values between these two clay soils along with the distinct spectra of these two soil types in the MIR range, indicates that pH is an important parameter that affects SOM content. Furthermore, our findings did not observe any bands related to carbonates. Pärnpuu et al. (2022) found a positive correlation between soil pH and absorbance at a specific wavenumber reflecting the carbonate content in the soil. Therefore, our results confirm that our soils are non-calcareous.

Land management practices can also influence soil properties by affecting soil carbon input (Baumman et al. 2016). According to our findings, Chernozem and Luvisol, that are characterized by silty clay textures and a high content of total N, plant available P and K, exhibited higher absorbances throughout the MIR range, compared to the other soil types. Our FTIR-ATR results indicate variations and extensive overlapping in spectral data among the soil types, confirming that soil composition is influenced by several factors, making it challenging to fingerprint SOM.

## 6. Conclusion

This research aimed to investigate the applicability of Fourier Transform Infrared-Attenuated Total Reflectance (FTIR-ATR) spectroscopy for soil organic matter characterization. The review of the existing literature regarding the use of FTIR spectroscopy in soil assessment identified distinct peaks of bands assigned to inorganic and organic soil components within the MIR spectral range. In this study, five distinct soil types collected from Croatia were analyzed using FTIR-ATR spectroscopy. According to our findings, FTIR-ATR spectroscopy has been demonstrated to be partially successful in fingerprinting SOM. The obtained FTIR spectra revealed prevalence of inorganic functional groups throughout the MIR range and only one peak indicative of the hydrophilic fraction of SOM. However, it can be assumed that the other SOM-specific bands are overlapped with the stronger signals of inorganic matter. Our findings indicate that the dominance of mineral constituents masks the spectral features of SOM and, as a result, is a major limitation of FTIR analysis for SOM determination. Besides, our results suggest that the formation of organo-mineral complexes facilitated by the high clay concentration of soil may hinder distinct spectral features of SOM. Overall, the FTIR-ATR spectra of all soil types displayed similar functional groups within the MIR range. The spectra of Luvisol and Chernozem showed higher absorbances throughout the MIR range, while Regosol acric and Gleysol vertic showed lower absorbances. It is also noteworthy that Luvisol's characteristic red color (*terra rosa*) is likely attributed to the high content in Fe oxides. The analyses of the two FTIR-ATR spectrometers highlighted the accuracy of the spectral results, further enhancing the reliability and applicability of this analytical approach in soil assessment. Finally, the observed spectral data did not reflect statistically significant correlations with the physicochemical data obtained by the conventional laboratory analysis, although there were some relationships between the spectral and the physicochemical data. The lack of statistical correlations might be attributed to the limited set of soil samples and lack of repetitions for each soil type.

To conclude, understanding the interactions between minerals and soil organic matter is crucial in order to improve FTIR analysis for SOM determination. FTIR spectroscopy enables the rapid and cost-effective analysis of a large number of soil samples. Therefore, a combined quantitative and qualitative analysis of soils coupled with chemometric modeling would be beneficial for fingerprinting SOM by FTIR-ATR spectroscopy. Advanced calibration modeling techniques that incorporate a larger set of soil samples or additional spectral data pretreatment methods could enhance the interpretation of spectral data, enabling better elucidation of the relationships between spectral and physicochemical characteristics of soils. This approach is essential for enhancing the applicability of FTIR analysis in fingerprinting SOM and advancing soil assessment.

## 7. References

1. Allo, M., Todoroff, P., Jameux, M., Sterna, M., Paulina, L., Albrecht, A. (2020). Prediction of tropical volcanic soil organic carbon stocks by visible-near- and mid-infrared spectroscopy. *Catena*. DOI: <https://doi.org/10.1016/j.catena.2020.104452>. – accessed May 2024
2. Artz, R. R. E., Chapman, S. J., Robertson, A. H. J., Potts, J. M., Laggoun-Défarge, F., et al. (2008). FTIR spectroscopy can predict organic matter quality in regenerating cutover peatlands. *Soil Biology and Biochemistry*, 40(2), 515 – 527. DOI: <https://doi.org/10.1016/j.soilbio.2007.09.019>. – accessed May 2024
3. Bašić, F. (2013). *The Soils of Croatia*. World Soils Book Series. Springer, Dordrecht. DOI: [https://doi.org/10.1007/978-94-007-5815-5\\_1](https://doi.org/10.1007/978-94-007-5815-5_1).
4. Baumann, K., Schöning, I., Schrupf, M., Ellerbrock, R. H., Leinweber, P. (2016). Rapid assessment of soil organic matter: Soil color analysis and Fourier transform infrared spectroscopy. *Geoderma*, DOI: <http://dx.doi.org/10.1016/j.geoderma.2016.05.012>. – accessed March 2024
5. Bot, A., Benites, J. (2005). *The importance of soil organic matter: Key to drought-resistant soil and sustained food and production*. Food and Agriculture Organization of the United Nations, ISBN 92-5-105366-9.
6. Breure, T. S., Prout, J. M., Haefele, S. M., Milne, A. E., Hannam, J. A., Moreno-Rojas, S., Corstanje, R. (2021). Comparing the effect of different sample conditions and spectral libraries on the prediction accuracy of soil properties from near- and mid-infrared spectra at the field-scale. *Soil and Tillage Research*. DOI: <https://doi.org/10.1016/j.still.2021.105196>. – accessed March 2024
7. Cooperband, L. (2002). *Building soil organic matter with organic amendments: A resource for urban and rural gardeners, small farmers, turfgrass managers, and large-scale producers*. Center for Integrated Agricultural Systems, University of Wisconsin-Madison.
8. Dhillon, G. S., Gillespie, A., Peak, D., Van Rees, K. C. J. (2017). Spectroscopic investigation of soil organic matter composition for shelterbelt agroforestry systems. *Geoderma*, 298, 1 – 13. DOI: <https://doi.org/10.1016/j.geoderma.2017.03.016>. – accessed June 2024
9. Fakhry, A., Osman, O., Ezzat, H., Ibrahim, M. (2016). Spectroscopic analyses of soil samples outside Nile Delta of Egypt. *Spectrochimica Acta Part A: Molecular and Biomolecular Spectroscopy*, 168, 244 – 252. DOI: <https://doi.org/10.1016/j.saa.2016.05.026>. – accessed June 2024
10. Fox, G. (2020). The brewing industry and the opportunities for real-time quality analysis using infrared spectroscopy. *Applied Sciences*, 10(2). <https://doi.org/10.3390/app10020616>. – accessed July 2024
11. Ghebleh Goydaragh, M., Taghizadeh-Mehrjardi, R., Golchin, A., Jafarzadeh, A. A., Lado, M. (2021a). Predicting weathering indices in soils using FTIR spectra and random forest models. *Catena*. DOI: <https://doi.org/10.1016/j.catena.2021.105437>. – accessed March 2024
12. Ghebleh Goydaragh, M., Taghizadeh-Mehrjardi, R., Jafarzadeh, A. A., Triantafilis, J., Lado, M. (2021b). Using environmental variables and Fourier Transform Infrared Spectroscopy

- to predict soil organic carbon. *Catena*, 202, 105280. DOI: <https://doi.org/10.1016/j.catena.2021.105280>. – accessed March 2024
13. Haynes (2005). Significance of labile Organic Matter fractions, Elsevier, *Advances in Agronomy*, Vol. 85, Chapter VII, pp. 222 – 257.
  14. Helfenstein, A., Baumann, P., Viscarra Rossel, R., Gubler, A., Oechlin, S., Six, J. (2021). Quantifying soil carbon in temperate peatlands using a mid-IR soil spectral library, *Soil*, 7, 193 – 215. DOI: <https://doi.org/10.5194/soil-7-193-2021>. – accessed November 2023
  15. International Organization for Standardization. (2004). Soil quality – Determination of organic carbon by sulfochromic oxidation (modified; titrimetric determination, Tjurin method, bichromate method) (ISO Standard No. 14235:2004).
  16. International Organization for Standardization. (2004). Soil quality – Determination of pH (ISO Standard No. 10390:2004).
  17. International Organization for Standardization. (2004). Soil quality – Determination of total nitrogen – Modified Kjeldahl method (ISO Standard No. 11261:2004).
  18. International Organization for Standardization. (2006). Soil quality – Pretreatment of samples for physico-chemical analysis (ISO Standard No. 11464:2006).
  19. Jensen, J. L., Schjønning, P., Watts, C. W., Christensen, B. T., Obour, P. B., Munkholm, L. J. (2020). Soil degradation and recovery - Changes in organic matter fractions and structural stability, *Geoderma*, 364, 114181, DOI: <https://doi.org/10.1016/j.geoderma.2020.114181>. – accessed November 2023
  20. Jiménez-González, M. A., Álvarez, A. M., Carral, P., Almendros, G. (2019). Chemometric assessment of soil organic matter storage and quality from humic acid infrared spectra. *Science of The Total Environment*, DOI: <https://doi.org/10.1016/j.scitotenv.2019.06.231>. – accessed March 2024
  21. Krivoshein, P. K., Volkov, D. S., Rogova, O. B., Proskurnin, M. A. (2022). FTIR Photoacoustic and ATR Spectroscopies of Soils with Aggregate Size Fractionation by Dry Sieving, *ACS Omega*, 7(2), 2177 – 2197. DOI: <https://doi.org/10.1021/acsomega.1c05702>. – accessed October 2023
  22. Lal, R., Negassa, W., and Lorenz, K. (2015). Carbon sequestration in soil. *Current Opinion in Environmental Sustainability*, 15, 79 – 86. DOI: <https://doi.org/10.1016/j.cosust.2015.09.002>. – accessed June 2024
  23. Lehman, R. M., Cambardella, C. A., Stott, D. E., Acosta-Martinez, V., Manter, D. K., Buyer, J. S., Karlen, D. L. (2015). Understanding and Enhancing Soil Biological Health: The Solution For Reversing Soil Degradation, *Sustainability*, 1(7), 988 – 1027, DOI: <https://doi.org/10.3390/su7010988> – accessed March 2024
  24. Ludwig, B., Nitschke, R., Terhoeven-Urselmans, T., Michel, K., Flessa, H. (2008). Use of mid-infrared spectroscopy in the diffuse-reflectance mode for the prediction of the composition of organic matter in soil and litter. *Journal of Plant Nutrition and Soil Science*, 171(4), 384 – 391, DOI: <https://doi.org/10.1002/jpln.200700022>. – accessed March 2024
  25. Ma, F., Zeng, Y., Du, C., Shen, Y., Ma, H., Xu, S., Zhou, J. (2017). Soil variability description using Fourier transform mid-infrared photoacoustic spectroscopy coupling with RGB method. *Catena*, 157, 79 – 88. <https://doi.org/10.1016/j.catena.2017.01.005>. – accessed June 2024

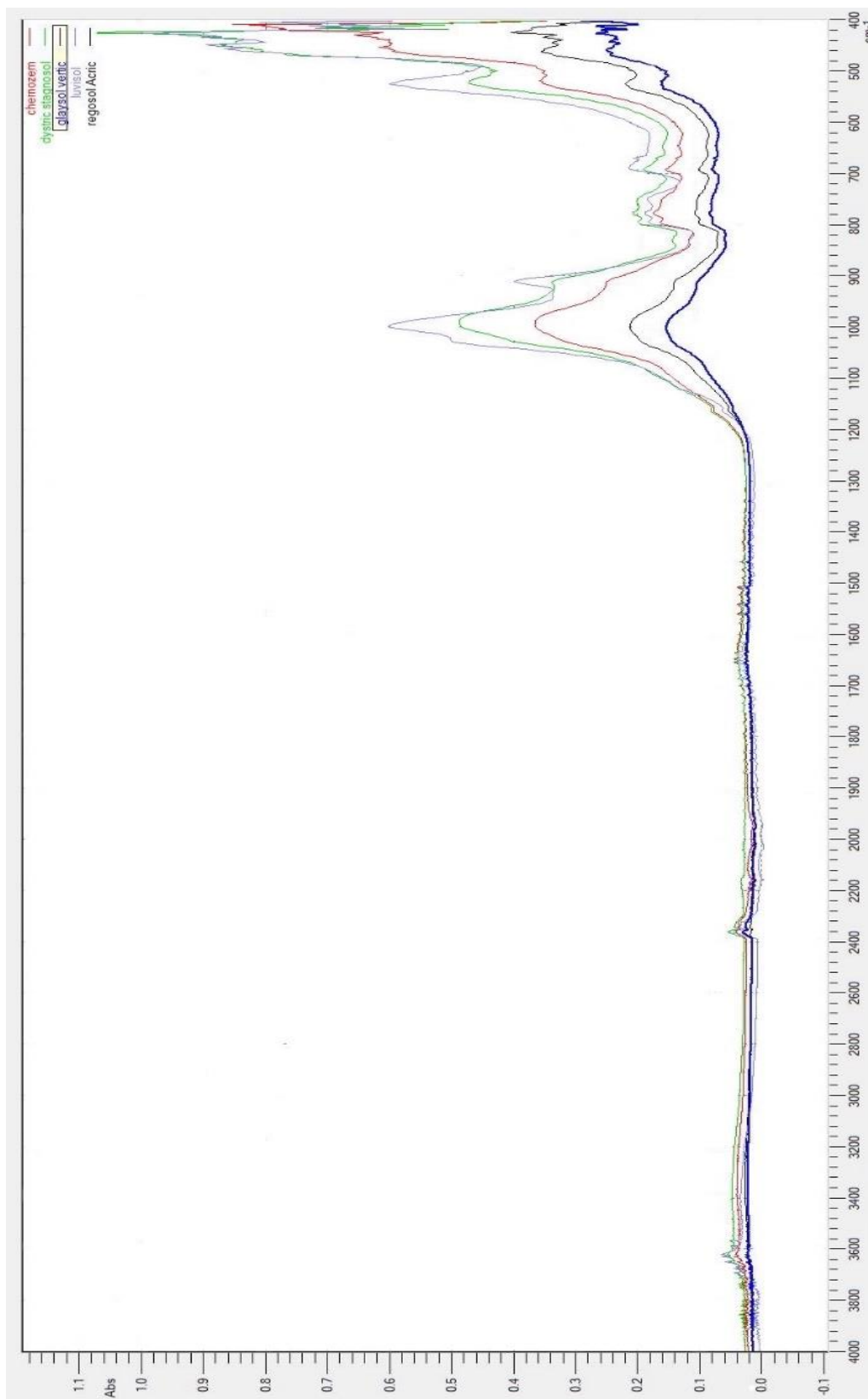
26. Margenot, A. J., Calderón, F. J., Goyne, K., Mukome, F., Parikh, S. J. (2017). Soil analysis, applications of IR and Raman spectroscopies, *Encyclopedia of Spectroscopy and Spectrometry*, 3rd Edition, 2, 448 – 454. Oxford Academic Press.
27. Maynard, J. J., Johnson, M. G. (2018). Applying fingerprint FTIR spectroscopy and chemometrics to assess soil ecosystem disturbance and recovery, *Journal of Soil and Water Conservation*, 73(4), 443 – 451. DOI: <https://doi.org/10.2489/jswc.73.4.443>. – accessed November 2023
28. Metzger, K., Zhang, C., Ward, M., Daly, K. (2020). Mid-infrared spectroscopy as an alternative to laboratory extraction for the determination of lime requirement in tillage soils, *Geoderma*, 364, DOI: <https://doi.org/10.1016/j.geoderma.2020.114171>. – accessed November 2023
29. Nath, D., Laik, R., Meena, V. S., Kumari, V., Singh, S. K., Pramanick, B., Sattar, A. (2022). Strategies to admittance soil quality using mid-infrared (mid-IR) spectroscopy an alternate tool for conventional lab analysis: A global perspective, *Environmental Challenges*, 7, 100469, DOI: <https://doi.org/10.1016/j.envc.2022.100469>. – accessed November 2023
30. Nuzzo, A., Buurman, P., Cozzolino, V., Spaccini, R., Piccolo, A. (2020). Infrared spectra of soil organic matter under a primary vegetation sequence, *Chemical and Biological Technologies in Agriculture*, 7(6), DOI: <https://doi.org/10.1186/s40538-019-0172-1>. – accessed October 2023
31. Obeng, A. S., Dunne, J., Giltrap, M., Tian, F. (2023). Soil organic matter carbon chemistry signatures, hydrophobicity, and humification index following land use change in temperate peat soils. *Heliyon*, 9 (e19347). DOI: <https://doi.org/10.1016/j.heliyon.2023.e19347>. – accessed March 2024
32. Padilla, J. E., Calderón, F. J., Acosta-Martinez, V., Van Pelt, S., Gardner, T., Baddock, M., Zobeck, T. M., Noveron, J. C. (2014). Diffuse-reflectance mid-infrared spectroscopy reveals chemical differences in soil organic matter carried in different size wind eroded sediments. *Aeolian Research*, 14, 99 – 108. DOI: <http://dx.doi.org/10.1016/j.aeolia.2014.06.003>. – accessed March 2024
33. Pärnpuu, S., Astover, A., Tõnutare, T., Penu, P., Kauer, K. (2022). Soil organic matter qualification with FTIR spectroscopy under different soil types in Estonia, *Geoderma Regional*, 28. DOI: <https://doi.org/10.1016/j.geodrs.2022.e00483>. – accessed October 2023
34. Parolo, M. E., Savini, M. C., Loewy, R. M. (2017). Characterization of soil organic matter by FT-IR spectroscopy and its relationship with chlorpyrifos sorption, *Journal of Environmental Management*,. 196, 316 – 322, ISSN 0301 – 4797. DOI: <https://doi.org/10.1016/j.jenvman.2017.03.018>. – accessed October 2023
35. Peltre, C., Bruun, S., Du, C., Thomsen, I. K., Jensen, L. S. (2014). Assessing soil constituents and labile soil organic carbon by mid-infrared photoacoustic spectroscopy. *Soil Biology and Biochemistry*, 77, 41 – 50. DOI: <https://doi.org/10.1016/j.soilbio.2014.06.022>. – accessed March 2024
36. Rial, M., Martínez Cortizas, A., and Rodríguez-Lado, L. (2015). Mapping soil organic carbon content using spectroscopic and environmental data: A case study in acidic soils from NW Spain. *Science of the Total Environment*. DOI: <https://doi.org/10.1016/j.scitotenv.2015.08.088>. – accessed March 2024

37. Robertson, A. H. J., Hill, H. R., Main, A. M. (2013). Analysis of soil in the field using portable FTIR. *International Workshop of Soil Spectroscopy: the present and future of Soil Monitoring*, FAO HQ. The James Hutton Institute.
38. Santos, U. J., Demattê, J. A. M., Menezes, R. S. C., Dotto, A. C., Barbosa Guimarães, C. C., Rodrigues Alves, B. J. R., Sá Barretto Sampaio E. V. S. (2020). Predicting carbon and nitrogen by visible near-infrared (Vis-NIR) and mid-infrared (MIR) spectroscopy in soils of Northeast Brazil. *Geoderma Regional*, 23, e00333. DOI: <https://doi.org/10.1016/j.geodrs.2020.e00333>. – accessed May 2024
39. Šestak, I., Mesić, M., Zgorelec, Ž., Perčin, A., Stupnišek, I. (2018). Visible and near infrared reflectance spectroscopy for field-scale assessment of Stagnosols properties. *Plant, Soil and Environment*, 64(6), 276-282. DOI: <https://doi.org/10.17221/220/2018-PSE>. – accessed July 2024
40. Šestak, I., Mihaljevski Boltek, L., Mesić, M., Zgorelec, Ž., Perčin, A. (2019). Hyperspectral sensing of soil pH, total carbon and total nitrogen content based on linear and non-linear calibration methods. *Journal of Central European Agriculture*, 20(1), 504-523. DOI: <https://doi.org/10.5513/JCEA01/20.1.2158>. – accessed July 2024
41. Šestak, I., Pereira, P., Telak, L. J., Perčin, A., Hrelja, I., Bogunović, I. (2022). Soil Chemical Properties and Fire Severity Assessment Using VNIR Proximal Spectroscopy in Fire-Affected Abandoned Orchard of Mediterranean Croatia. *Agronomy*, 12(1), 129. DOI: <https://doi.org/10.3390/agronomy12010129>. – accessed July 2024
42. Šoštarić, M., Zgorelec, Ž., Babić, D. et al. (2017). Radioactivity of Selected Agricultural Soils in Croatia: Effects of Soil Properties, Soil Management, and Geological Parameters. *Water Air Soil Pollution*, 228, 218. DOI: <https://doi.org/10.1007/s11270-017-3398-1>. – accessed October 2023
43. Škorić, A. (1982). Priručnik za pedološka istraživanja (engl. Handbook for pedological research). Fakultet poljoprivrednih znanosti, Zagreb. – accessed October 2023
44. Teong, I. T., Felix, N. L. L., Mohd, S., Sulaeman, A. (2016). Characterization of Soil Organic Matter in Peat Soil with Different Humification Levels using FTIR, IOP Conference Series: Materials Science and Engineering, 136, 1, 012010. DOI: 10.1088/1757-899X/136/1/012010. – accessed March 2024
45. Tinti, A., Tugnoli, V., Bonora, S., Francioso, O. (2015). Recent applications of vibrational mid-infrared (IR) spectroscopy for studying soil components: A review. *Journal of Central European Agriculture*, 16(1), 1 – 22. DOI: <https://doi.org/10.5513/JCEA01/16.1.1535>. – accessed October 2023
46. United Nations (2015). Transforming our world: The 2030 Agenda for Sustainable Development.
47. University of California (2023). FTIR indicators of soil organic matter quality across a landscape of organic management, Jackson Soil and Root Ecology Lab, Division of Agriculture and Natural Resources.
48. Volkov, D. S., Rogova, O. B., Proskurnin, M. A. (2021). Organic Matter and Mineral Composition of Silicate Soils: FTIR Comparison Study by Photoacoustic, Diffuse Reflectance, and Attenuated Total Reflection Modalities, *Agronomy*, 11, 1879. DOI: <https://doi.org/10.3390/agronomy11091879>. – accessed October 2023

49. Wang, J., Zhen, J., Hu, W., Chen, S., Lizaga, I., Zeraatpisheh, M., Yang, X. (2023). Remote sensing of soil degradation: Progress and perspective, *International Soil and Water Conservation Research*, 11, 429 – 454. DOI: <https://doi.org/10.1016/j.iswcr.2023.03.002>. – accessed October 2023
50. Williams, M. I., Farr, C. L., Page–Dumroese, D. S., Connolly, S. J. (2020). Soil Management and Restoration, In *Forest and Rangeland Soils of the United States Under Changing Conditions*, ISBN: 978-3-030-45215-5. – accessed November 2023
51. WRB-FAO (2015). IUSS Working Group WRB - World Reference Base for Soil Resources 2014 update 2015. International soil classification system for naming soils and creating legends for soil maps. *World Soil Resources Reports No. 106*, Food and Agriculture Organization of UN. DOI: <https://www.fao.org/3/i3794en/I3794en.pdf>. – accessed November 2023
52. Xing, Z., Du, C., Tian, K., Ma, F., Shen, Y., Zhou, J. (2016). Application of FTIR-PAS and Raman spectroscopies for the determination of organic matter in farmland soils. *Talanta*, 156 – 157, 197 – 205. DOI: <https://doi.org/10.1016/j.talanta.2016.05.076>. – accessed November 2023
53. Xing, Z., Du, C., Shen, Y., Ma, F., Zhou, J. (2021). A method combining FTIR-ATR and Raman spectroscopy to determine soil organic matter: Improvement of prediction accuracy using competitive adaptive reweighted sampling (CARS). *Computers and Electronics in Agriculture*, 191, 106549. DOI: <https://doi.org/10.1016/j.compag.2021.106549>. – accessed May 2024
54. Xu, X., Du, C., Ma, F., Shen, Y., Zhou, J. (2020). Forensic soil analysis using laser-induced breakdown spectroscopy (LIBS) and Fourier transform infrared total attenuated reflectance spectroscopy (FTIR-ATR): Principles and case studies. *Forensic Science International*. DOI: <http://dx.doi.org/10.1016/j.forsciint.2020.110222>. – accessed May 2024
55. Zebec, V., Rastija, D., Lončarić, Z., Bensa, A., Popović, B., Ivezić, V. (2017). Comparison of Chemical Extraction Methods for Determination of Soil Potassium in Different Soil Types, *Eurasian Soil Science*, 50(12), 1420 – 1427. DOI: <https://doi.org/10.1134/S1064229317130051>. – accessed March 2024

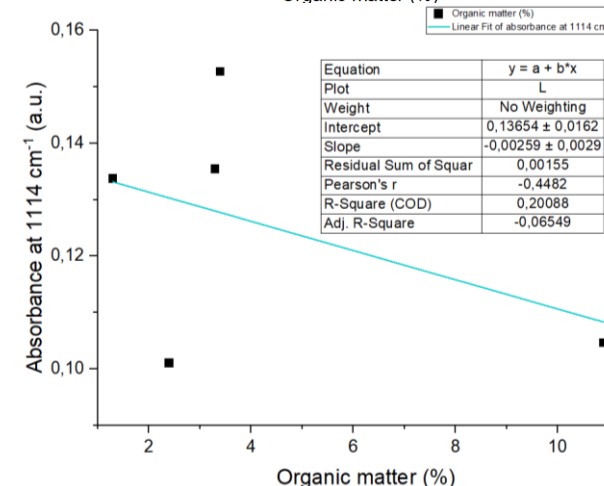
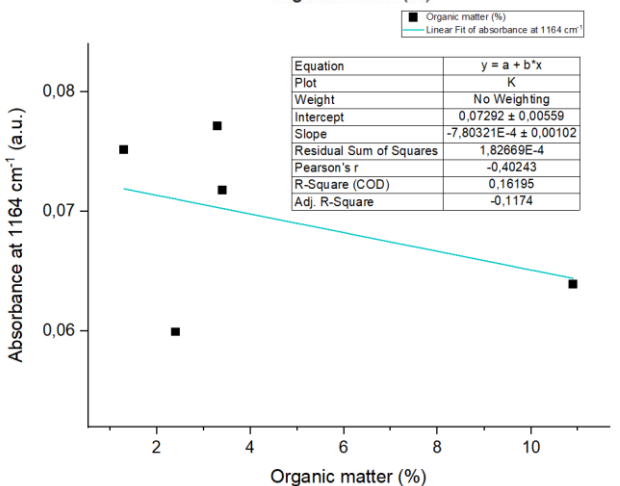
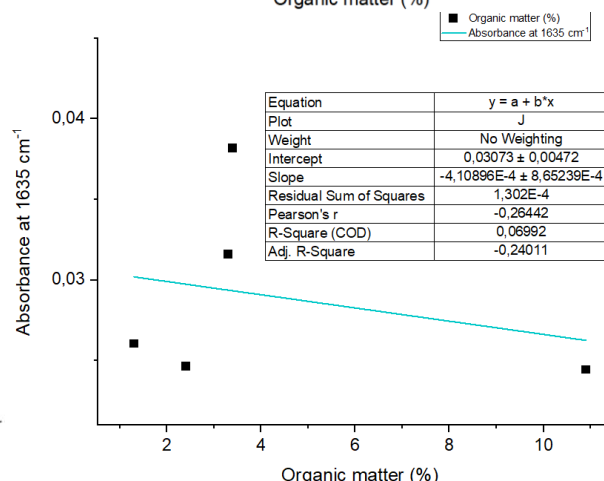
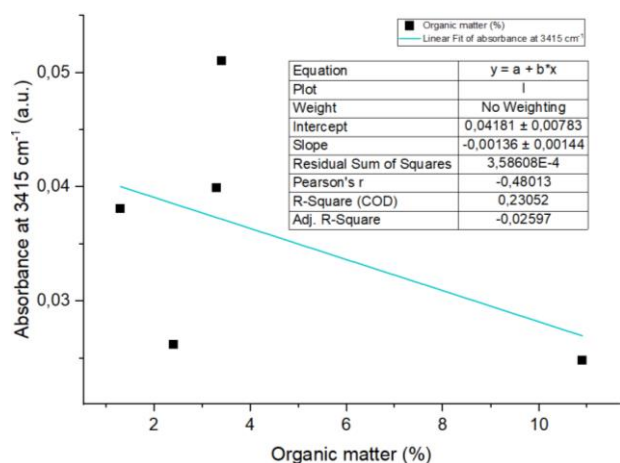
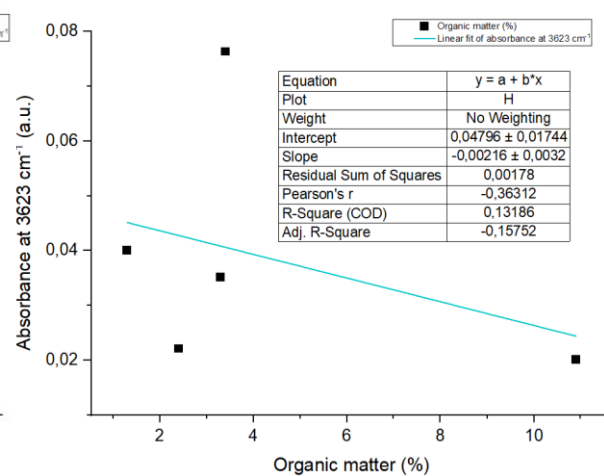
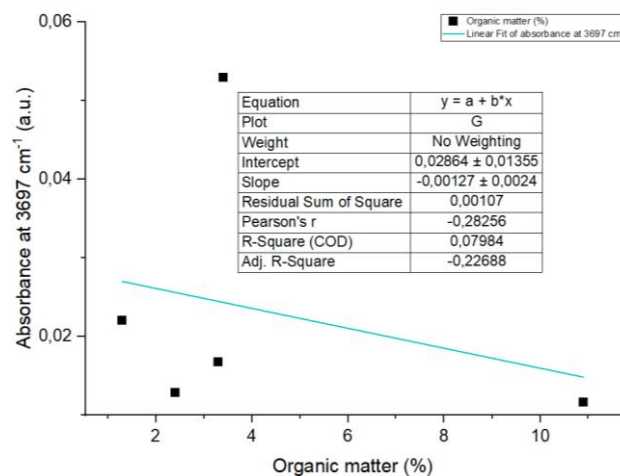
## 8. Appendices

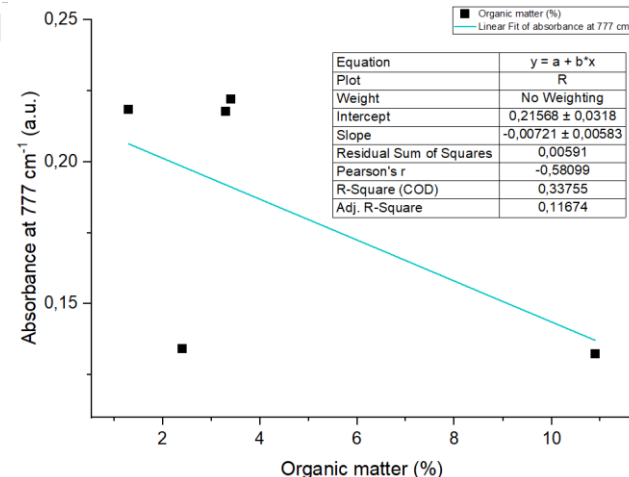
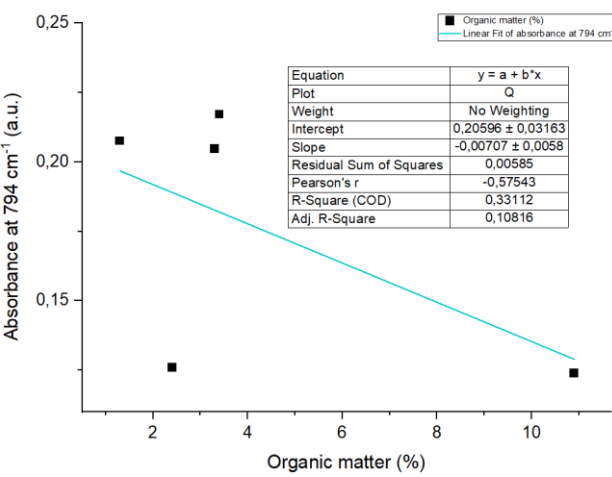
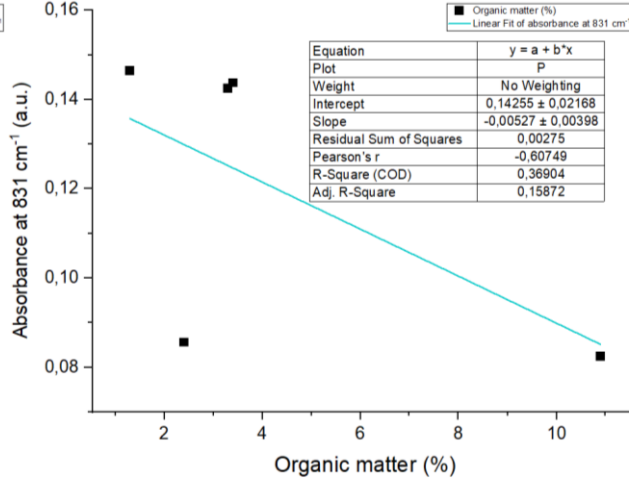
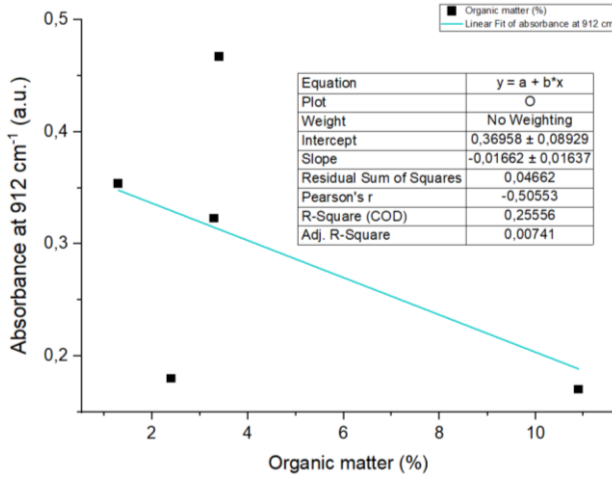
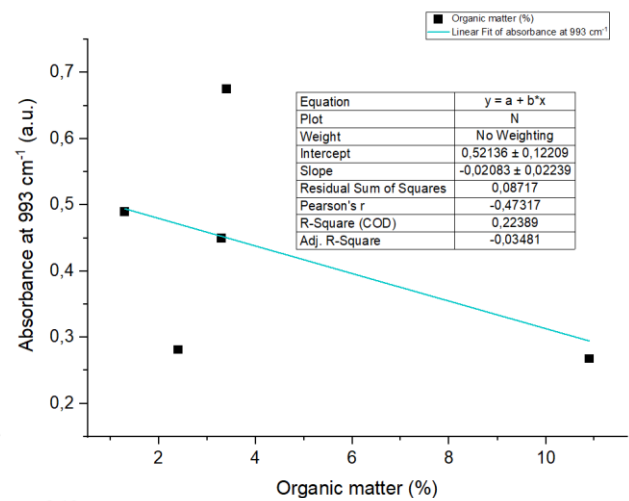
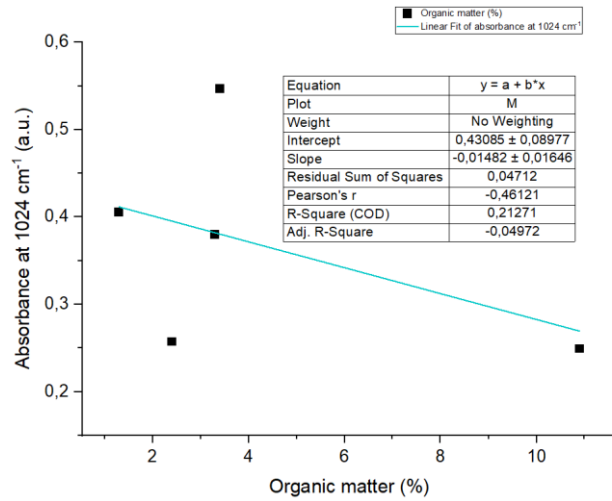
### 8.1 Average FTIR-ATR spectra obtained by Shimadzu IRTracer 100 Spectrometer.

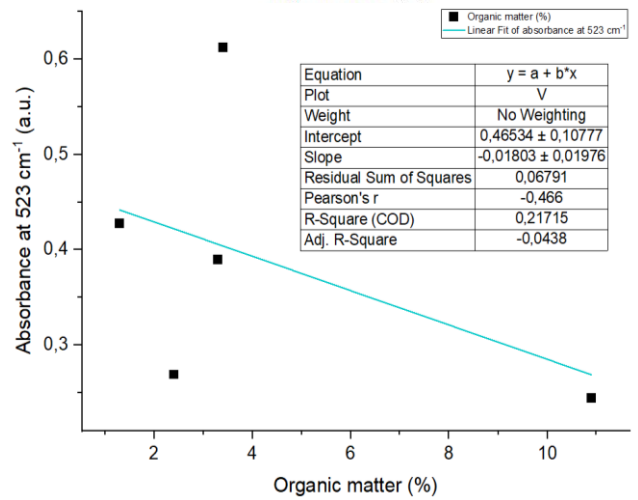
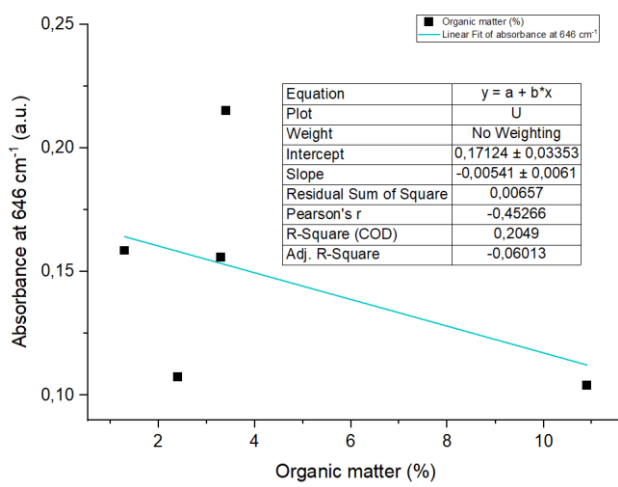
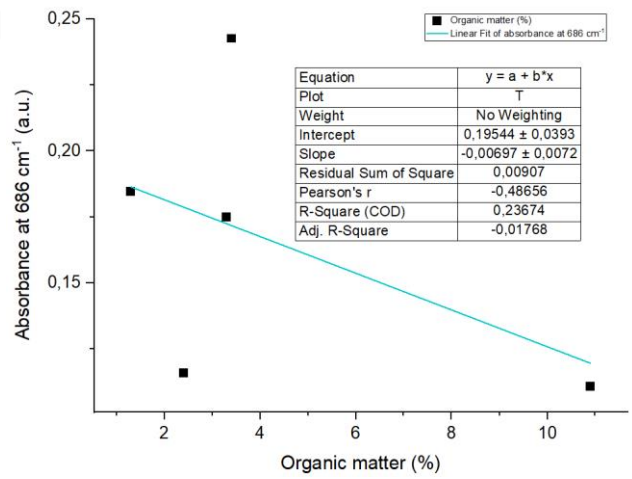
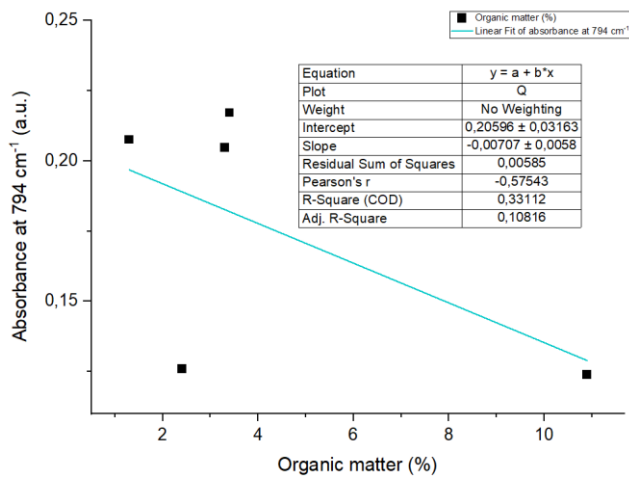




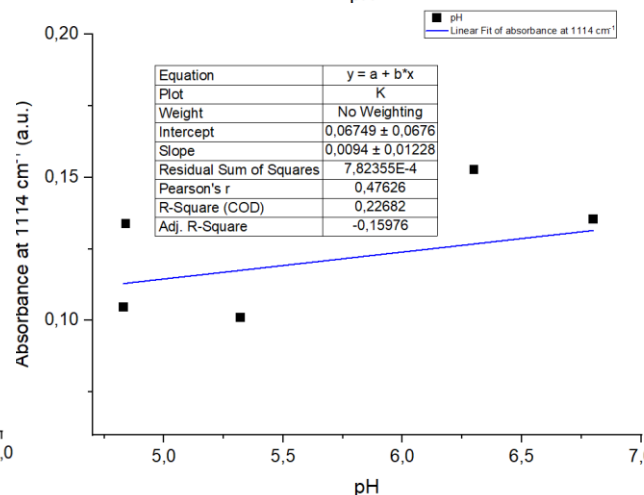
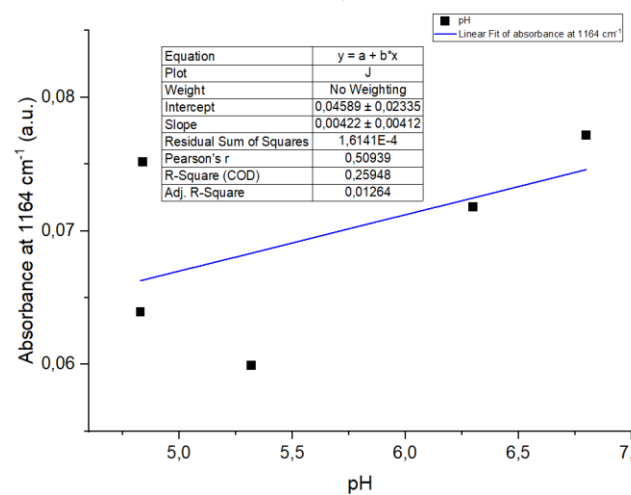
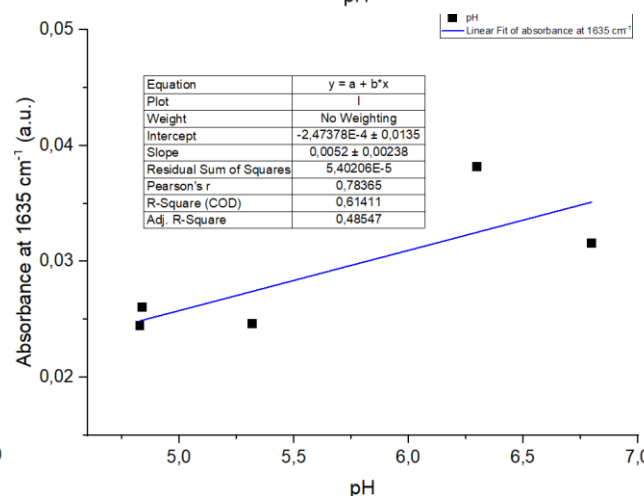
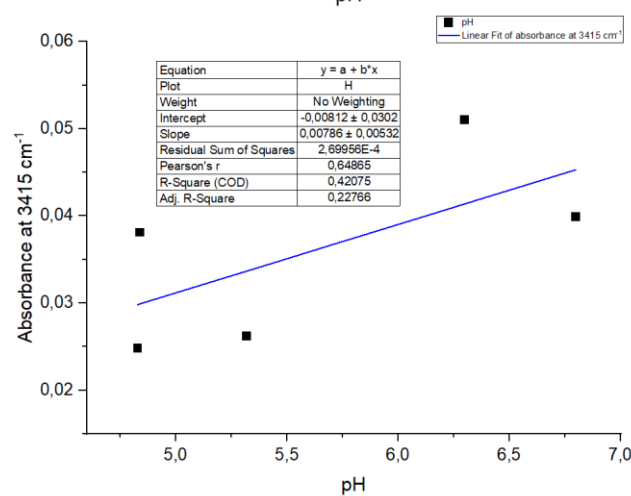
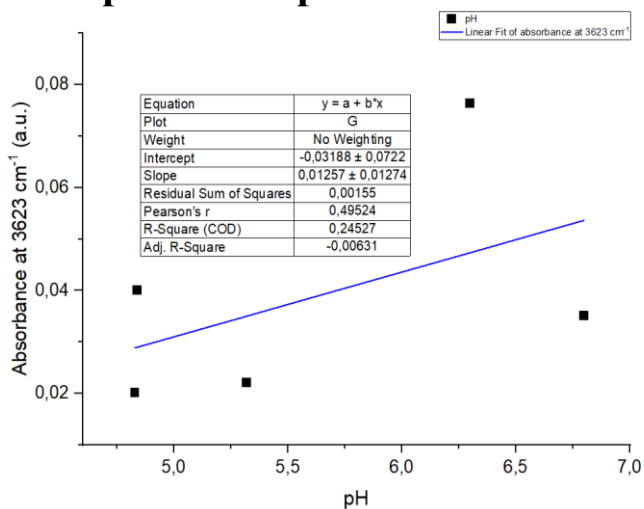
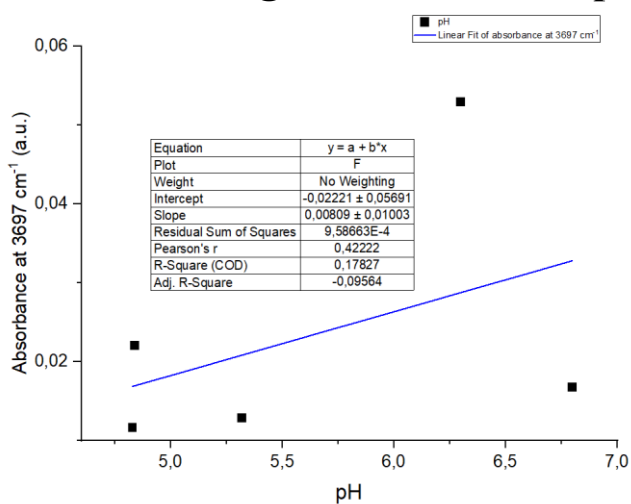
## 8.2 Linear Regression of FTIR spectral peaks and Organic Matter Content (OM%).

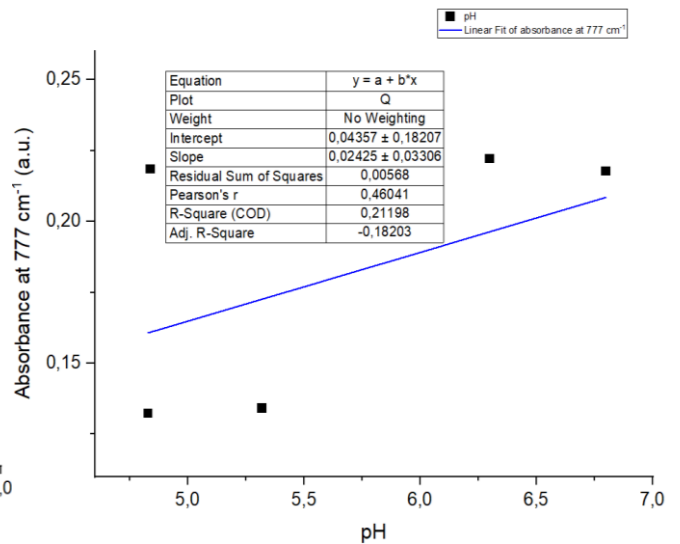
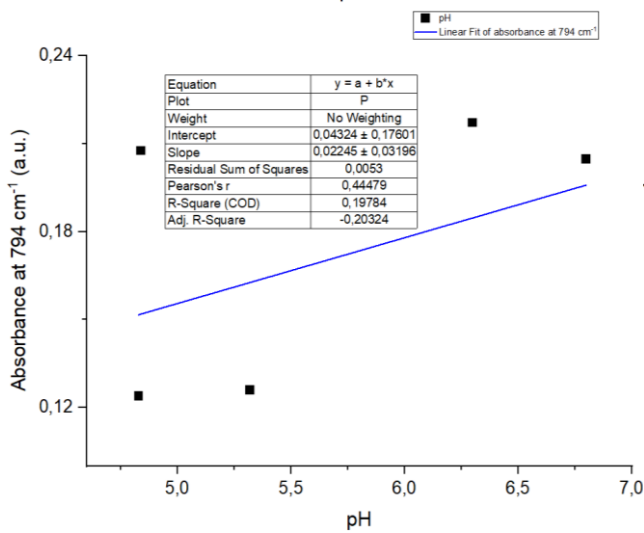
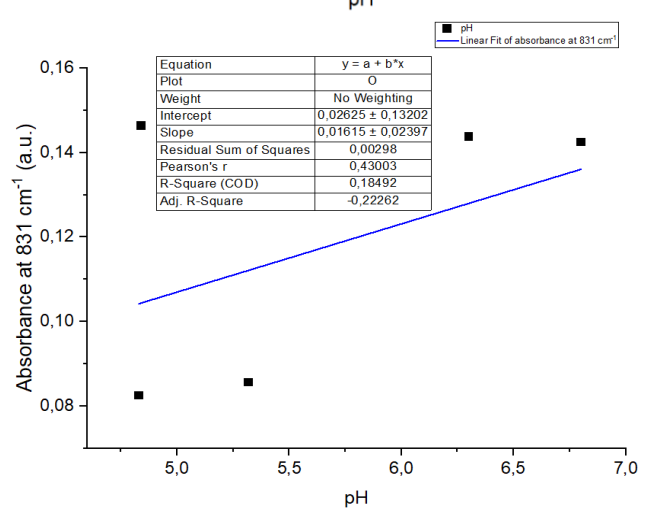
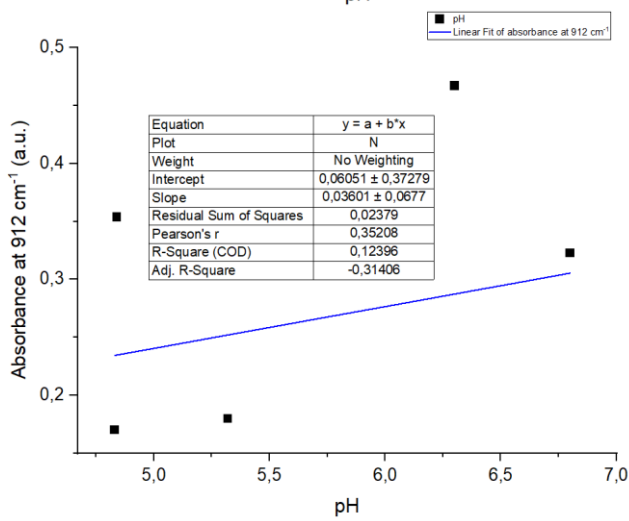
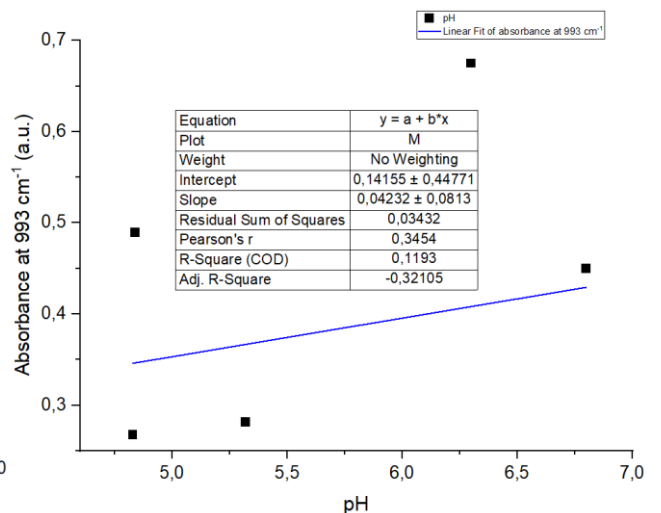
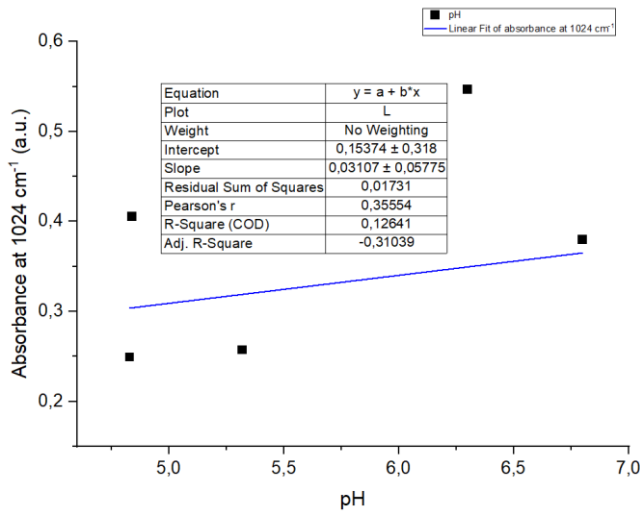


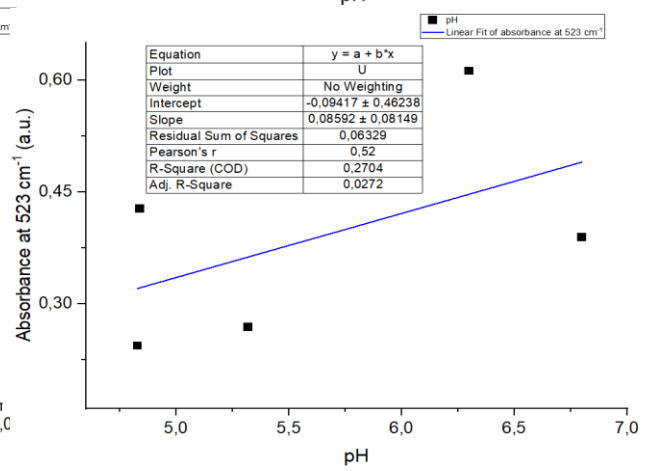
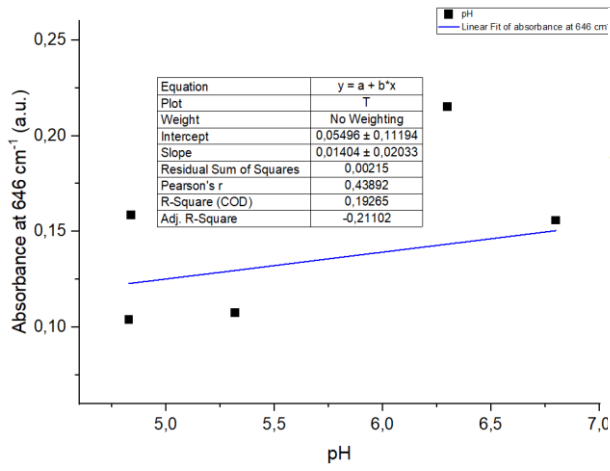
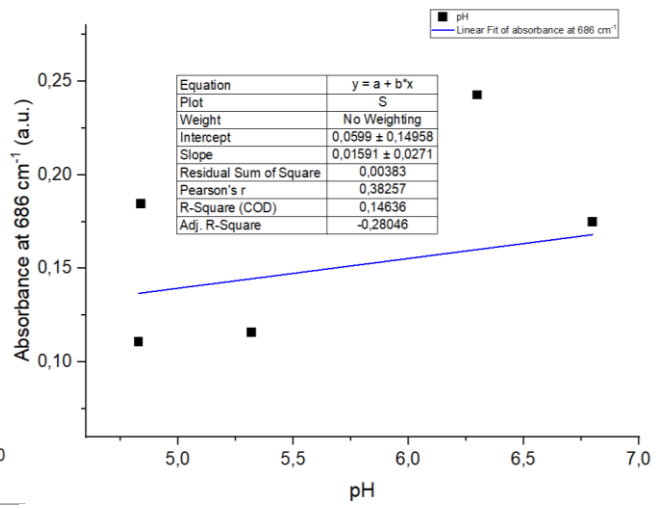
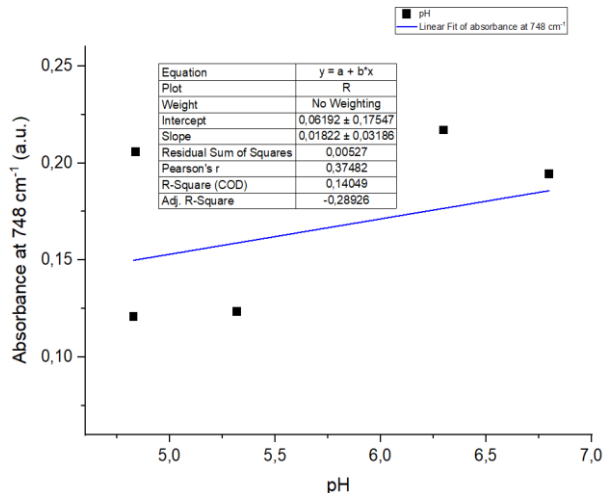




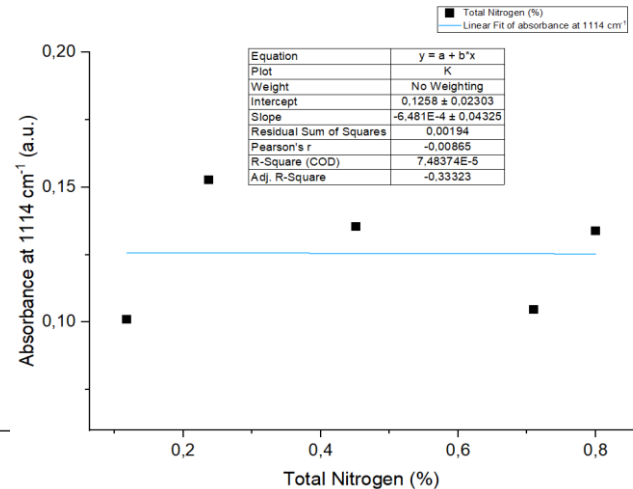
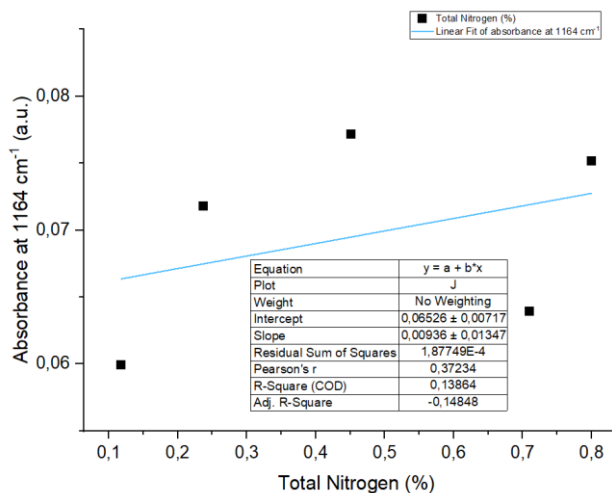
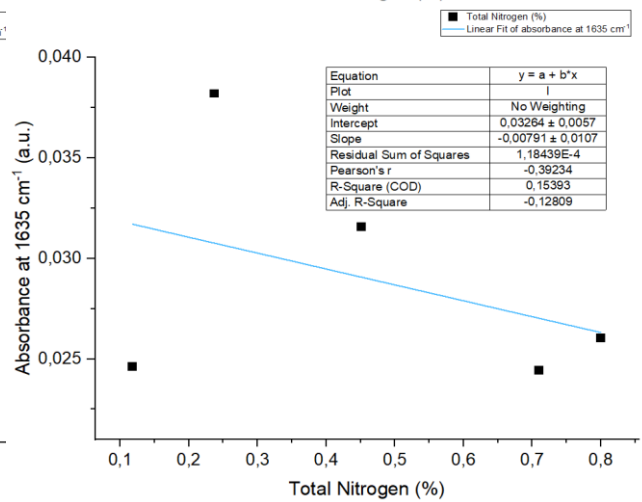
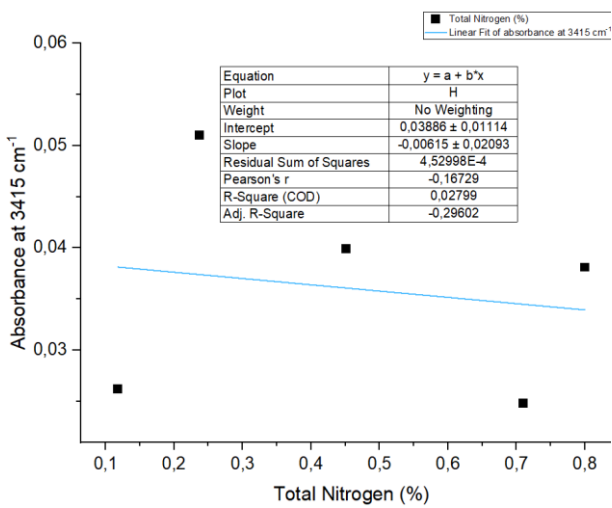
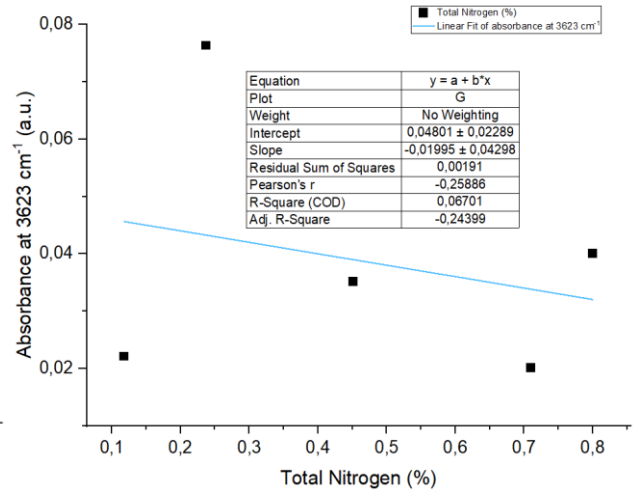
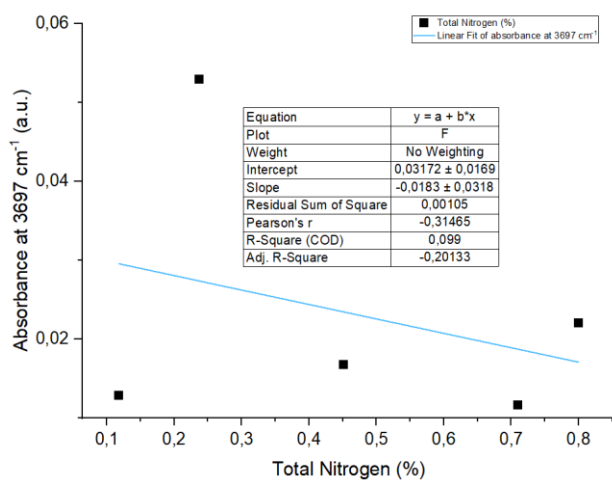
### 8.3 Linear Regression of FTIR spectral peaks and pH.

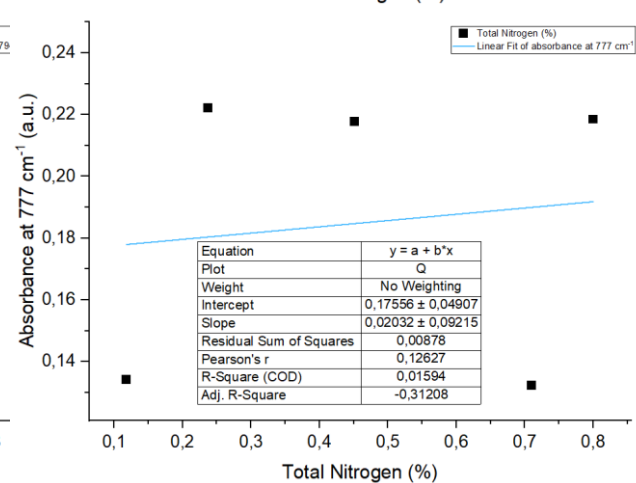
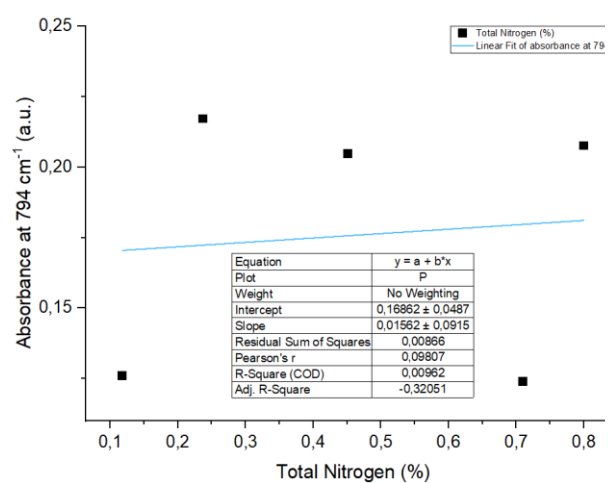
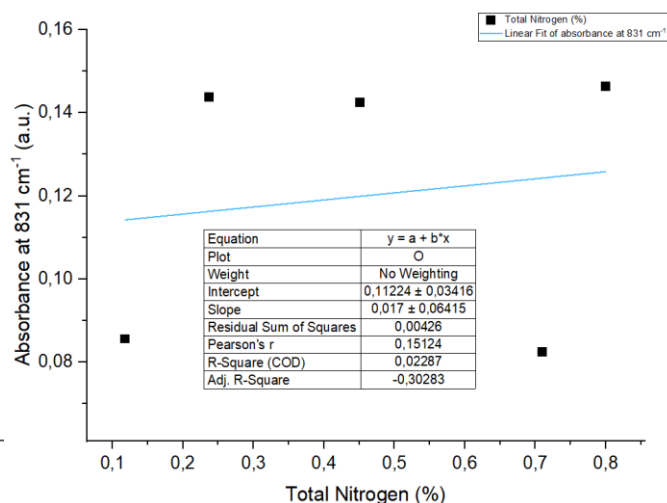
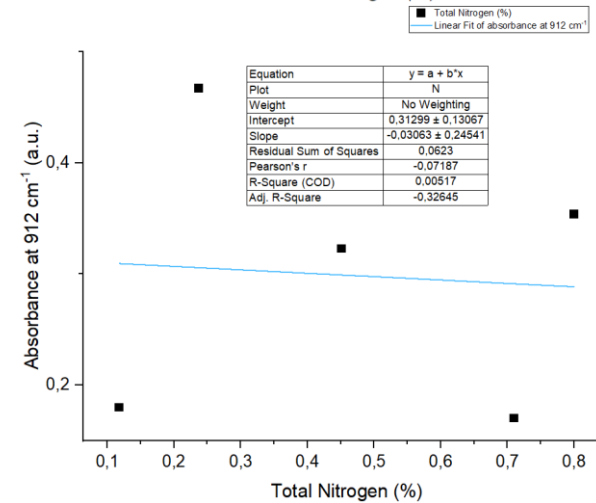
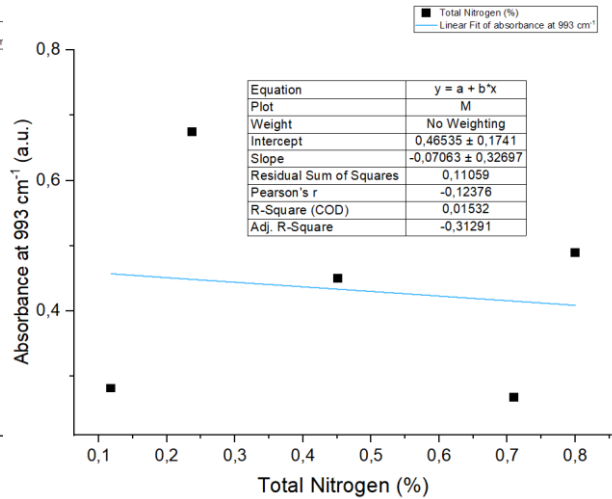
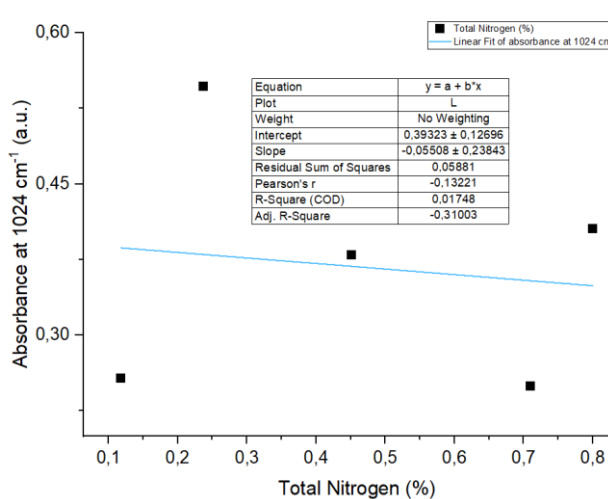




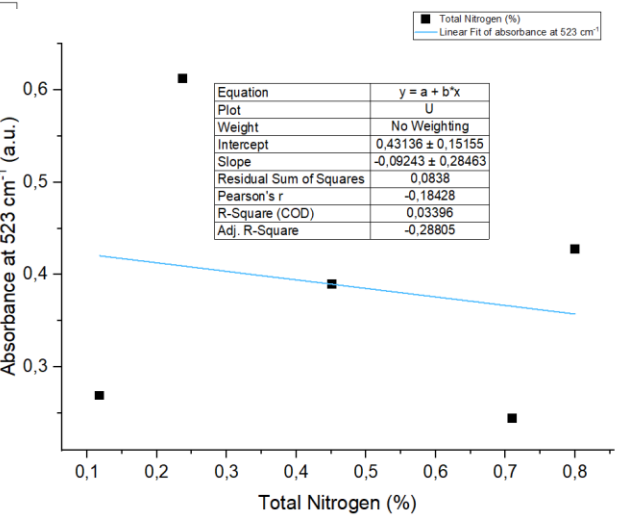
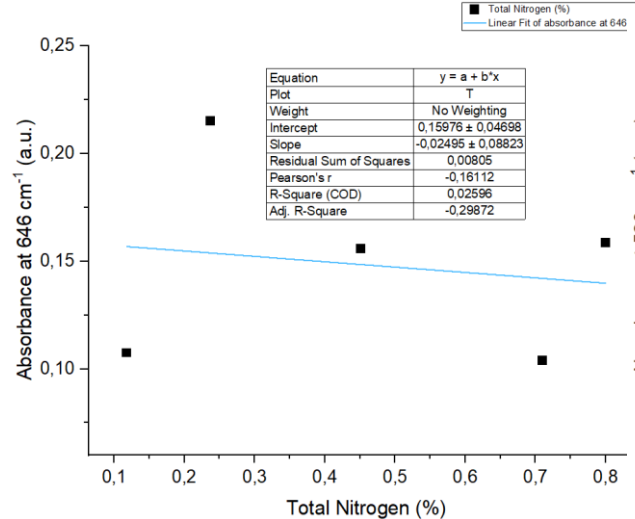
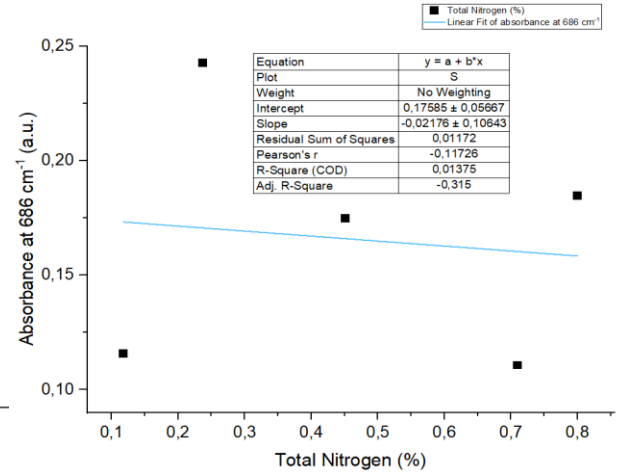
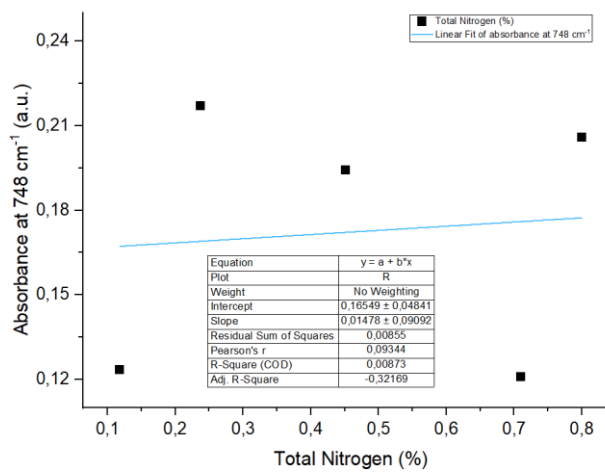


## 8.4 Linear Regression of FTIR spectral peaks and Total Nitrogen Content (TN%).

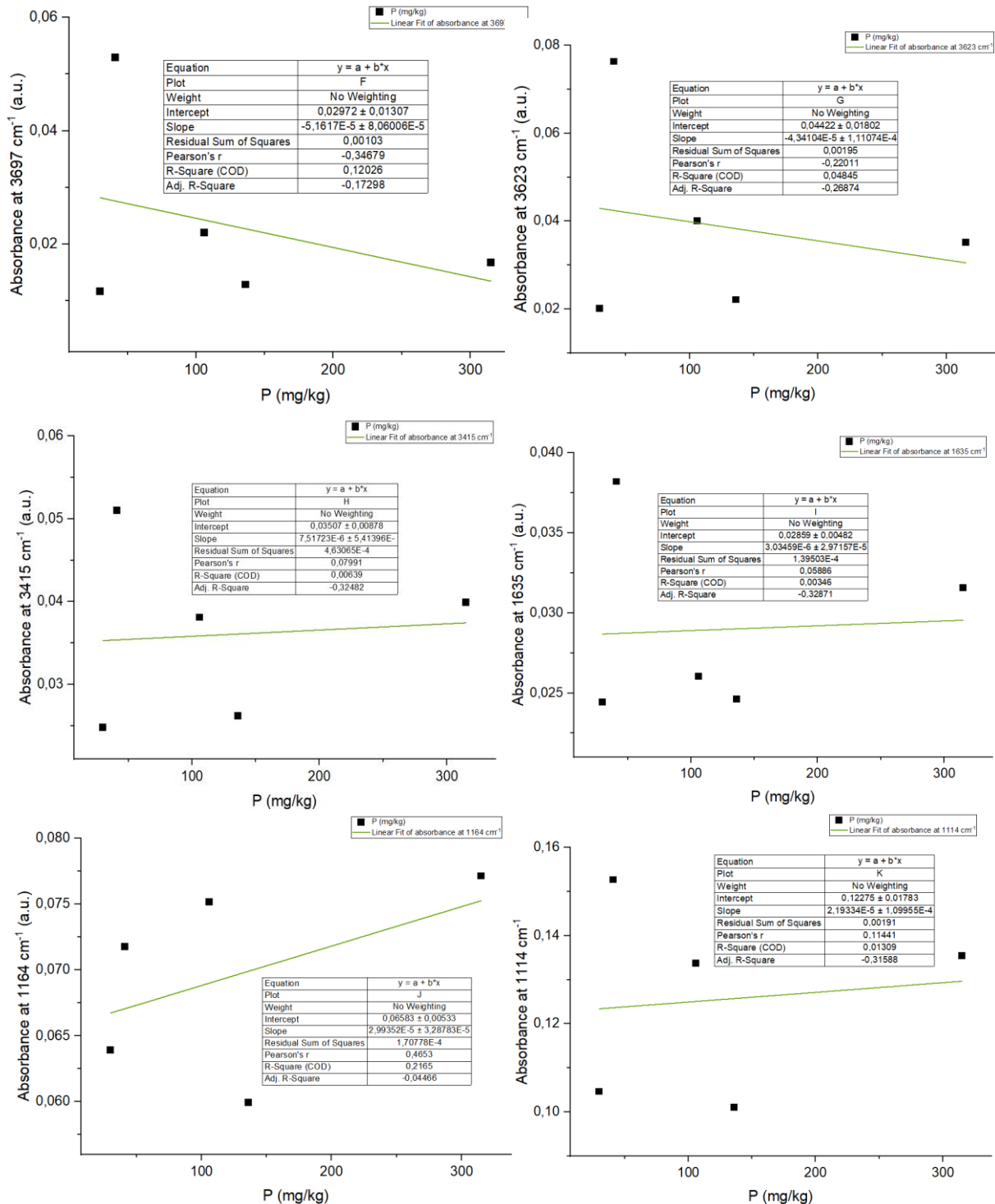


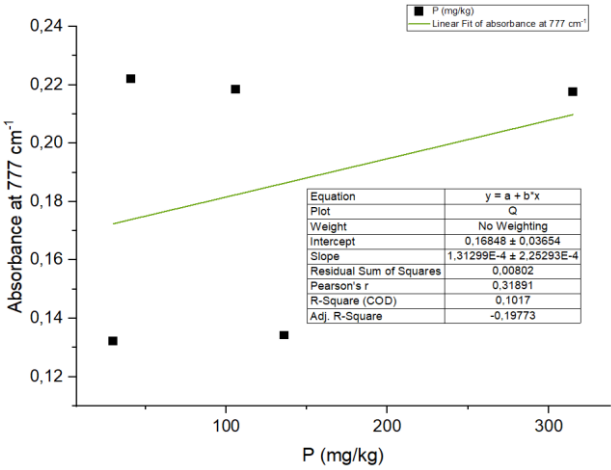
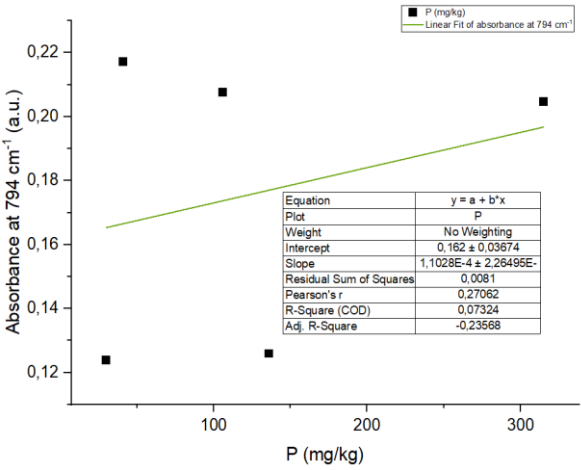
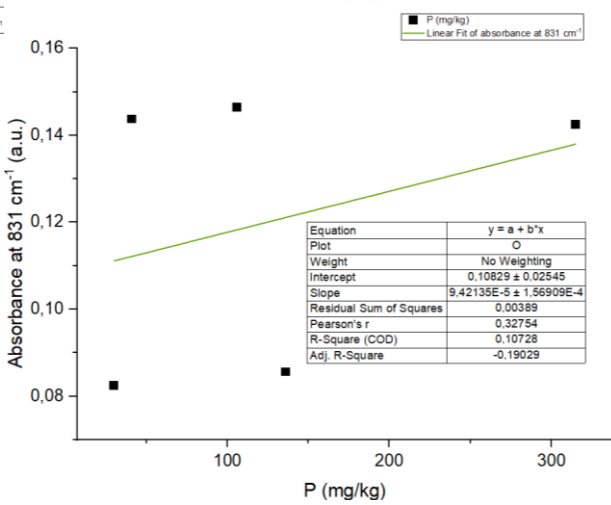
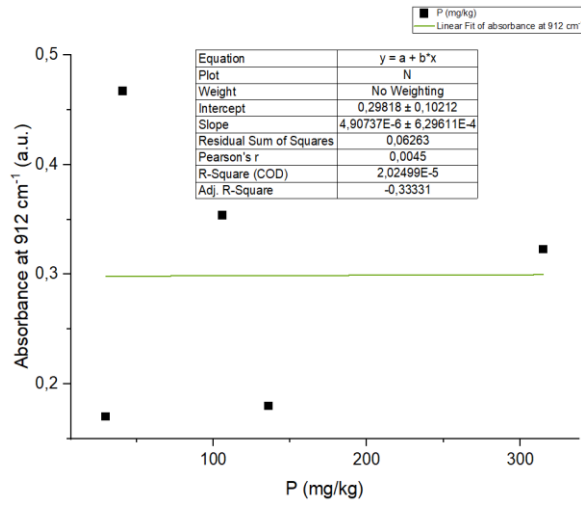
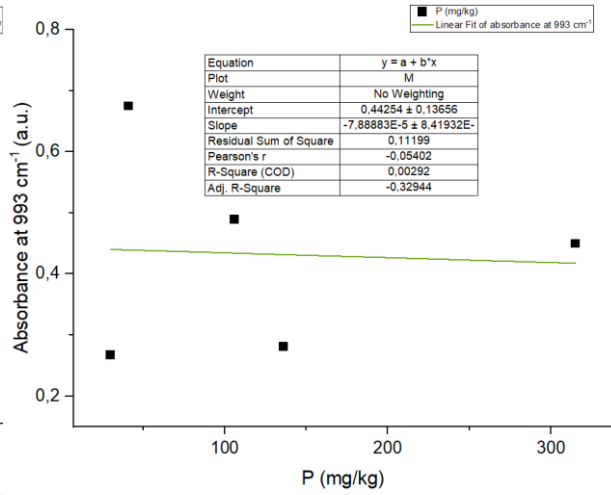
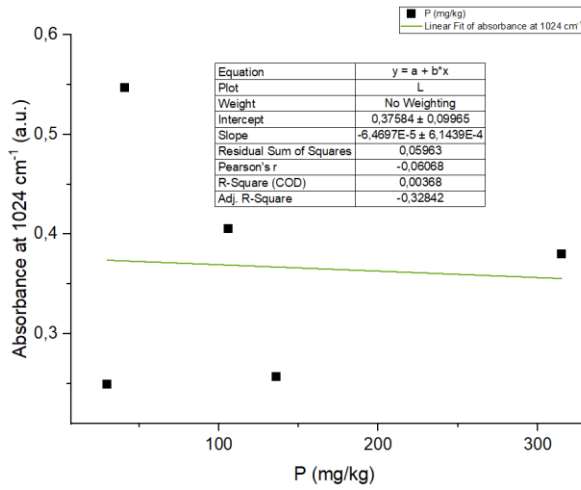


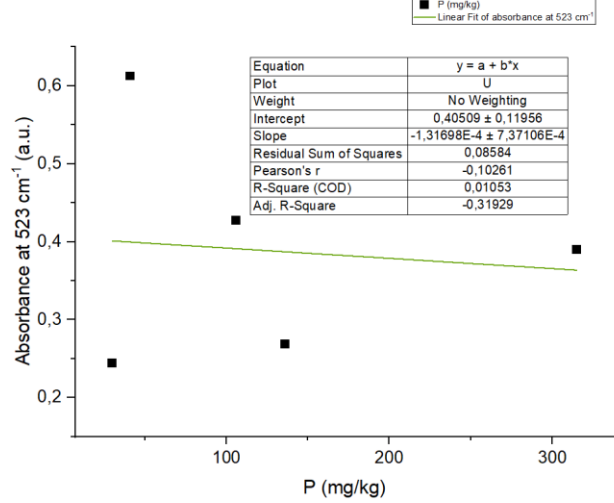
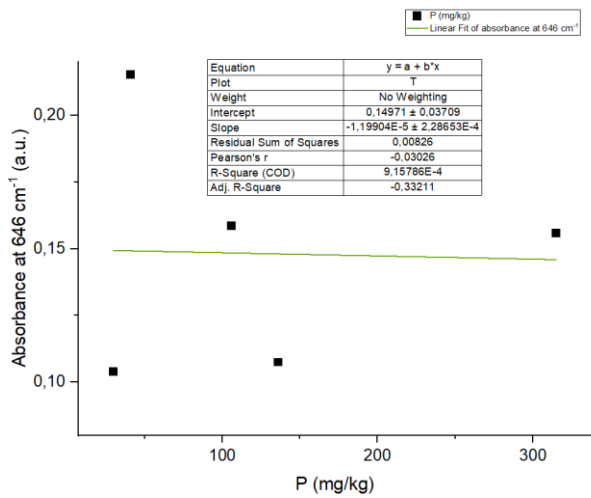
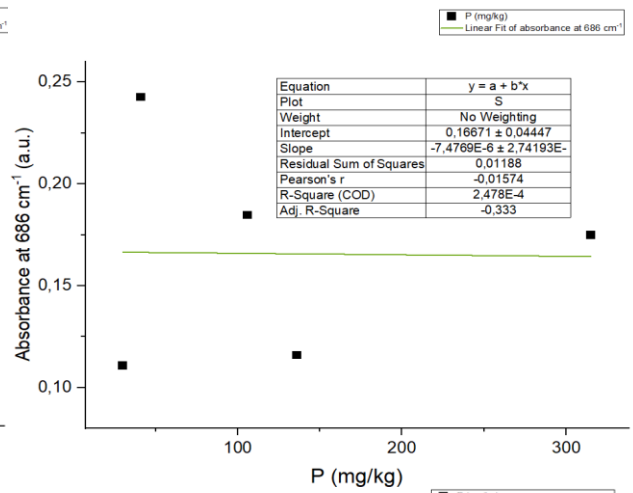
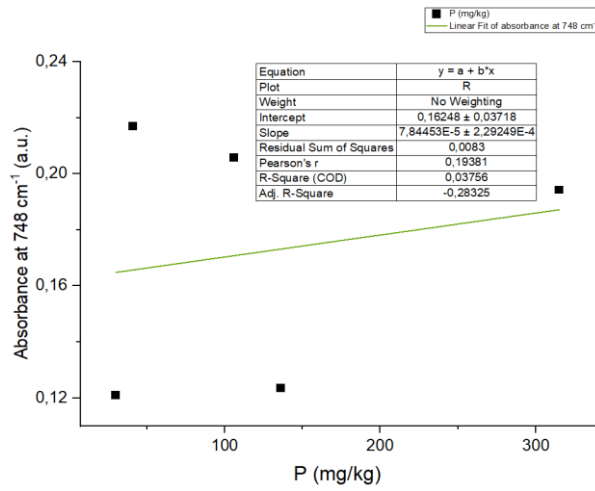




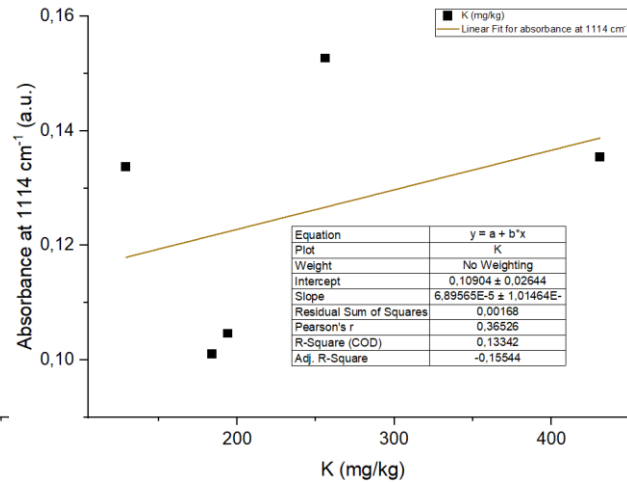
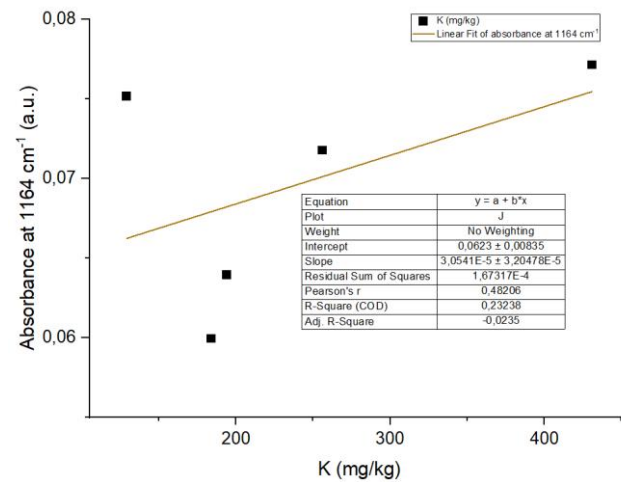
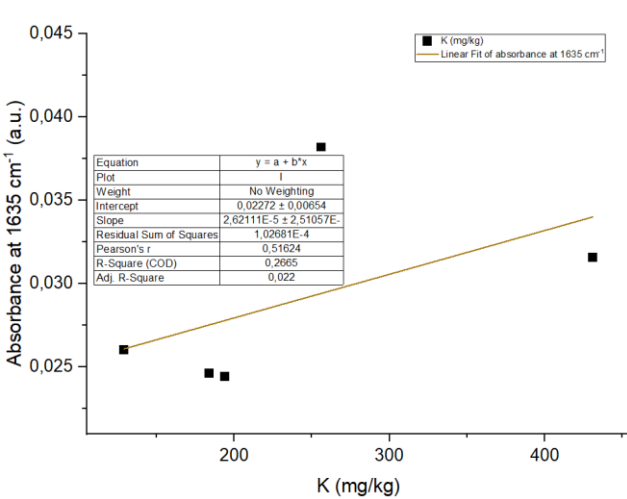
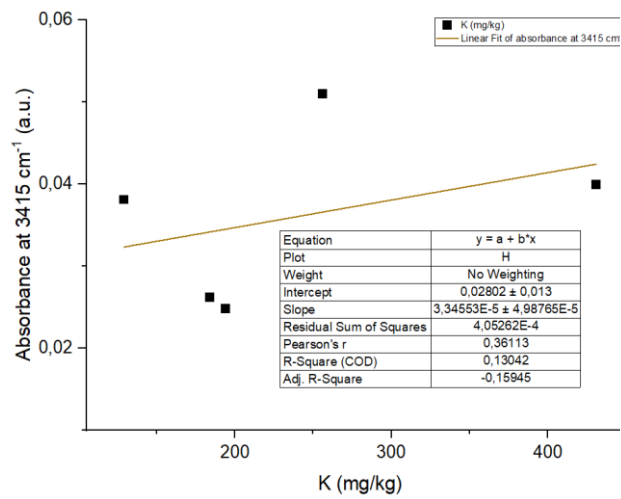
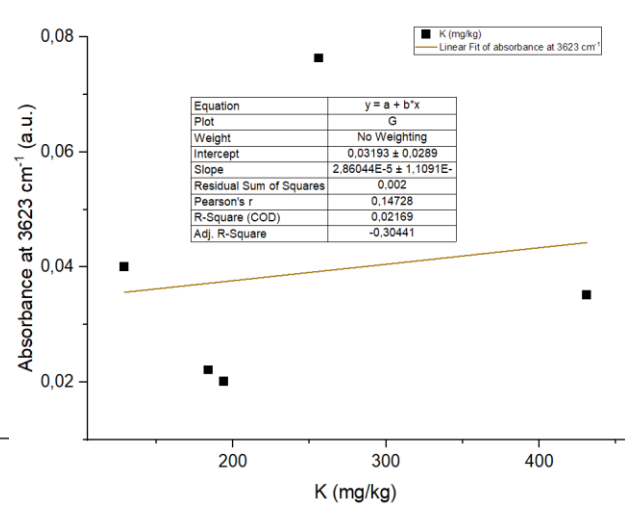
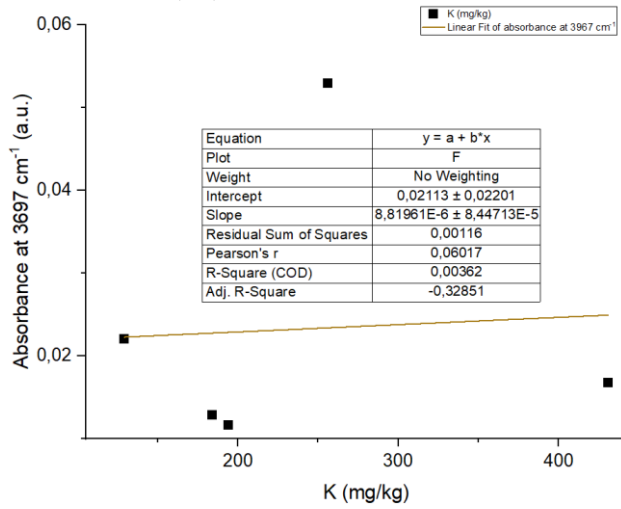
## 8.5 Linear Regression of FTIR spectral peaks and Phosphorus Content (P).

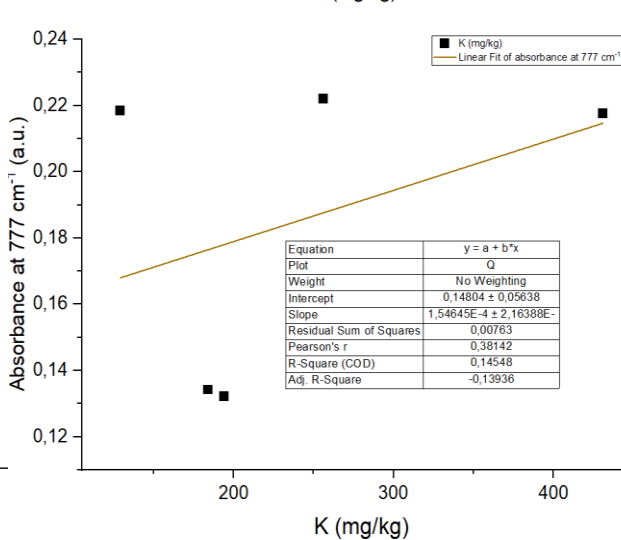
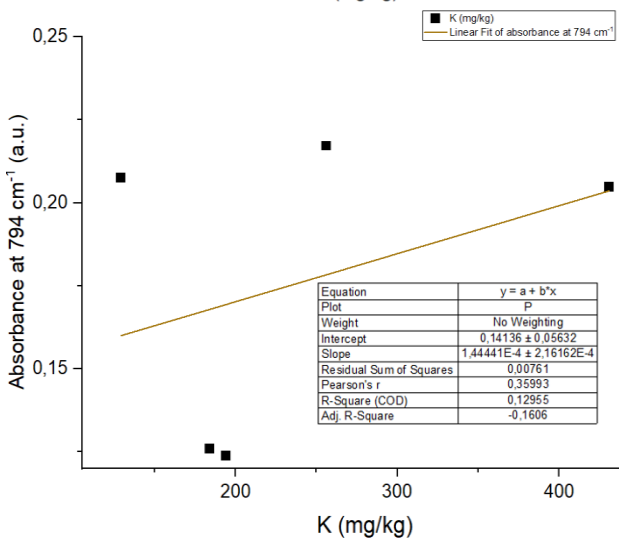
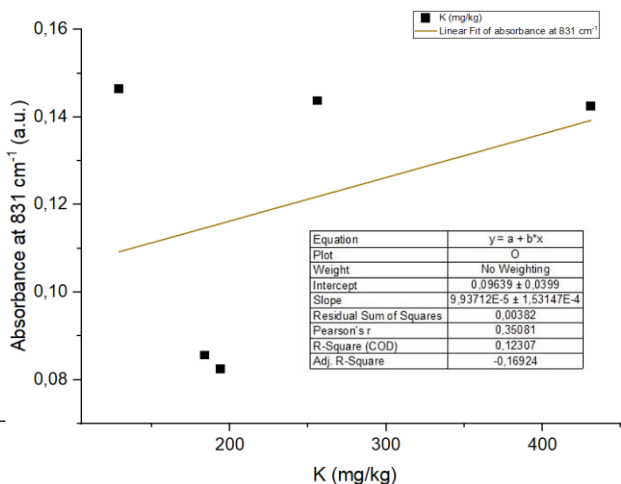
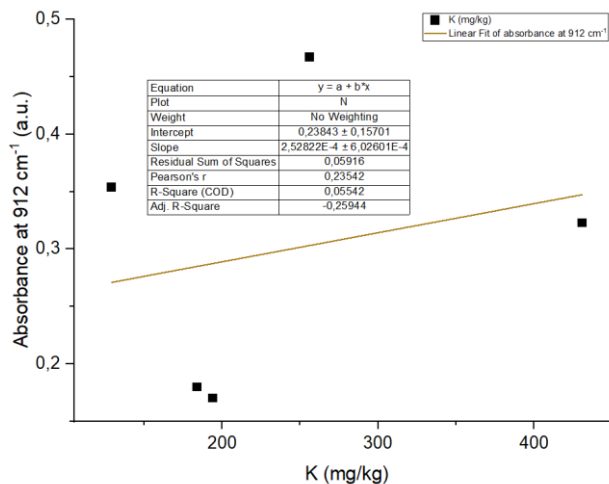
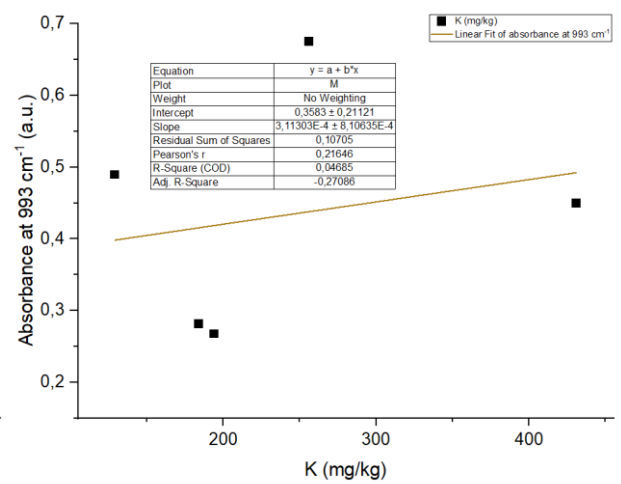
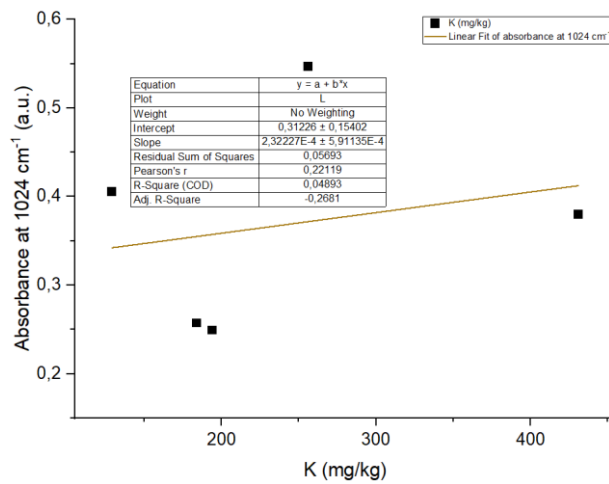


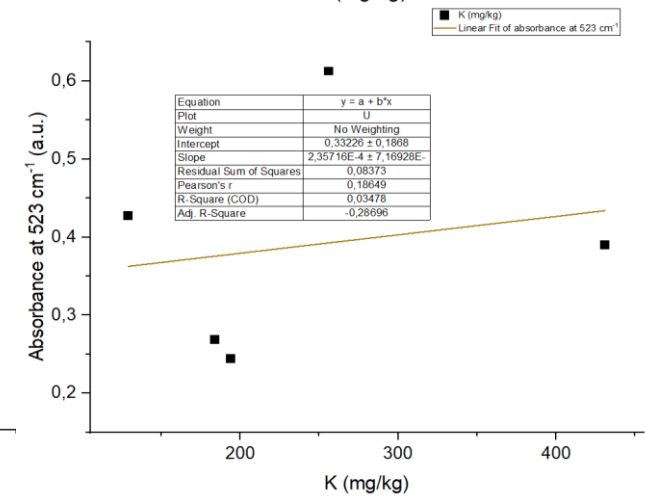
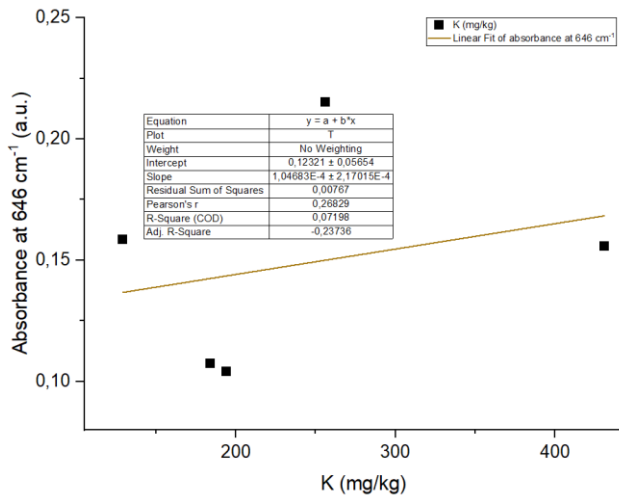
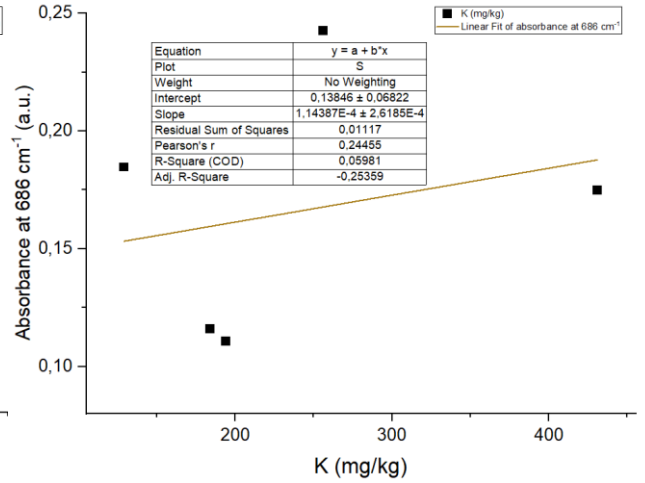
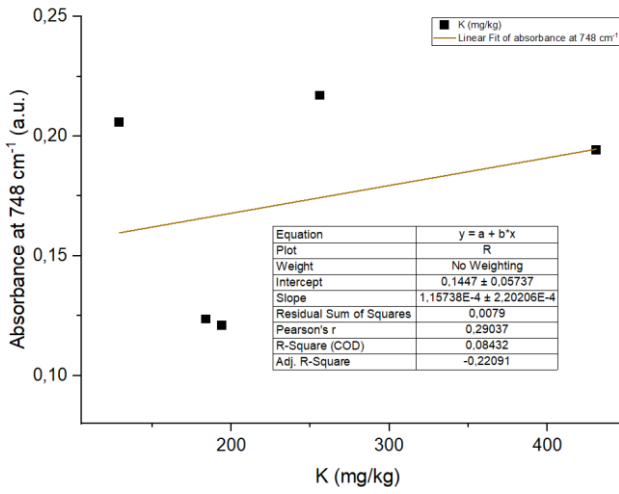




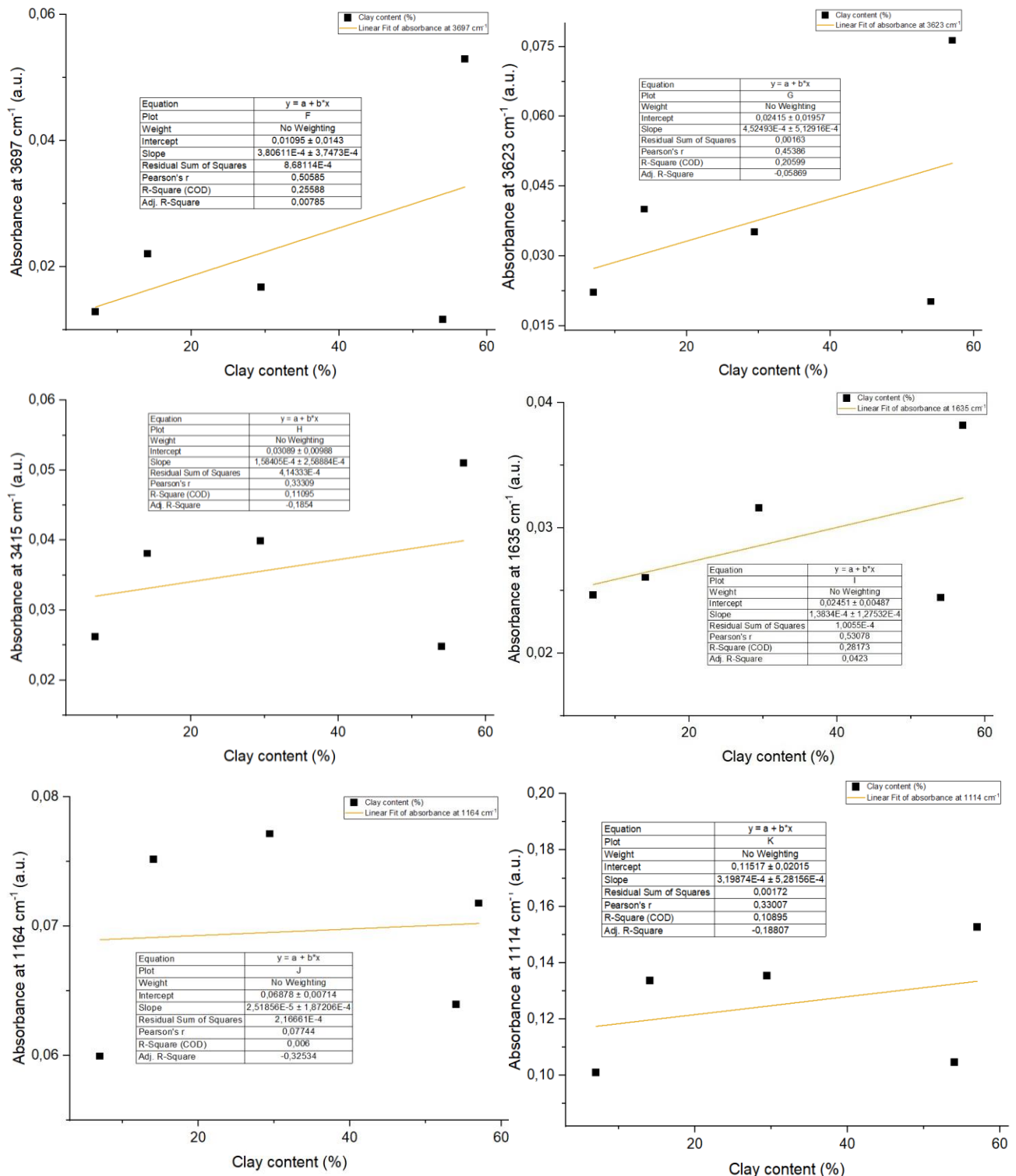
## 8.6 Linear Regression of FTIR spectral peaks and Potassium Content (K).



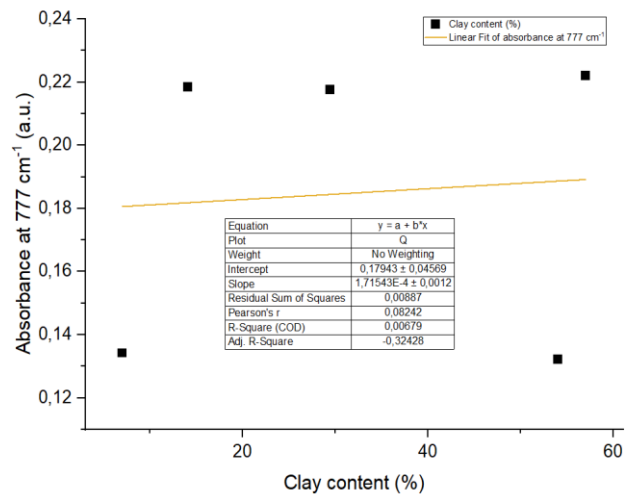
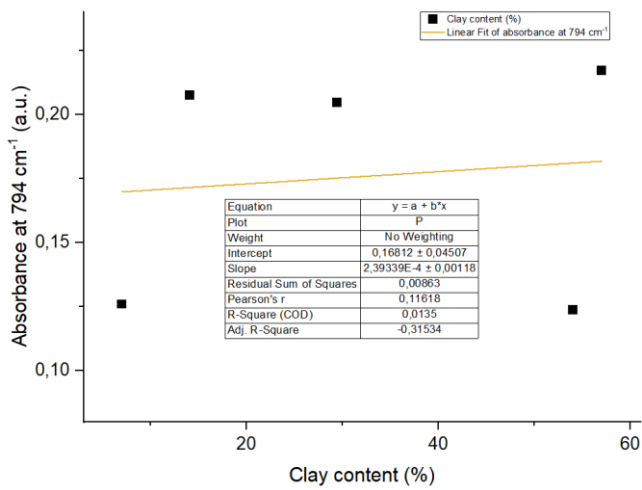
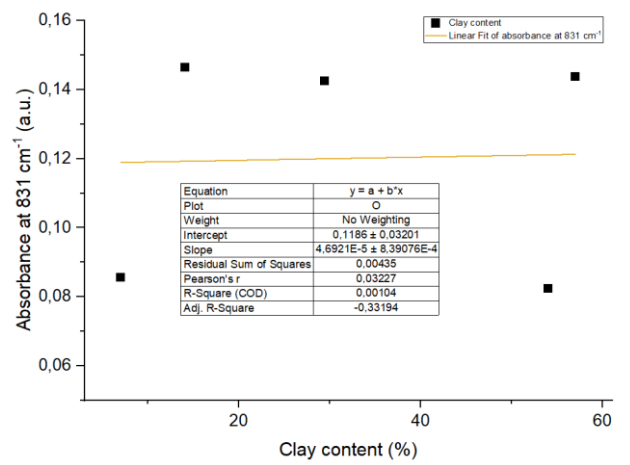
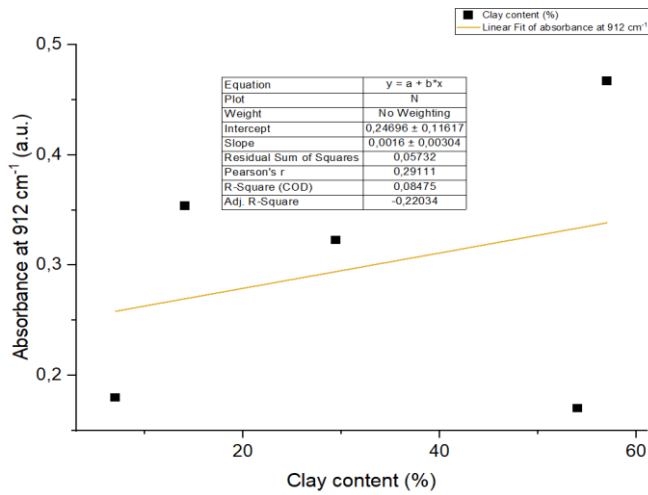
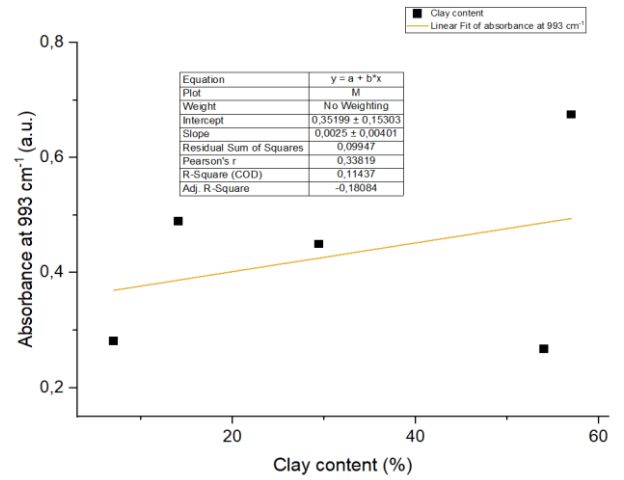
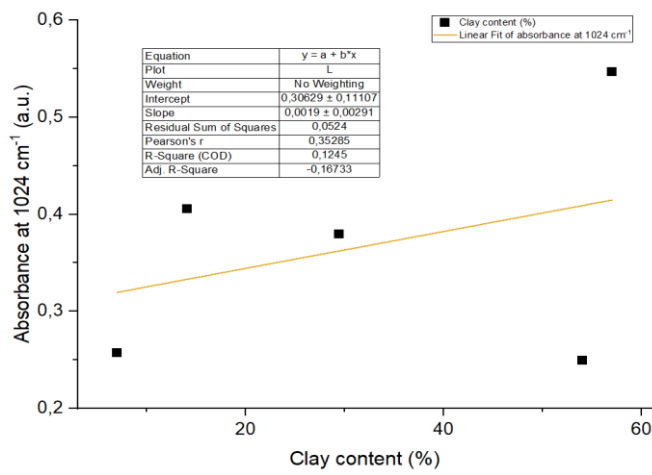


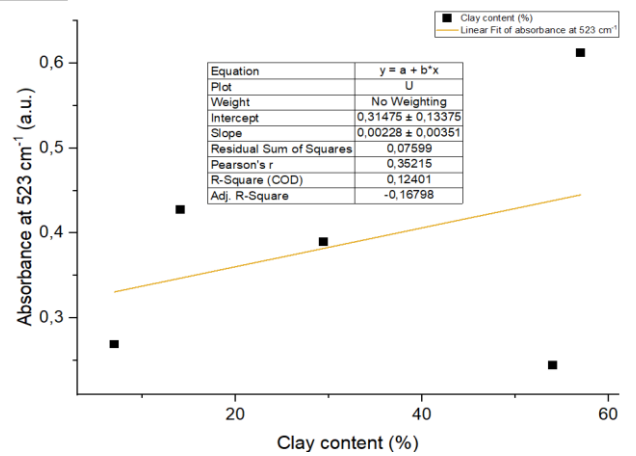
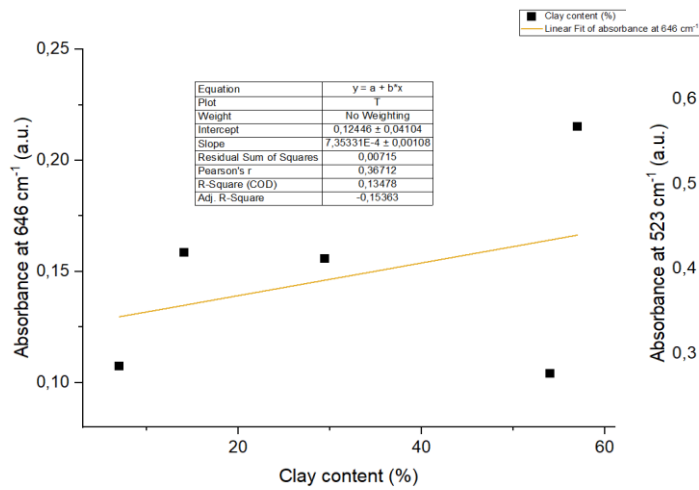
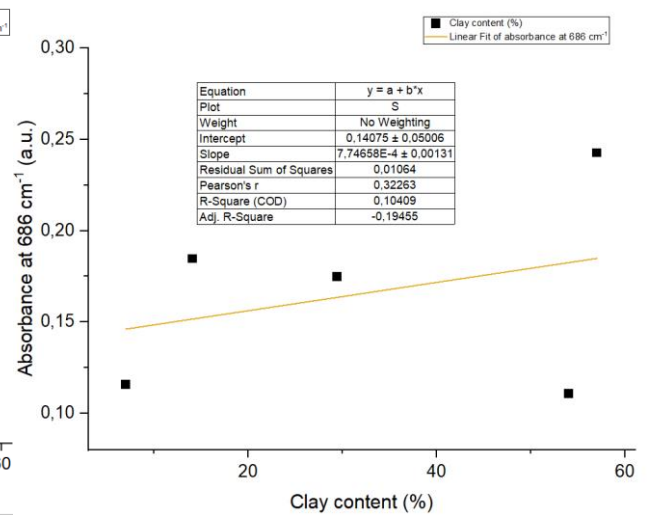
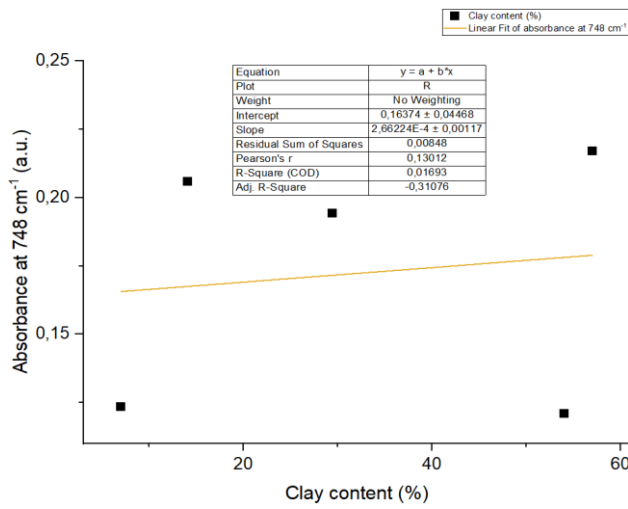


## 8.7 Linear Regression of FTIR spectral peaks and Clay Content (%)









## Biography

Sofia Kapeni was born in Athens, Greece, on March 27, 1999. During her childhood, she lived in a small village, Agios Loukas, on Evia island with her parents and brother. She was always enthusiastic about learning new things, and as a child, she learned English and German and engaged in various sports such as rhythmic gymnastics and kickboxing. In 2017, after graduating from the 2<sup>nd</sup> High School of Aliveri, she enrolled in the International Hellenic University, in Thessaloniki, where she studied Agricultural Technology until 2022. During her studies, she participated in a 6-month Erasmus exchange program at the Estonian University of Life Sciences and completed a 6-month internship at HAS University of Applied Sciences in the Netherlands. These multicultural experiences enabled Sofia to develop a strong interest in the field of research along with her will to explore the world. As a result, she participated in several Erasmus youth exchanges over the years. After completing her bachelor's degree, she decided to continue her academic career by applying to the Erasmus Mundus Master in Sustainable Agriculture, Food Production, and Food Technology. This new journey took her to Hungary, where she studied at the Hungarian University of Life Sciences for her first year of master's studies. After completing her first year, she continued her studies at the Faculty of Agriculture at the University of Zagreb, where she developed a keen interest in environmental health and sustainability. Upon graduating, her goal is to remain in academia by pursuing a PhD and contributing to the research community. In the long-term future, she hopes to also engage in youth exchange programs, fostering personal and cultural development opportunities that Erasmus provides, as it enriched her own development. Ideally, she hopes to continue living in the country that appealed to her the most, Croatia.